Integrated Process Design, Control and Analysis of Intensified Chemical Processes

Mansouri, Seyed Soheil

Publication date:
2016

Document Version
Peer reviewed version

Integrated Process Design, Control and Analysis of Intensified Chemical Processes

Seyed Soheil Mansouri

PhD Thesis

August 2016

DTU Chemical Engineering
Department of Chemical and Biochemical Engineering

Technical University
of Denmark

Integrated Process Design, Control and Analysis of Intensified Chemical Processes

PhD Thesis

Seyed Soheil Mansouri

August 31, 2016

KT-Consortium
Department of Chemical and Biochemical Engineering
Technical University of Denmark
Kongens Lyngby, Denmark

This thesis has been submitted as partial fulfillment of the requirements for the degree of Doctor of Philosophy at the Technical University of Denmark

DTU Chemical Engineering
Department of Chemical and Biochemical Engineering

ABSTRACT

Process design and process control have been considered as independent problems for many years. In this context, a sequential approach is used where the process is designed first, followed by the control design. However, this sequential approach has its limitations related to dynamic constraint violations, for example, infeasible operating points, process overdesign or under-performance. Therefore, by using this approach, a robust performance is not always guaranteed. Furthermore, process design decisions can influence process control and operation. To overcome these limitations, an alternative approach is to tackle process design and controllability issues simultaneously, in the early stages of process design. This simultaneous synthesis approach provides optimal/near optimal operation and more efficient control of conventional (non-reactive binary distillation columns) as well as complex chemical processes; for example, intensified processes such as reactive distillation. Most importantly, it identifies and eliminates potentially promising design alternatives that may have controllability problems later. To date, a number of methodologies have been proposed and applied on various problems to address the interactions between process design and control, and they range from optimization-based approaches to model-based methods.

In this work, integrated process design and control of reactive distillation processes is considered through a computer-aided framework. To assure that design decisions give the optimum operational and economic performance, operability and controllability issues are considered simultaneously with the process design issues. Operability issues are addressed to ensure a stable and reliable process design at pre-defined operational conditions whereas controllability is considered to maintain desired operating points of the process at imposed disturbances in the feed under normal operating conditions. First, a set design methods, similar in concept to design of non-reactive distillations, such as McCabe-Thiele and driving force approach are selected to design the reactive distillation column. Next, these design methods are extended using element concept to also include ternary as well as multicomponent reactive distillation processes. The element concept is used to translate a ternary system of compounds (A + B $\leftrightarrow$ C) to a binary system of elements (W_A and W_B). When only two elements are needed to represent the reacting system of more than two compounds, a binary element system is identified. In the case of multi-element reactive distillation processes (where more than two elements are encountered) the equivalent element concept is used to translate a multicomponent (multi-element) system of compounds (A + B $\leftrightarrow$ C + D) to a binary system of key elements (elements W_{HK} and W_{LK}). For an energy-efficient design, non-reactive driving force (for binary non-reactive distillation), reactive driving force (for binary element systems) and binary-equivalent driving force (for multicomponent reactive distillation) were employed. For both the McCabe-Thiele and driving force method, vapor-liquid equilibrium data are based on elements. It has been is demonstrated that designing a reactive distillation column at the maximum driving force will result in the minimum energy consumption. Note, that the same principles that apply to a binary non-reactive compound system are valid also for a binary-element or a multi-element system. Therefore, it is advantageous to employ the element based method for multicomponent reaction-separation systems.

It is shown that the same design-control principles that apply to a non-reacting binary system of compounds are also valid for a reactive binary system of elements or multi-elements for distillation columns. Application of this framework shows that designing the reactive distillation process at the maximum driving force results in a feasible and reliable design of the process as well as the controller structure. Through analytical, steady-state and closed-loop dynamic analysis it is verified that the control structure, disturbance rejection and energy requirement of the reactive distillation column is better than any other operation point that is not at the maximum driving force. Furthermore, it is shown that the design at the maximum driving force can be both controlled using simple controllers such as PI as well as advanced controllers such as MPC.

RESUMÉ PÅ DANSK

Procesdesign og processtyring er blevet betragtet som selvstændige problemer i mange år. I denne forbindelse anvendes en sekventiel tilgang, hvor processen er konstrueret først, efterfulgt af kontrol design. Men denne sekventielle tilgang har sine begrænsninger relateret til dynamiske constraint krænkelser, for eksempel tidsbegrænsninger arbejdspunkter, proces overdesign eller under-performance. Derfor, ved at bruge denne metode, en robust ydeevne er ikke altid garanteret. Desuden kan processen designbeslutninger påvirke processtyring og drift. For at overvinde disse begrænsninger, en alternativ metode er at tackle proces design og styrbarhed spørgsmål samtidigt, i de tidlige stadier af processen design. Denne samtidige syntese tilgang giver optimal / nær optimal drift og mere effektiv styring af konventionelle (ikke-reaktive binære destillationskolonner) samt komplekse kemiske processer; for eksempel intensiveret processer såsom reaktiv destillation. Vigtigst er det identificerer og fjerner potentielt lovende design alternativer, der kan have styrbarhed problemer senere. Til dato har en række metoder blevet foreslået og anvendt på forskellige problemer at løse samspillet mellem proces design og kontrol, og de spænder fra optimering tilgange til at modellere-baserede metoder.

I dette afhandling, er integreret proces design og kontrol af reaktive destillation processer betragtes gennem en computerstøttet rammer. For at sikre, at beslutninger om design giver de optimale operationelle og økonomiske resultater, anvendelig og styrbarhed spørgsmål behandles samtidig med proces design spørgsmål. Operabilitet problemer løses for at sikre en stabil og pålidelig proces design på foruddefinerede driftsbetingelser mens styrbarhed anses for at opretholde ønskede arbejdspunkter i processen på pålagte forstyrrelser i foderet under normale driftsforhold. Først et sæt design metoder, der ligner i koncept til design af ikke-reaktive destillationer, såsom McCabe-Thiele og drivkraft tilgang valgt at designe den reaktive destillationskolonne. Dernæst er disse designmetoder udvides ved hjælp element koncept til også at omfatte ternære samt flerkomponent reaktive destillation processer. Elementet begrebet anvendes til at oversætte et ternært system med forbindelserne ($A + B \leftrightarrow C$) til et binært system af elementer (W_A og W_B). Når kun to elementer er nødvendige for at repræsentere den reagerende system med mere end to forbindelser, er et binært element system har identificeret. I tilfælde af multi-element reaktiv destillation processer (hvor mere end to elementer er stødt) den ækvivalente element begrebet anvendes til at oversætte en multikomponent (multi-element-system) i forbindelserne ($A + B \leftrightarrow C + D$) til et binært system af centrale elementer (elementer W_{HK} og W_{LK}). For et energieffektivt design, ikke-reaktivt drivkraft (for binær ikke-reaktivt destillation), reaktiv drivkraft (for ternære sammensatte reaktiv destillation) og binær-ækvivalent drivkraft (for flerkomponent reaktiv destillation) blev anvendt. For både McCabe-Thiele og drivkraft metode, er damp-væske ligevægt data baseret på elementer. Det har været påvist, at designe en reaktiv destillationskolonne ved maksimal drivkraft vil resultere i minimalt energiforbrug. Bemærk, at de samme principper, som gælder for en binær ikke-reaktiv forbindelse systemet gælder også for et binær-element eller et multi-element-system. Derfor er det fordelagtigt at anvende elementet metode til flerkomponent reaktion-separation.

Det er vist, at de samme design-kontrol principper, der gælder for en ikke-reagerende binære system af forbindelser gælder også for et reaktivt binært system af grundstoffer eller multi-elementer til destillationskolonner. Anvendelsen af denne ramme viser, at designe den

reaktive destillation ved de maksimale drivkraft resulterer i en gennemførlig og pålidelig udformning af processen samt controller struktur. Gennem analytiske, steady-state og lukket-sløjfe dynamisk analyse er det bekræftet, at kravet om kontrol struktur, forstyrrelse afvisning og energi af den reaktive destillationskolonne er bedre end nogen anden operation punkt der er slet ikke den maksimale drivkraft. Endvidere er det vist, at designet ved maksimal drivkraft kan både styres ved hjælp af simple regulatorer såsom PI samt avancerede regulatorer såsom MPC.

PREFACE

This thesis is submitted as partial fulfilment of the requirements for the degree of Doctor of Philosophy (PhD) in chemical engineering at the Technical University of Denmark (DTU). The PhD-project was carried out at the Department of Chemical and Biochemical Engineering, DTU from September 2013 to August 2016 under main supervision of Professor Rafiqul Gani, and co-supervision of Associate Professor Jakob Kjøbsted Huusom and Professor John M. Woodley.

Firstly, I would like to express my sincere gratitude to my main supervisor Professor Rafiqul Gani for his continuous and persistent support of my PhD study, his meticulous supervision, his patience, motivation, and immense knowledge. I would also like to thank Rafiqul for giving me the opportunity as well as the trust he invested in me to excel; at various scientific platforms around the globe presenting my work and developing my personal and professional skills. It has been a pleasure for me to have Rafiqul as an instructor in several MSc and PhD courses and as my supervisor for my MSc and PhD projects for the last five years. He has been and will be definitely a source of inspiration for me when it comes to scientific leadership and professionalism.

Besides my main supervisor, I would like to also express my sincere gratitude to Associate Professor Jakob Kjøbsted Huusom. He has been an excellent source of inspiration both on academic and personal levels over the last three years. He has not been only an academic advisor to me but also a trustworthy and humble friend. I would like to thank him for countless number of hours that he has spent on helping me solving various challenges, both academic and personal, through his wide perspective and depth of knowledge.

I would also like to thank Professor Mauricio Sales-Cruz with whom my collaboration kicked-off in September 2014 while he was on sabbatical at DTU. I would like to thank him for hosting me for an external stay from February 2016 to May 2016 at Universidad Autónoma Metropolitana (Mexico) working on some of the concepts developed in this work. I have enjoyed a lot of scientific discussions and his true friendship. I have not only learnt a lot from him about computer-aided modeling, but also I have learnt the most from his humane personality and the love and care he has for his friends and family. Mexico has been one of the best experiences that I have had in my entire life until today. This experience would not have been so pleasant without the hospitality of Mauricio, his family and Mauricio Robles-Valle. While there, I also benefitted from many hours of scientific/non-scientific discussions and lengthy lunches on Fridays at Abastos Hotel Plaza with Professor Eduardo S. Pérez-Cisneros (also at Universidad Autónoma Metropolitana).

It has been a long journey for me to come to the point writing this acknowledgement. Therefore, I would like to take this opportunity to thank a few other influential people in my life that made this journey possible for me. I start with my high school mentors, Dr. Reza Namin and Dr. Margaret R. Farrar at Cambridge Rindge and Latin School (Massachusetts, USA), in early 2000s, who were the first people encouraging me to pursue science and technology. I am indebted to them for showing me the horizons, giving me the courage to set foot in it, until today that I have been able to push those horizons a little bit further and continue doing so in future. I sincerely thank Margaret, my advanced placement chemistry teacher, for many hours she spent talking to me about science after school. I also thank Reza

for giving me so much courage and support to finish my high school as one of the youngest ever before my sixteenth birthday. I would like to thank my undergraduate mentor, supervisor and friend, Dr. Sattar Ghader (Shahid Bahonr University of Kerman, Iran) who gave me the opportunity to work on some of his ongoing projects and giving me so much courage and impetus to write my first journal paper when I was only twenty-one years old. He is definitely one of those whom I am thankful forever. This acknowledgement will be incomplete for me without mentioning Professor Zainuddin Abd Manan (Universiti Teknologi Malaysia, Malaysia) and Dr. Gholamreza Zahedi (currently with Design Tanks LLC, USA). I would like to thank them for introducing me to the field of process systems engineering and giving me the opportunity to stay as a visiting researcher at Process Systems Engineering Center (PROSPECT) during the final year of my undergraduate studies. I would also like to thank Dr. Mohammad R. Hajaligol (formerly a principal scientist at Philip Morris, USA) for guiding me throughout my chemical engineering education at all levels until now. I am indebted to him for all his support over the last ten years.

I would like to sincerely thank my best friends Dr. Ali Farsi, Stefano Cignitti, Masoud Malek-Shah and Pouya Hassanpour for their brotherhood, care and friendship over many years of my life. Each one of them has been a detrimental element in what I am achieving today. Furthermore, I would like to thank my colleagues at DTU, Emmanouil P., Anjan T., Amata A., Mohammad A., Marina F., Sawitree K., Olivia P., Zainatul H., Rebecca F., Mariona B., Deenesh B., Amol H., Peam C., Alberto Q. and Michele M. I would also like to thank all the wonderful colleagues at CAPEC-PROCESS research center. If you are reading this and I have missed any of my friends, forgive me, it is just a bad memory problem, but not of my heart.

Finally, I would like to dedicate this thesis to my beloved wife, Tannaz. I would have not been able to conclude this thesis without her patience, love, unconditional support and sacrifice. I would also like to dedicate this thesis to my mother and father – Minoo and Hossein. They have been continuously a source of support and love all throughout my life, especially my father that has held my back unconditionally no matter where I have been on the surface of this planet. I would like to thank also my sisters – Katayoun and Saara – whom I am indebted to for being there for me in many difficult situations in my life.

Seyed Soheil Mansouri

Kongens Lyngby, August 2016

CONTENTS

LIST OF FIGURES

LIST OF TABLES

1
INTRODUCTION

As a result of increased industrial developments together with economic, environmental and societal constraints, there is a need for improved design of chemical processes. This is to overcome challenges associated with energy consumption, raw material depletion and environmental impacts in order to achieve a sustainable development. Therefore, identification, design and development of appropriate processes are important for the industry to remain competitive and to adapt to the new realities of globalization. Nonetheless, the ability to profitably maintain a process operation at its desired conditions (such as product specifications, safety and environmental requirements) must be taken into account. This is the main objective of process control in chemical processes. In control design, operability addresses stability and reliability of the process using *a priori* operational conditions and controllability addresses maintenance of process at desired operating points subject to disturbances (Gollapalli et al., 2000).

Chemical process design and process control are usually considered as independent problems. In this context, a sequential approach is used where the process is designed first, followed by the design of process control. However, as it is well-known, this sequential approach has limitations related to dynamic constraint violations, for example, infeasible operating points, process overdesign or under-performance. Therefore, a robust performance may not always be guaranteed (Dimian et al., 2014a; Seferlis and Georgiadis, 2004) as process design decisions can influence process control and operation. This concept is illustrated in Figure 1.1.

To overcome these limitations, alternatives to tackle process design and controllability issues simultaneously, in the early stages of process design have been proposed and several reviews on this topic have been published recently. Huusom

(2015) discussed the drivers for an integrated approach and outlines the challenges in formulation of such a multi-objective synthesis problem. Sharifzadeh (2013) and Ricardez-Sandoval et al. (2009) extensively reviewed the current state-of-the-art in integration of process design and control, while, Yuan et al. (2012) performed the review of the literature with a focus on optimization-based simultaneous design and control of chemical processes.

This simultaneous synthesis approach provides optimal/near optimal operation and more efficient control of chemical processes (Nikačević et al., 2012). Most importantly, it is possible to identify and eliminate potentially promising design alternatives that may have controllability problems. To date, a number of methodologies have been proposed and applied on various problems to address the interactions between process design and control, and they range from mathematical programming optimization-based approaches (Kookos and Perkins, 2001) to model-based decomposition methods (Hamid et al., 2010).

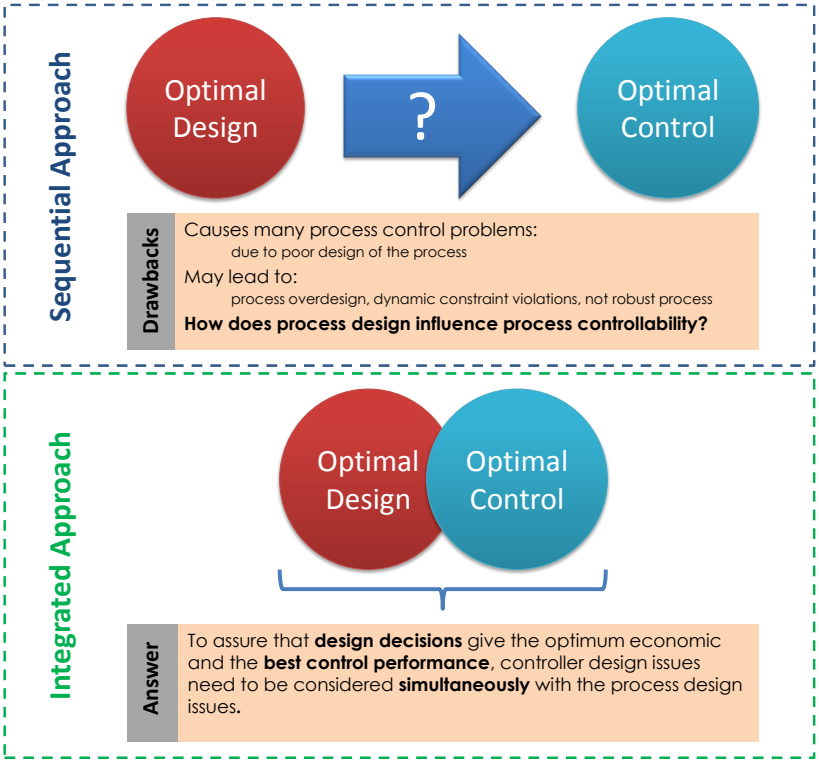

Figure 1.1 Cenceptual comparison of sequential and integrated approaches for integrated process design and control problem

A chemical plant may have thousands of measurements and control loops. By the term plant wide control it is not meant the tuning and behavior of each of these loops, but rather the control philosophy of the overall plant with emphasis on the structural

decisions. The structural decisions include the selection/placement of manipulators and measurements as well as the decomposition of the overall problem into smaller sub-problems (the control configuration) (Larsson et al., 2003). However, synthesis strategies and methodologies have been developed for determining the interconnections between manipulated and controlled variables, which is also termed as control structure selection.

From mid-1980s initial efforts were directed towards steady-state indicators and control indices that address potential control problems. Grossmann and Morrari (Grossmann and Morari, 1983) shown that the heuristic approach is not only often costly and ineffective but that it can have an adverse effect: a design modification intended to improve operability can actually make it worse. They reviewed systematic methods to include operability as a design objective. To this end, they defined the following objectives to be achieved in the operability of a chemical plant:

- Feasibility of steady-state operation for a range of different feed conditions and plant parameter variations
- Fast and smooth changeover and recovery from process disturbances
- Safe and reliable operation despite equipment failures
- Easy start-up and shut-down

In their work, through various application examples, they demonstrated that the fact that it is not always a trivial problem to incorporate properly the objective of operability in design in which intuition and heuristics failed greatly. The common ideas of oversizing for flexibility, identifying "obvious" worst conditions for feasible operation, and avoiding long dead times for dynamic resiliency proved to be all incorrect in those example problems. Furthermore, the importance of selecting proper process configurations and equipment sizes to achieve flexibility, as well as the impact of design changes on the sensitivity of dynamic resilience were also established. Pistikopoulos and Grossmann (Pistikopoulos and Grossmann, 1988) posed the problem of determining minimum cost modifications for redesigning existing process flowsheet systems so as to achieve a specified level of flexibility. In their work, they proposed a novel computational strategy for nonlinear models which relies on the iterative solution of an optimal design formulation that features as constraints a relaxation of the feasibility function for the specified region of flexibility. Special structures of nonlinear models were exploited, in particular models that were bilinear in the uncertain parameters and control variables.

During the 1990s, the importance of a simultaneous approach, considering operability together with the economic issues, was widely recognized. Straub and Grossmann (Straub and Grossmann, 1990) addressed the problem of developing a quantitative measure for the flexibility of a design to withstand uncertainties in the continuous parameters and discrete states. For a given a linear model, a joint distribution for the parameters and probabilities of failure for the discrete states, the proposed metric predicts the probability of feasible operation for a design. A novel inequality reduction scheme is proposed to aid in performing the integration over the feasible region characterized by inequalities. Through an application example, they demonstrated the fact that the proposed measure provides a framework for integrating flexibility and reliability in process design. In their example, the they have not only

shown the computational feasibility of the proposed measure, but also the fact that it provides more complete information than when flexibility and reliability are treated as separate measures. Mohideen *et al*. (Mohideen et al., 1997) proposed a method for the incorporation of robust stability criteria in the design of dynamic systems under uncertainty because in spite of their industrial relevance, operability criteria such as flexibility, controllability and stability have not typically been considered in most process synthesis tools as distinct design objectives. In their approach, process systems were modelled via dynamic mathematical models, variations include both uncertain parameters and time-varying disturbances, while control structure selection and controller design was considered as part of the design optimization problem. Stability criteria were included, based on the concept of the measure of a matrix, to maintain desired dynamic characteristics, in a multi-period design formulation. A combined flexibility-stability analysis procedure was also introduced to ensure feasible and stable operation of the dynamic system in the presence of parametric uncertainties and process disturbances. Fraga *et al*. (Fraga et al., 2000) proposed a discrete programming approach, implemented in a computer-aided tool (Jacaranda), incorporating dynamic modelling for the generation of process designs, which met specified criteria for operability or flexibility. Particular attention is given to implementation issues, including especially how to incorporate dynamic modelling efficiently in an automated environment. Their results have demonstrated that even with a coarse discretization procedure, alternative process structures can be generated using a variety of evaluation criteria. Although they made use of simplified models for computational efficiency, the underlying procedures are suitable for high fidelity models. Furthermore, the models can be extended to include alternative control strategies, enabling the simultaneous generation of the process structure and its control system.

1.1 State-of-the-art in integration of process design and control

In mathematical optimization approaches, the process design problem is usually formulated as a mixed integer non-linear programming (MINLP) optimization problem. The continuous variables are linked with design variables (such as, flow rates, heat duties) and process variables (temperatures, pressures, compositions), while binary (decision) variables are used to model logical decisions related to choices between different process flowsheet alternatives. In the integrated process design-control context, the variables considered in the process model represent both steady-state and dynamic behavior of the process and in this case the optimization problem is referred to as mixed integer dynamic optimization (MIDO)(Flores-Tlacuahuac and Biegler, 2007). Meidanshahi and Adams (Meidanshahi and Adams, 2016), addressed integrated process design and control of semi-continuous processes using a MIDO approach. Their results show that the MIDO approach using an outer approximation (OA) method was able to find similar solutions obtained with particle swarm optimization (PSO). Therefore, since the OA method proved to be faster than PSO, they recommended using PSO only when an OA method is not available.

In decomposition-based approach, the main idea is to decompose the original MINLP problem into an ordered set of sub-problems. Each sub-problem, except the last one, requires only the solution of a subset of the original constraints set. The final sub-problem contains the objective function and the remaining constraints. In this way, the solution of the decomposed set of sub-problems is equivalent to that of the original optimization problem. The advantage is a more flexible solution approach together with relatively easy to solve sub-problems while the disadvantage is that a global optimal solution cannot be guaranteed (Hamid et al., 2010). Mehta and Ricardez-Sandoval (Mehta and Ricardez-sandoval, 2016), recently proposed a new methodology for integration of process design and control using power series expansion (PSE) approximations. The main idea in this approach is to back-off from the optimal steady-state design that is often found to be dynamically inoperable. However, the challenge in their approach is to determine the magnitude of the back-off needed to accommodate the transient and feasible operation of the process in the presence of disturbances and parameter uncertainty. Sharifzadeh and Thornhill (Sharifzadeh and Thornhill, 2013), proposed a new framework that utilizes a multi-objective function to explore the trade-off between process and control objectives. They applied two parallel solution strategies, dynamic optimization based on sequential integration and full discretization. Recently, Patil et al. (2015) proposed a methodology that addresses the simultaneous design, scheduling, and control of multiproduct processes. The proposed methodology takes into account the influence of disturbances by the identification of their critical frequency, which is used to quantify the worst-case variability in the controlled variables via frequency response analysis. Another decomposition-based optimization approach has been proposed to tackle the integration of process design and controller design for reactor-separator-recycle processes (Hamid, 2011). The employed solution strategy is based on the targeted reverse design approach and employs thermodynamic-process insights, for example, the attainable region (Diane Hildebrandt and Glasser, 1990) and the driving force concept (Bek-Pedersen and Gani, 2004), to decompose the integrated design-control problem into four sequential hierarchical sub-problems. Based on the solution of the decomposed set of hierarchical sub-problems, large number of infeasible solutions within the search space are identified and eliminated. Hence, it is able to obtain a final sub-problem that is significantly smaller in size.

Huusom (Huusom, 2015) discussed the drivers for an integrated approach and outlines the challenges in formulation of such a multi-objective synthesis problem. He outlines four main opportunities for integration of process design and control:

i. *Defining operational constraints in process synthesis.* The integrated process design and control problem (that is a dual multi-objective optimization problem: one is the optimal steady-state process design objectives, and two is dynamic controller performance objectives) may be solved through a controllability index approach without fundamentally changing the problem definition and solution strategy as opposed to the conventional process synthesis approaches. Therefore, from an industrial point of view this approach more viable compared to the sequential process design and control approach. Here, the challenge is finding mathematically simple enough controllability index measures for a wide range of process.

ii. *Enabling process integration by model based control*. Efficiency of many processes can be realized by application of model based control. This is primarily due to the decoupling effect and feed forward properties that can be utilized through the embedded process model. There is a potential in advanced control, which is significant, that is development of process models by more efficient and cheap procedures for many production companies to get more involved in developing the right automation strategies for their own processes rather than relying on off the shelf solutions.

iii. *Analyzing operation of novel unit operations.* Currently many solution strategies and approaches have been developed to address the conflicting trade-offs between process design and control of conventional unit operations (for example, single reactor, distillation, etc.). However, there is a need for solution strategies for new hybrid and intensified unit operations of future given the needs of the society in future. The advantages of such units can be associated with challenges in terms of operation (Nikačević et al., 2012). As part of the challenge is a high degree of dynamic coupling in such systems, the solution is a control system which implements decoupling and coordination through a model based control approach. This therefore put some requirements on the need for development of accurate process models.

iv. *The need for a plantwide process design and operation benchmark problem.* In the integrated process design and control area, there is a need for a generally accepted and validated benchmark problem, also from and industrial perspective, similar to Tennessee-Eastman problem (Downs and Vogel, 1993). Such benchmark problem(s) can be used to perform both steady-state and dynamic simulation using predefined performance scenarios and metrics. Therefore, from a design point of view the best solution can be easily identified and from a control point of view the none-trade-off solution can be identified.

1.2 Integrated process design and control of intensified processes

Integrated approach can be achieved by identifying variables together with their target values that have roles in process-controller design. The solution to this optimization problem must address the trade-offs between conflicting design and control objectives for the intensified processes. Therefore, a systematic analysis for identifying optimal design together with design-manipulated variables *u*, process-controlled variables *y*, their target set points, and their pairing significantly contributes to the integration of process design, operation and control. Nonetheless, this systematic analysis may provide additional and or innovative options to address the conflicting trade-offs between process design, control and operation of intensified processes. Thus, through such a systematic analysis, new choices for actuators may identify.

Lutze et al. (2010) have defined process intensification as "a process development/design option which focuses on improvements of a whole process by adding/enhancing of phenomena through integration of unit operations, integration of functions, and integration of phenomena and/or targeted enhancement of a phenomenon within an operation". There is an increasing interest in application of intensified and multi-functional processes in chemical industry (Nikačević et al.,

2012). Several applications of process intensification principles are realized so far on an industrial scale including reactive distillation, micro-reactors, rotating packed bed systems, etc. However, reactive distillation with already over 150 industrial applications is one of the most successful intensified processes on an industrial scale (Harmsen, 2007). Some of the applications of reactive distillation in industry are for example, production of methyl-tert-butyl-ether (MTBE) (Panda and Kannan, 2014), ethyl-tert-butyl-ether (ETBE) (Sneesby et al., 1999a) and methyl-acetate (Pöpken et al., 2001). Intensified processes, including reactive distillation, possess specific and/or unique properties that may result in a difficult or complex operation in presence of disturbances. This is mainly due to the loss in degrees of freedom because of integration of unit operations, functions or phenomena (see Figure 1.2). Therefore, one alternative to tackle this challenge is to address to process design and control problems simultaneously in the early stages of process design. Beside reactive distillation which is widely implemented in the chemical industry (Schoenmakers and Bessling, 2003), the other combinations of chemical reaction and separation, or two separation processes in one unit are also promising such as membrane-based reactors or distillations. However, these novel hybrid schemes, as it was also mentioned earlier, have less degrees of freedom compared to conventional process which compose of separate consecutive tasks or unit operations (see Figure 1.3).

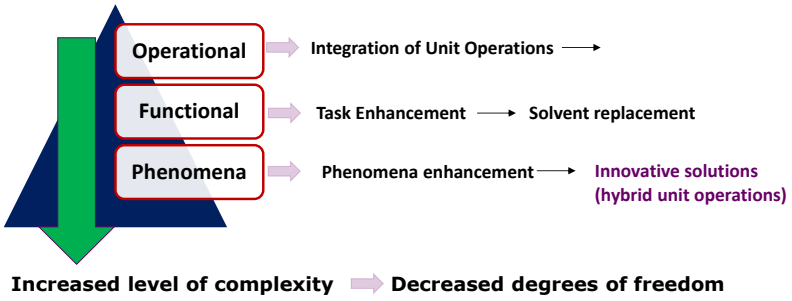

Figure 1.2 Complexity pyramid in integration of unit operations/functions/phenomena to achieve process intensification.

Reactive distillation column (RDC) is a unit operation in which separation and reaction take place in a single operation, thus making it a multi-functional unit operation. Due to its very successful application in the industry it has attracted considerable amount of research both from academia and industry (Tuchlenski et al., 2001). It offers substantial advantages, such as higher reaction rate and selectivity (Lee et al., 2010), avoidance of azeotropes and reduced energy consumption as well as solvent usage (Babi et al., 2014; S. Mansouri et al., 2013). However, it must be noted that as a result of integration of functions/operations into a single unit operation, the control and operation of the RDC poses a challenge due to the loss in degrees of freedom.

Various studies have addressed the design-control of reactive distillation processes. Al-Arfaj and Luyben (Al-Arfaj and Luyben, 2000) explored six alternative control structures for an ideal two-product reactive distillation column. They illustrated the

interaction between design and control by the impact of holdup in the reactive zone. Georgiadis *et al*. (Georgiadis et al., 2002) investigated the design and control of a RDC via two different optimization approaches. In the first approach, the steady-state process design and the control system are optimized sequentially. They confirmed that operability is strongly influenced by process design. In the second approach, the process design and the control system are optimized simultaneously using mixed integer dynamic optimization leading to a more economically beneficial and better controlled system than that obtained using the sequential approach. Therefore, the objective (or target) for the integrated process design and control is to overcome the bottlenecks associated with the sequential approach and to obtain optimal/near optimal design of a reactive distillation column which is also the easiest to control and operate.

Sneesby et al. (1999) explored the interactions between design and control where they focused on control schemes for reactive distillation taking into account effect of the principal operating parameters on the reactant conversion. For this purpose, they proposed a standard regulatory control system for an ETBE reactive distillation column where the reboiler duty (or the bottoms draw rate) to control the bottoms composition inferred via a stripping section temperature was used. They found their structure to be closed-loop stable, unlike many other control schemes which used other temperatures (e.g. the reboiler temperature) to infer the ether purity. However, the scheme that Sneesby et al. (1999) reported had a major deficiency which was its inability to control the composition to a set-point.

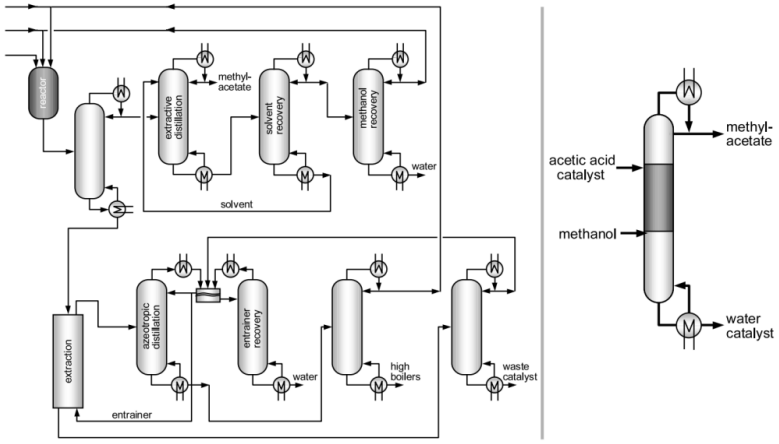

Figure 1.3 Production of methyl-acetate at Eastman-Kodak. Left: without intensification; Right: with intensification – reactive distillation column (Schoenmakers and Bessling, 2003).

Chung et al. (2015) addressed design and control of reactive distillation process for esterification of levulinic acid and n-butanol. They performed sensitivities of some design variables such as feed ratio of raw materials and operating pressure for

economic production of n-butyl levulinate. They obtained the optimal steady-state design through total annual cost analysis using iterative optimization.

1.3 Objectives of the work

The objective of this work is to develop a systematic methodology to address the integrated process design and control of intensified chemical processes. The aim is to use efficient, simple and easy to use design methods that are similar in concept to design of non-intensified processes. The methodology is based on decomposing the problem into a sub-set of smaller sequential hierarchical problems. Figure 1.4, shows a representative scheme of the integrated process design-control methodology that has been developed in this work.

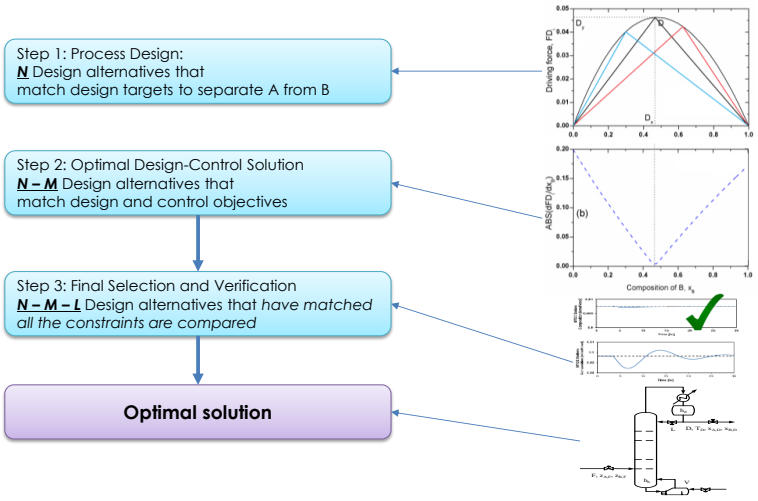

Figure 1.4 Representative scheme of the design-control methodology for intensified processes.

It must be noted that this framework is mainly addressing the integrated process design and control of intensified processes. In this work, integrated design and control of reactive distillation processes and reaction-separation processes is considered through a systematic hierarchical approach implemented through a computer-aided framework. The framework, based on the method proposed by Hamid et al. (2010), consists of four hierarchical steps by which, (1) the objectives and design targets are set, (2) the number of elements in the system is identified, (3) the reactive distillation column is designed and the control structure is determined, and (4) the designed operation is verified by rigorous dynamic analysis.

1.4 Thesis organization

This PhD-thesis consists of five chapters (including this chapter, Introduction). A brief summary of the contents given in each chapter is listed below:

Chapter 1: Introduction
The main drivers for an integrated approach for process design and control of intensified chemical processes are highlighted in this chapter. The opportunities and the needs to develop a systematic methodology to address the integrated process design and control are also given. Finally, a more specific objective of the present work is given which will be elaborated in next chapters.

Chapter 2: Review of the methodologies for integrated process design and control
The most important methodologies for addressing the integrated process design and control are reviewed in this chapter. These approaches are classified as: dynamic optimization approach, embedded control optimization, and decomposition-based methods.

Chapter 3: Concepts and theories for integrated process design and control
Although the integrated process design and control of chemical processes is an elaborate problem, in this chapter only the concepts and theories which are associated with the decomposition-based methodology, developed in this work, are explained and reviewed. The concepts and theories are similar in concept to design of non-reactive separation processes. Here, the main concepts that are addressed are: the driving force concept (from a thermodynamic and design point of view), the element-based method for design of multi-component reaction-separation processes together with the physical and chemical equilibrium concept, and the driving force based integrated process design and control.

Chapter 4: Methodology for integrated process design and control
In this chapter, the methodology for integrated process design and control of a class of intensified processes (i.e. reactive distillation processes) is presented and implemented through a hierarchical computer-aided framework. The framework is capable of handling large variety of reactive distillation configurations (single feed, multiple feed, with or without non-reactive stages). Each step of the framework together with the description of any corresponding algorithm being applied in that step of the framework is given and explained.

Chapter 5: Application examples
This chapter starts with two conceptual examples to illustrate the interactions of design and control and how process design decisions influence process control and operation. The first conceptual example is MTBE production process represented by a reactor-separator-recycle system is presented. The second conceptual example is methyl-acetate production via a membrane-assisted intensified process, which is also a reactor-separator-recycle system.

This chapter continues with applications of the methodology which are demonstrated through three case studies. The first case study involves production of MTBE by a reactive distillation process (single feed, binary element system). The second case study is also concerned with MTBE production by reactive distillation but for a multi-element system (single feed and more than two elements). The third case study is the famous production of methyl-acetate by reactive distillation process (multi-element, double feed).

2
REVIEW OF METHODOLOGIES FOR INTEGRATED PROCESS DESIGN AND CONTROL

Recent developments in the field suggest that if process design and controller design are performed simultaneously, it may result in improved performance in terms of process economics and operation. The drawback in sequential approaches for integrated process design and control is that they are mainly focused on individual problems, such as controller structure selection or controller design. However, these methods lack the considerations for interactions between process control issues and process design issues. According to Morari (1983), it is very well recognized that controllability is inherently dominated by the process design and does not depend on the controller design – that is, it is not possible to overcome issues associated with controllability in a process by designing more sophisticated controllers. Therefore the drivers to integrate controllability and controller performance into process design, as they were elaborated in the introduction of this thesis, have led to development of new methodologies for integration of process design and control.

In the current review, the focus is given to the methodologies that are developed for integration of process design and control. These methodologies can be categorized as (1) dynamic optimization approach, (2) embedded control optimization, and (3) decomposition approach. In the forthcoming text, some of the main contributions under the aforementioned categories are highlighted. Note however, recently, Sharifzadeh (2013) and Yuan et al. (2012) have extensively reviewed the methods and current state-of-the-art for integrated process design and control.

Here, in all the methodologies that are reviewed, the process flowsheet is known, as well as the design targets, feed specifications and process conditions. Therefore, the objective is to find the design variables, the operating conditions (including set-points for controlled variables) and controller structure that optimize the plant economics and, simultaneously, a measure of the plant controllability, subject to a set of constraints which also include the process model to ensure appropriate dynamic behavior and process specifications. The general formulation of the problem is (Sendin et al., 2004) give as follows. Note that the original notation has been used.

$$\min_{x} F\left(\dot{z}, z, p, x\right) = \begin{bmatrix} F_1\left(\dot{z}, z, p, x\right) \\ F_2\left(\dot{z}, z, p, x\right) \end{bmatrix} \tag{2.1}$$

Subject to:

$$f\left(\dot{z}, z, p, x\right) = 0 \tag{2.2}$$

$$z\left(t_0\right) = z_0 \tag{2.3}$$

$$h\left(z, p, x\right) = 0 \tag{2.4}$$

$$g\left(z, p, x\right) \leq 0 \tag{2.5}$$

$$x^L \leq x \leq x^U \tag{2.6}$$

Here x is the vector of decision variables, z is the vector of dynamic state variables, F is the vector of objective functions (F_1 is a combination of capital and operation costs, and F_2 is the controllability measure), f is the set of differential and algebraic equality constraints describing the system dynamics (mass, energy and momentum balances, i.e. the non-linear process model), and h and g are possible equality and inequality path and/or point constraints which express additional requirements for the process performance.

2.1 Dynamic optimization approach

There is a need to consider process design and process control issue at the early stages of process design. Over the years, there have been a number of methodologies that have been developed based on dynamic optimization where the problem is posed as mixed-integer dynamic optimization (MIDO). In this approach, the problem is formulated as a mixed integer non-linear programming (MINLP) optimization problem. The continuous variables are linked with design variables (such as, flow rates, heat duties) and process variables (temperatures, pressures, compositions), while binary (decision) variables are used to model logical decisions such as whether to choose between different possible flowsheet structures and/or controller structures. In the integrated process design-control context, the variables considered in process model are such that they represent both steady-state and dynamic behavior of the problem. Therefore, in this case the optimization problem is referred to as MIDO. Disturbance rejection is an important feature for the closed-loop control performance of chemical processes. In order to get minimum time closed-loop disturbance rejection, the following optimization problem can be formulated to use a MIDO approach (Flores-Tlacuahuac and Biegler, 2007):

$$\min \int_0^{t_f} \left\| z(t) - \hat{z}(t) \right\|^2 dt \tag{2.7}$$

s.t. Semi-explicit DAE model of a dynamic process

$$\frac{dz(t)}{dt} = F\left(z(t), x(t), u(t), t, p\right) \tag{2.8}$$

$$0 = G\left(z(t), x(t), u(t), t, p\right) \tag{2.9}$$

Initial conditions:

$$z(0) = z^0 \tag{2.10}$$

Bounds:

$$\begin{aligned} z^L \le z(t) \le z^U \\ x^L \le x(t) \le x^U \\ u^L \le u(t) \le u^U \\ p^L \le p \le p^U \end{aligned} \tag{2.11}$$

Disjunctions:

$$\bigvee_{j \in D} \left\{ a_j \le g_j(w) \le b_j \right\} \tag{2.12}$$

where F is the vector of right-hand sides of differential equations in the DAE model of a dynamic process system, G is the vector of algebraic equations, assumed to be index one, $t \in [0, t_f]$ the time, z the differential state vector, z^0 the initial values of z, $\hat{z}$ is the set-point vector, x the algebraic state vector, u the control profile vector and p is a time-independent parameter vector. Also, we define $w = [z^T, x^T, u^T, p^T]^T$ and D is the set of disjunctions with the inequality constraints having the property $g_j(0) = 0$ in the j^{th} disjunction. These disjunctions can be obtained and derived in a systematic manner taking into account the logical expressions. A number of approaches can be taken to solve Eqs. (7) – (11). Currently, DAE optimization problems are solved using a variation approach or by various strategies that apply non-linear programming (NLP) solvers to the DAE model (Biegler, 2007a). Until the 1970s, these problems were solved using an indirect or variational approach, based on the first order necessary conditions for optimality obtained from Pontryagin's Maximum Principle (Berkovitz, 1961). For problems without inequality constraints, these conditions can be written as a set of DAEs (Lewis et al., 2015). Obtaining a solution to these equations requires careful attention to the boundary conditions. Often the state variables have specified initial conditions and the adjoint variables have final conditions; the resulting two-point boundary value problem (TPBVP) can be addressed with different approaches, including single shooting, invariant embedding, multiple shooting or some discretization method such as collocation on finite elements or finite differences. On the other hand, if the problem requires the handling of active inequality constraints, finding the correct switching structure as well as suitable initial guesses for state and adjoint variables is often very difficult.

Methods that employ NLP solvers can be classified into two groups, *sequential* and *the simultaneous* strategies (Biegler, 2007b). The sequential methods which are also known as control vector parameterization; it is only the control variables that are discretized. Therefore, the control variables are given as piecewise polynomials as

described by Barton *et al*. (Barton et al., 1998); thus, the optimization is carried out taking into account the polynomial coefficients. Provided that the initial conditions and a set of control parameters are given, the DAE model is solved in the frame of an inner loop controlled by an NLP solver; parameters that represent the control variables are updated by the NLP solver. Gradients of the objective function with respect to the control coefficients and parameters are calculated either from direct sensitivity equations of the DAE system or by integration of the adjoint equations (Biegler, 2007b). Sequential strategies are easier to build and to be employed as they include the components of reliable DAE solvers (e.g., DASSL, DASOLV, and DAEPACK) as well as NLP solvers (NPSOL, SNOPT). Moreover, repeated numerical integration of the DAE model is required. This may become computationally expensive for large-scale problems. Nonetheless, it is well known that sequential approaches have properties of single shooting methods and are not able to handle open-loop instability. Finally, path constraints can be handled only approximately, within the limits of the control parameterization. An application example is the work of Flores-Tlacuahuac *et al*. (Flores-Tlacuahuac et al., 2005) where they considered dynamic optimization strategies for grade transitions for high-impact polystyrene reactors. Because their desired operating conditions were at unstable points, state and control variables in the optimal control problem were discretized and a large-scale nonlinear programming solver was applied.

Multiple shooting is a simultaneous approach that inherits many of the advantages of sequential approaches. Here the time domain is partitioned into smaller time elements and the DAE models are integrated separately in each element. Control variables are parametrized as in the sequential approach and gradient information is obtained for both the control variables as well as the initial conditions of the state's variables in each element. Finally, equality constraints are added to the NLP to link the elements and ensure that the states are continuous across each element. As with the sequential approach, inequality constraints for states and controls can be imposed directly at the grid points. For piecewise constant or linear controls this approximation is accurate enough, but path constraints for the states may not be satisfied between grid points. In the simultaneous approach, also known as direct transcription, both the state and control profiles are discretized in time using collocation of finite elements. This approach corresponds to a particular implicit Runge-Kutta method with high order accuracy and excellent stability properties. Also known as fully implicit Gauss forms, these methods are usually too expensive (and rarely applied) as initial value solvers. However, for boundary value problems and optimal control problems, which require implicit solutions anyway, this discretization is a less expensive way to obtain accurate solutions. On the other hand, the simultaneous approach leads to large-scale NLP problems that require efficient optimization strategies. One of the application examples is proposed by Biegler *et al*. (Biegler et al., 2002) which is an improved algorithm for simultaneous strategies for dynamic optimization. This approach addresses two important issues for dynamic optimization. First, an improved nonlinear programming strategy is developed based on interior point methods. This approach incorporates a novel filter-based line search method as well as preconditioned conjugate gradient method for computing search directions for control variables. This leads to a significant gain in algorithmic performance. On a dynamic optimization case study, they have shown that nonlinear programs (NLPs) with over

800,000 variables can be solved in less than 67 CPU minutes. Second, they addressed the problem of moving finite elements through an extension of the interior point strategy. With this strategy they developed a reliable and efficient algorithm to adjust elements to track optimal control problem breakpoints and to ensure accurate state and control problems. This is demonstrated on a dynamic optimization for two distillation columns. As a result, these methods, such as the aforementioned one, directly couple the solution of the DAE system with the optimization problem; the DAE system is solved only once, at the optimal point, and therefore can avoid intermediate solutions that may not exist or may require excessive computational effort.

Areas of application of MIDO frameworks are as follows: batch process synthesis and development (Capón-García et al., 2013; Nie et al., 2012), reduction of kinetic mechanisms (Petzold et al., 1999), solvent design in batch processes (Giovanoglou et al., 2003), optimization of hybrid discrete/continuous systems (Barton and Lee, 2004), biochemical process such as optimal chemotherapy (Dua et al., 2006). Meidanshahi and Adams (Meidanshahi and Adams, 2016), addressed integrated process design and control of semi-continuous processes using a MIDO approach. MIDO approach has been increasingly used as a result of the advancements in computational power and dynamic programming algorithms (Dimian et al., 2014b). Various algorithms and solutions strategies have been developed to solve MIDO problems. Note however, the major drawback of MIDO methodologies is the complexity that is associated with computations. Therefore, their application on large or industrial problems is difficult due to very long computational times (Ricardez-Sandoval et al., 2009). A comprehensive review of state-of-the-art and progress in the optimization-based simultaneous design and control for chemical processes has been performed by Yuan *et al.* (Yuan et al., 2012). Some of these methods are categorized and presented in Table 1 (updated from Yuan *et al.* (2012)) and further details can be found in the given references.

Table 2.1 Methods for addressing MIDO problems

Authors	Key Features	Applications	Controller
Androulakis (Androulakis, 2000)	Complete discretization on the dynamic system. The transformed MINLP problem is solved using the BB method.	Kinetic mechanism reduction	–
Avraam (Avraam et al., 1999, 1998)	Complete discretization on the dynamic system. The MIDO problem is transformed to a large MINLP problem. This problem is solved using the OA method.	Safety analysis of a surge drum	–
Asteasuain (Asteasuain et al., 2004)	Used gPROMS/gOPT to solve MIDO	Semi-batch polymerization reactor	PI
Asteasuain (Asteasuain et al., 2006)	Implemented a multi-objective optimization to minimize the cost	Styrene polymerization reactor	Multivariable PI

Asteasuain (Asteasuain et al., 2007)	Performed a simultaneous design and control under uncertainty for optimal grade transition operation	Polymerization reactor	Multivariable PI
Bahri (Bahri et al., 1997)	Back-off minimization to capture uncertainty	Two series CSTRs	PI
Bansal (Bansal et al., 2000, 1998)	Applied Mohideen's framework in a rigorous distillation model	Binary distillation; double-effect distillation	PI
Bansal (Bansal et al., 2002)	Developed a novel, multi component, mixed integer dynamic optimization algorithm	Distillation column	PI
Bansal (Bansal et al., 2003)	Proposed a new MIDO algorithm without the solution of an intermediate adjoin problem	Binary distillation	PI
Dimitriadis (Dimitriadis and Pistikopoulos, 1995)	Complete discretization on the dynamic system. The transformed MINLP problem is solved using the GBD method.	Batch reactor	PI
Flores-Tlacuahauc (Flores-Tlacuahuac and Grossmann, 2006)	Non-convex formulation, Big-M formulation, and GDP based MINLP	Two series CSTRs	PI
Flores-Tlacuahauc (Flores-Tlacuahuac and Grossmann, 2011)	Full discretization approach; MINLP was solved by a full nonconvex optimization formulation	Polymerization reactor	PI
Kookos (Kookos and Perkins, 2001)	Infinite-dimensional; stochastic, mixed integer dynamic optimization	Evaporator system; Binary distillation	Multivariable PI
Khajuria (Khajuria and Pistikopoulos, 2011)	Incorporating highly non-linear and dynamics nature into dynamic optimization framework	Pressure swing adsorption systems	PI
Lopez-Negrete (Fuente and Flores-Tlacuahuac, 2009)	Full discretization approach; Relaxed versions based composition approach	Binary distillation	PI
Mohideen (M J Mohideen et al., 1996; M. Jezri Mohideen et al., 1996; Mohideen et al., 1997)	Mixed integer stochastic optimal control formulation; Multi-period decomposition approach	Ternary distillation column	PI
Paramasivan (Paramasivan and Kienle, 2010)	Full discretization approach; Formulate MIDO to determine the optimal control structure and controller parameters	Reactive distillation	PID
Panjwani (Panjwani et al., 2005)	Used a high fedility dynamic model to predict the behavior	Reactive distillation	PI

	under varying disturbances		
Ross (Ross et al., 2001)	The simplification involves fixing the integer decisions pertaining to the existing process and control structure	High purity industrial distillation system	PI
Sakizlis (Sakizlis et al., 2003)	Presented a novel method for integrating advanced controller in a simultaneous design and control	Binary distillation; Evaporator system	PI
Schweiger (Schweiger and Floudas, 1998)	Used control vector parameterization (CVP). OA method for treating the integers		
Banga and Moles (Banga et al., 2004; Moles et al., 2003)	Used stochastic global optimization (GO) method to locate the region of global solutions		
Esposito and Moles (Esposito and Floudas, 2000; Moles et al., 2003)	Used deterministic GO methods to locate the optimal performance		

2.2 Embedded control optimization

This approach is based on a novel mathematical formulation to render the combinatorial complexity of the integrated process design and control problem. Therefore, the problem is formulated as a bi-level optimization problem, which is then solved using a two-stage sequential approach (Malcolm et al., 2007). This formulation separates design decisions from control decisions to keep the problem size manageable by significantly reducing the complexity. The first stage (usually called master level) seeks optimal design decisions while the second stage tests the dynamic performance based on design decisions obtained previously by fixing a particular control strategy (for example model predictive control) alongside its tuning parameters. Fixing a particular control strategy in the second stage, therefore, eliminates integer decisions for selecting controller structures, and the problem complexity is reduced. From a computational point of view, the currently proposed solution strategies are able to reduce the combinatorial complexity of the problem and solving with less effort compared to the dynamic optimization-based solution strategies. Although the design solution obtained from the embedded control optimization approach may result in suboptimal design solutions, it is attractive from a computational point of view and offers better practicality for solving industrial problems. The embedded control approaches can be divided into two groups, mathematical programming format and intelligent-based control.

2.2.1 Mathematical programming format

Malcolm et al. (2007) proposed a procedure for integrated process design and control. This is based on process dynamics and advanced control by a novel embedded control optimization approach. Their work suggests a two-stage problem decomposition

leading to a massive reduction of problem size and complexity. Therefore, their work presents a decision-making hierarchy that allows designers to arrive at key structural decisions for process flowsheet and control layout, and to optimize them simultaneously for high-performance under realistic uncertain operating conditions. Conceptual approaches to achieve the desired integration of design and control were made possible using a novel problem formulation that implicitly relates closed-loop dynamics with design decisions. As a result, an integrated optimal design with feedback control was obtained. This new integrated design can satisfactorily operate under adverse input conditions, while delivering products within desired quality specifications. Rigorous mathematical programming approaches are presented for optimizing parametric design variables, as well as structural alternatives. Their novel design and control integration also provides analytical methods to ensure desired production quality standards in the presence of uncertainty. Moon et al. (2011) and (2009a) introduced a new mathematical formulation to reduce combinatorial complexity of integrating design and control. They have shown that a substantial reduction in problem size can be achieved using embedded control decisions within specific designs. These embedded control decisions avoid a combinatorial explosion of control configuration, using a full state space model that does not require a pairing of control variables and loops. Patel et al. (2008) proposed a bi-level dynamic optimization approach for achieving IPDC. The principal idea proposed was to utilize an optimal controller (a modified linear quadratic regulator) to practically evaluate the best achievable control performance for each candidate design during process design. The evaluation of complete, closed-loop system dynamics can then be meshed with a superstructure-based process design algorithm, thus enabling considering both cost and controllability in design of a process. The practicality of the introduced approach enables a solution of this complex dynamic optimization problem within reasonable computational requirements, as demonstrated in an evaporator case study. Ricardez Sandoval et al. (2008) proposed a new methodology to integrate process design and control. In their work, they have assumed availability of the complete dynamic model of the system to be design and a fixed (known) control structure. The key idea in this method is to represent the system's closed-loop nonlinear behavior as a linear state space model complemented with uncertain model parameters. Then, robust control tools are applied to calculate bounds on the process stability, the process feasibility and the worst-case scenario. Their new methodology was applied to the simultaneous design and control of a mixing tank process. The resulting design avoids the solution of computationally intensive dynamic optimizations since the integration of design and control problem is reduced to a nonlinear constrained optimization problem.

2.2.2 Intelligence-based control

Lu et al. (2010) performed Particle Swarm Optimization (PSO-based) intelligent integration of design and control for one kind of non-linear curing process. This method combines the merits of both fuzzy modeling/control and PSO method, where fuzzy modeling/control is proposed to approximate/control the nonlinear process in a large operating region and the PSO-based intelligent optimization method is developed to solve non-convex and non-differential integration problem with design

and control optimized simultaneously. Finally, the proposed method is compared with the traditional sequential method on controlling the temperature profile of a nonlinear curing process. Bhat *et al*.(Bhat and McAvoy, 1990) discussed the use of backpropagation neural nets for dynamic modeling and control of chemical process systems. The backpropagation algorithm and its rationale were reviewed. The algorithm was applied to model the dynamic response of pH in a CSTR. Comparing the results to traditional modeling, the backpropagation technique is shown to be able to pick up more of the nonlinear characteristics of the CSTR. The use of backpropagation models for control, including learning process inverses, was also briefly discussed. To summarize the approaches named in this section, Table 2 gathers the different embedded control optimization approaches together and presents the main feature of each method.

Table 2.2 Methods for embedded control optimization

Method	
Mathematical programming format	
Malcolm and Moon (Malcolm et al., 2007; Moon et al., 2011, 2009b)	Developed an embedded control optimization approach, which is used to recast the IPDC problem into a solvable mathematical programming format
Patel (Patel et al., 2008)	Utilized an optimal controller (a modified linear quadratic regulator – mLQR) to practically evaluate the best achievable control performance for each design candidate.
Ricardez-Sandoval (Ricardez-Sandoval et al., 2008)	Proposed a robust modeling approach for large-scale chemical processes. They used a fixed control structure and applied advanced and feedback controllers and local solutions are only obtained.
Intelligence-based control	
Lu (Lu et al., 2010)	Intelligence-based method which combines fuzzy modeling/control and particle swarm optimization.
Bhat (Bhat and McAvoy, 1990)	Applied backpropagation neural nets for dynamic modeling and control of chemical process systems.

2.3 Decomposition approach

The decomposition approach offers an effective solution strategy and several applications of this approach have been reported in the literature in solving different optimization problems in chemical engineering (for example, design of optimal solvents and solvent mixtures (Karunanithi et al., 2005), process synthesis and intensification (Mansouri et al., 2013) and process control (Hamid et al, 2010).

The main idea in the decomposition-based approach is to decompose the integrated process design and control problem into an ordered set of sub-problems. Each sub-problem, except the last one, requires only the solution of a subset from the original

constraints set. The final sub-problem contains the objective function and the remaining constraints. In this way, the solution of the decomposed set of sub-problems is equivalent to that of the original optimization problem. The advantage is a more flexible solution approach together with relatively easy to solve sub-problems. Recently, a decomposition-based optimization approach is proposed to tackle the integration of process design and controller design for single reactor, single separator and reactor-separator-recycle processes (Alvarado-Morales et al., 2010; Hamid et al., 2010). The main merit of this proposed solution strategy is, based on the reverse approach and thermodynamic-process insights (for example attainable region (D. Hildebrandt and Glasser, 1990) and driving force approach (Gani and Bek-Pedersen, 2000)) to decompose the whole framework into sequential hierarchical sub-problems. There are two points that need to be clarified: First, the resulting final optimal design and control scheme cannot be guaranteed feasibility under parameter/model uncertainties and external disturbances; second, this work does not explicitly consider the closed-loop stability and, consequently, the final design could be unstable. Nonetheless, global optimal solution cannot be guaranteed using this approach.

Here, only a few decomposition algorithms in the area of integration of process design and control that have been proposed are reviewed. Mohideen et al. (1996), proposed a unified decomposition-based process design framework for obtaining integrated process and control systems design based on a dynamic mathematical model describing the process, including path constraints, interior and end-point constraints, a model that describes uncertain parameters and time-varying disturbances and a set of process design and control alternatives. Kookos and Perkins (2001) developed an algorithm based on the systematic generation of lower and upper bounds on the best achievable dynamic economics of the combined plant to effectively reduce the size of the search space. Sanchez-Sanchez and Ricardez-Sandoval (2013) proposed a methodology that includes process synthesis and control structure decisions for the optimal process and control design of dynamic systems under uncertainty. The key feature introduced by this method is the simultaneous evaluation of dynamic flexibility and feasibility for optimal process synthesis and control structure design. Trainor et al. (2013) developed a new simultaneous design and control methodology that accounts for structural decisions in the analysis. Their proposed approach involves an iterative decomposition framework that includes a robust feasibility analysis and a robust asymptotic stability test. Their results illustrated through a case study indicates that their methodology is a suitable tool to simultaneously design and control systems that can maintain dynamically feasibility and asymptotically stability in the presence of critical time-dependent realizations in the disturbances. Pistikopoulos and Diangelakis (2015), raised the concern that while significant progress has been achieved over the years at the moment there is not a generally accepted methodology and/or “protocol” for integrated process design, control and scheduling, also currently, there is not a commercially available software [or even in a prototype form] system to fully support such an activity. They presented the foundations for such an integrated framework and especially a software platform that enables such integration based on research developments. They particularly emphasized on PAROC, a prototype software system which allows for the

representation, modeling and solution of integrated design, scheduling and control problems.

The feasible solutions to integrated process design and control problem may be located in a relatively small region of the search space. This is due to the large number of constraints involved. Therefore, the capability of solving such a problem largely falls into the effectiveness of the solution strategy and locating the feasible solutions (one of these solutions is the optimal solution).

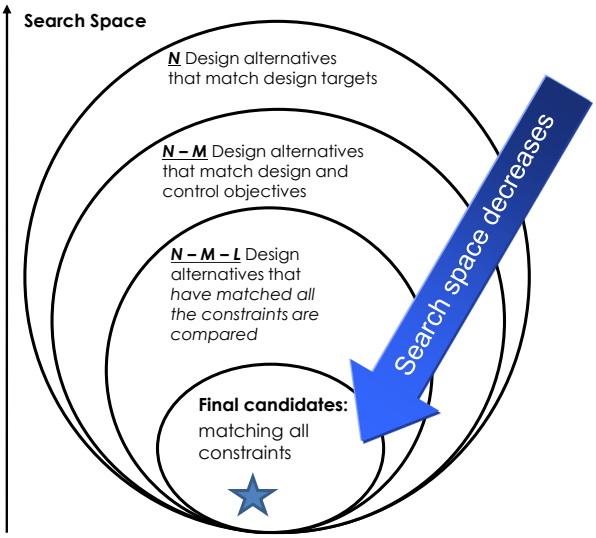

Figure 2.1 Onion diagram showing that the number of solutions is reduced after each sub-problem.

Thus, one approach as an alternative to solve a dynamic optimization (or an embedded control optimization) and in order to manage the complexity is using a decomposition-based solution strategy. In this approach, the problem is decomposed into a set of sub-problems that are solved according to pre-defined calculation order. In this way, after every sequential sub-problem, the search space for feasible solutions is reduced and a sub-set of design-manipulated and/or decision variables are fixed.

When all the constraints are satisfied, it remains to calculate the objective function for all the identified feasible solutions to locate the optimal solution. This leads to a problem that is significantly smaller and can be solved more easily. Therefore, while the sub-problem complexity may or may not increase with every subsequent stage, the number of feasible solutions is reduced after each stage. Figure 2.1 shows a schematic diagram of how the integrated process design and control can be tackled using a decomposition-based solution strategy.

The application of model predictive control (MPC) has been scarcely addressed in the literature on the integrated process design and control. Note however, there are a few decomposition-based works that have looked at this in the literature which are also briefly reviewed here. Francisco et al. (2011) proposed a methodology for the simultaneous design of processes with linear MPC, providing simultaneously the plant dimensions, the control system parameters and a steady state working point. They illustrated the application of their methodology on the activated sludge process of a wastewater treatment plant. Bahakim and Ricardez-sandoval (2014) proposed a methodology based on stochastic simultaneous design and control for chemical processes under uncertainty. They also proposed an optimization framework to obtain a feasible and stable process design in presence of stochastic disturbances. Advanced model-based control schemes such as MPC were also used. Their stochastic-based methodology represents a practical approach to address the integration of design and control while using advanced model-based control strategies such as MPC.

Even though the decomposition approach offers an effective solution strategy and several applications of this approach have been reported in the literature in solving different optimization problems in chemical engineering (for example, design of optimal solvents and solvent mixtures (Karunanithi et al., 2004), sustainable process design (Carvalho et al., 2008), process flowsheet design and reverse approach (Anterroches and Gani, 2006), process synthesis and intensification (Mansouri et al., 2013)) no methodology based on the decomposition-based approach, beside the ones mentioned above, has been reported for solving the integrated process design and control problems. Therefore, there is a need for a decomposition-based methodology to solve the IPDC problem and to facilitate its application in practice.

3
CONCEPTS AND THEORIES FOR INTEGRATED PROCESS DESIGN AND CONTROL

In this chapter, the concepts and theories that are being used in this work will be elaborated. These concepts and their associated theory will be later embedded in the various stages of the integrated process design and control methodology.

First, the chemical and physical equilibrium concept with be explained together with relevant mathematical information to guide the reader in better understanding this concept. Furthermore, the element-based method which is based on the chemical and physical equilibrium concept is elaborated. Second, the driving force concept for designing reactive and non-reactive separation processes will be discussed. Driving force approach is a method of distillation process design that its objective is to achieve the design at the maximum available driving force for separation of a given mixture (reactive or non-reactive). Finally, the driving force based integrated process design and control is presented. That is, from a process design point of view optimal/near optimal design in terms of energy consumption is obtained at the highest driving force; and from a controller design point of view, the best controller structure and set-point values for controlled and manipulated variables are obtained at this point. Therefore, with an analytical analysis it is demonstrated that at the maximum driving force is, the sensitivity of the controlled variables to disturbances is the lowest and at the same time, the sensitivity of controlled variables to manipulated variables (actuators) is the highest.

3.1 The chemical and physical equilibrium and element-based method

This concept is derived from chemical model theory, where the equations of chemical equilibrium together with any appropriate physical model yielding the chemical potentials are embedded into an element-based model (called the chemical model) (Michelsen, 1994). The solution of the chemical model equations together with the condition of equilibrium (equality of the component chemical potentials in all co-existing phases) provides the element phase compositions for the reactive system. One attractive feature of this concept is its capability to handle the problem of reactive-phase equilibrium in the same manner as the case when no reactions are taking place in the system. That is, this approach reduces the chemical and physical equilibrium problem to an identical physical equilibrium problem for a mixture of elements representing the system.

3.1.1 Thermodynamic fundamentals

For a system with *NP* phases and *NC* chemical species, the fundamental thermodynamic relation is given by the Gibbs free energy as:

$$G = G\left(T, P, n_i^{\beta}\right) \tag{3.1}$$

where n_i^{β} (i = 1,2,...,*NC*; β = 1,2,..,*NP*) represents the number of moles of species i in phase β. The Gibbs free energy is an extensive property, proportional to the amount of material in the system. From Euler's theorem on homogeneous functions one readily has that:

$$G = \sum_{\beta=1}^{NP}\sum_{i}^{NC} \mu_i^{\beta} n_i^{\beta} \tag{3.2}$$

where the chemical potential μ^{β}_i is defined to be:

$$\frac{\partial G}{\partial n_i^{\beta}} = \mu_i^{\beta}\left(T, P, n_j^{\beta}\right) \tag{3.3}$$

and it is a homogeneous function of degree zero in n_j^{β}; that is, μ^{β}_i is an intensive property. The total differential of G from Eq. (3.1) is given by:

$$dG = \left(\frac{\partial G}{\partial T}\right)_{P,n} dT + \left(\frac{\partial G}{\partial P}\right)_{T,n} dP + \sum_{\beta=1}^{NP}\sum_{i=1}^{NC}\left(\frac{\partial G}{\partial n_i^{\beta}}\right)_{T,P} dn_i^{\beta} \tag{3.4}$$

for fixed T and P, Eq. (3.4) is reduced to:

$$dG = \sum_{\beta=1}^{NP}\sum_{i=1}^{NC}\left(\frac{\partial G}{\partial n_i^{\beta}}\right)_{T,P} dn_i^{\beta} = \sum_{\beta=1}^{NP}\sum_{i=1}^{NC} \mu_i^{\beta} dn_i^{\beta} \tag{3.5}$$

The total differential of G from Eq. (3.3) is given by:

$$dG = \sum_{\beta=1}^{NP}\sum_{i=1}^{NC} \mu_i^{\beta} dn_i^{\beta} + \sum_{\beta=1}^{NP}\sum_{i=1}^{NC} n_i^{\beta} d\mu_i^{\beta} \tag{3.6}$$

Combining Eqs. (3.5) and (3.6) gives the well-known Gibbs-Duhem equation (Jenkins, 2008). When the Gibbs function is used to describe a thermodynamic system, the condition for thermodynamic equilibrium of a closed system is defined as the state for which the total Gibbs free energy attain its minimum with respect to all possible changes at the given *T* and *P*.

$$0 = \sum_{\beta=1}^{NP}\sum_{i}^{NC} n_i^{\beta} d\mu_i^{\beta} \tag{3.7}$$

This can be formulated mathematically as

$$\min G = \sum_{\beta=1}^{NP}\sum_{i=1}^{NC} \mu_i^{\beta} n_i^{\beta} \tag{3.8}$$

s.t

$$\sum_{\beta=1}^{NP}\sum_{i=1}^{NC} A_{ji} n_i^{\beta} - b_j = 0 \qquad j = 1,2,..,M \tag{3.9}$$

In the above equations, *G* as it is described by Eq. (3.1) is the total Gibbs free energy of a system that has *NC* species and *NP* phases. Eq. (3.9) represents the *M* independent element mass balances, where the coefficients A_{ji} denote to the number of elements *j* in molecule *i* in the reaction mixture. The formula matrix $\boldsymbol{A}$ as a full rank matrix of $M \times NC$ elements and b_j is the total number of moles of element *j* in the system. Note that, the total number of independent elements (*M*), (they may be atoms, molecules or groups) is smaller than the number of components (*NC*) in the reactive system. The solution of the constrained optimization problem represented by Eqs. (3.8) and (3.9) is obtained through the Lagrange multiplier formulation. The corresponding Lagrangian function $\hat{L}$ is defined as follows and Further details can be obtained from Pérez-Cisneros (1997).

$$\hat{L} = \sum_{\beta=1}^{NP}\sum_{i=1}^{NC} \mu_i^{\beta} n_i^{\beta} - \sum_{j=1}^{M} \lambda_j \left(\sum_{\beta=1}^{NP}\sum_{i=1}^{NC} A_{ji} n_i^{\beta} - b_j \right) \tag{3.10}$$

3.1.2 Phase rule for reacting systems

An important aspect in the computation of the chemical-physical equilibrium is the correct characterization and identification of the reactive system. This characterization must be carried out by using the phase rule for reactive systems. In addition to Eq. (3.8) and (3.9) there are equations of chemical equilibrium of the form:

$$\sum_{i=1}^{NC} Z_{ij} \mu_i^{\beta} = 0 \qquad j = 1,2,..,NR \tag{3.12}$$

Where Z_{ij} are the stoichiometric coefficients and *NR* is the number of independent chemical reactions. In some cases, there may be stoichiometric constraints which apply and therefore provide additional equations (for example, the requirement of electrical neutrality in a system of electrolytes). The number of these constraints will be *S*. The total number of equations involving intensive variables for a two phase system is: (*NC* +2) (*NP*-1) + *NR* +*S*. The degree of freedom for the equilibrium system is given as follows:

$$F = (2 + NC) - (NP + NR + S) \tag{3.12}$$

This is the phase rule for a reacting system at equilibrium (Pérez-Cisneros, 1997). The phase rule for a nonreactive system with N*C* species and *NP* phases is given as:

$$F = 2 + NC - NP \tag{3.13}$$

Thus, comparing Eqs. (3.12) and (3.13), it is observed that these equations can be written as follows, taking into account the number of elements in a given system:

$$F = 2 + M - NP \tag{3.14}$$

Therefore, the number of elements in a reactive system is identified by the following:

$$M = NC - NR - S \tag{3.15}$$

Thus, this reactive system could always, in principle, be obtained from its *M* independent constituent *elements*. To determine *M*, it is clear that, if the number of components (*NC*) and the number of independent chemical reactions (*NR*) are known, the number of independent elements *M* is simply obtained from Eq. (3.15).

3.1.3 Equilibrium Conditions

In order to explain the chemical and physical equilibrium concept, only chemical and physical equilibrium for $\beta = 1$ (a single phase). For simplicity, the superscript β in Eq. (3.2) is omitted. This discussion has been originally made by Pérez-Cisneros (1997).

Together with the stationary point conditions (Pérez-Cisneros, 1997), into Eq. (3.2) the following Gibbs free energy equation at equilibrium is obtained:

$$G_{eq} = \sum_{i=1}^{NC} n_i \mu_i = \sum_{i=1}^{NC} n_i \left(\sum_{j=1}^{M} A_{ji} \lambda_j \right) = \sum_{j=1}^{M} b_j \lambda_j \tag{3.16}$$

The relationship between the vector **λ** (Lagrange multiplier) and the vector ***b*** (element composition) is identical to the relationship between vector ***n*** (molar composition) and the vector **μ (**chemical potential). Thus, a completely consistent thermodynamic representation of a phase at chemical equilibrium is obtained in terms of ***b*** as the (element) composition vector and **λ** as the corresponding element potential vector. This description can be extended to a system consisting *NP* number of phases; for more details, interested reader can refer to Pérez-Cisneros (1997).

One exciting feature of the chemical model approach is that the equations are identical to the set of equations being used to solve a non-reactive phase equilibrium problem. This implies that the same computational methods and tools can be used for reactive systems in the same way as for non-reactive systems. Furthermore, it has the potential to define element mole fractions similar to mole fractions on a compound basis for non-reactive systems. The total element amount in any phase β is given as follows:

$$b_T^\beta = \sum_{j=1}^{M} b_j^\beta \tag{3.17}$$

then the element "mole" fractions are given as

$$W_j^\beta = \frac{b_j^\beta}{b_T^\beta} = \frac{b_j^\beta}{\sum_{k=1}^{M} b_k^\beta} \tag{3.18}$$

3.1.4 Element selection

It is clear that the choice of elements plays a significant role in the current formulation. The elements can be selected as the constituent chemical elements (*NE*) that are present in a given reaction mixture. However, there is always the possibility to choose a fragment of a reactant as an element. Therefore, from the discussion in the previous sections, it is readily known how to determine the number of elements in a reaction mixture. Here we classify the element mixtures into two categories: (i) binary element systems which are the reactive systems that can be represented by two elements, and (ii) multi-element systems which are the systems that are represented by more than two elements. Below, these categories are illustrated through two examples.

Example 3.1: Binary element system

Consider the following reaction which is the reaction between formaldehyde (CH_2O) and water (H_2O) to produce methylene glycol ($HOCH_2OH$) and the further polymerization of methylene glycol to polyoxymethylene ($HO(CH_2O)_2$). The reaction scheme considering only the first polymerization reaction is as follows (Albert et al., 1996):

$$CH_2O + H_2O \rightarrow HOCH_2OH$$

$$2HOCH_2OH \rightarrow HO(CH_2O)_2 + H_2O$$

Using equation (3.17), it is known that there are four compounds and two reactions. Therefore, the above reaction system can be represented in terms of two *elements*, **A** (formaldehyde) and **B** (water) by the following reactions:

$$A + B \rightarrow AB$$

$$2(AB) \rightarrow A_2B + B$$

Consequently, the element matrix is written as follows where the columns are elements and the rows are compounds:

Compound	CH_2O	H_2O	$HOCH_2OH$	$HO(CH_2O)_2$
Element				
A (CH_2O)	1	0	1	2
B (H_2O)	0	1	1	1

Example 3.2: Multi-element systems

The production of ethyl acetate ($CH_3COOC_2H_5$) by the esterification of acetic acid (CH_3COOH) with ethanol (C_2H_5OH) has the following reaction scheme where water (H_2O) is also produced as a byproduct:

$$CH_3COOH + C_2H_5OH \rightarrow H_2O + CH_3COOC_2H_5$$

There are four compounds and one reaction. Therefore, the above reaction system can be represented in terms of two *elements*, **A** (C_2H_2O), **B** (C_2H_5OH) and **C** (H_2O) by the following reactions:

$$AC + B \leftrightarrow AB + C$$

Similarly, the element matrix is constructed as follows:

Compound	CH_3COOH	C_2H_5OH	H_2O	$CH_3COOC_2H_5$
Element				
A (C_2H_2O)	1	0	0	1
B (C_2H_5OH)	0	1	0	1
C (H_2O)	1	0	1	0

3.1.5 Equivalent binary elements

Looking at Example 3.1, it is also possible to represent a multi-element system in terms of equivalent binary elements (Jantharasuk et al., 2011). The key elements are noted as the binary elements (light key element (LK) and heavy key element (HK)). One can assign any pair of elements (or compounds) as LK and HK, with the lower boiling compound in the pair being the LK and the heavier boiling compound in the pair being the HK. For all other non-key compounds, those that have lower boiling points are therefore lighter than the light key and go with the LK, while those that have higher boiling points are heavier than the HK and go with the HK compound. This representation is similar in concept to the method of distillation design for a non-reactive multicomponent system proposed by (Hengstebeck, 1961). Note that LK and HK are selected according to the rules of key element selection given by Jantharasuk *et al*. (2011). It is well-known that the sum of mole fractions is always equal to 1. Therefore, it is also the case when the mole fractions are given in terms of elements. Thus, the sum of mole fractions in a multi-element system is as follows:

$$W_{LK}^{\beta} + W_{HK}^{\beta} + W_{LNK}^{\beta} + W_{HNK}^{\beta} = 1 \tag{3.19}$$

Having the above summation, now one can represent the multi-element system in a new composition domain termed as "equivalent binary element composition" as follows (Jantharasuk et al., 2011):

$$W_{eq}^{\beta} = W_{LK}^{\beta} + W_{HK}^{\beta} = 1 - \sum \left(W_{LNK}^{\beta} + W_{HNK}^{\beta} \right) \tag{3.20}$$

where, the light key equivalent element composition is given as follows:

$$W_{LK,eq}^{\beta} = \frac{W_{LK}^{\beta}}{W_{LK}^{\beta} + W_{HK}^{\beta}} \tag{3.21}$$

and the element composition is given as below (Pérez-Cisneros et al., 1997):

$$W_{j}^{\beta} = \frac{\sum_{i=1}^{NC} A_{j,i} x_{i}^{\beta}}{\sum_{i=1}^{NC} \sum_{j=1}^{M} A_{j,i} x_{i}^{\beta}} \tag{3.22}$$

3.2 Driving force concept for reactive and non-reactive separations

The driving force approach is a method to design distillation operations (reactive or non-reactive) which was first proposed by Gani and Bek-Pedersen (Gani and Bek-Pedersen, 2000). Like the McCabe-Thiele method (McCabe and Thiele, 1925) it is based on the graphical representation of vapor-liquid data. However, in this approach, driving force (*DF*), which is a function of vapor and liquid composition is plotted against, liquid (or vapor) composition. It is defined as the difference between two co-existing phases (vapor and liquid) and can only represent binary interaction between compounds (for non-reactive systems) or elements (for reactive systems) in two coexisting phases. Furthermore, Sanchez-Daza et al. (Sánchez-Daza et al., 2003) extended the application of the driving force approach to design of reactive distillation columns. A generic driving force diagram is given in Figure 3.1.

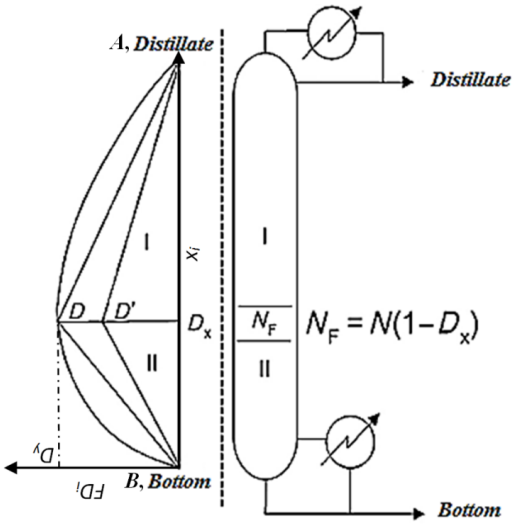

Figure 3.1 Driving force based design of distillation columns – on the left is the driving force diagram and on the right is the corresponding design of the reactive distillation column (adapted from Babi and Gani (Babi and Gani, 2014)).

To date, driving force approach has been applied in numerous process synthesis (Babi et al., 2014; Tula et al., 2015), design (Bek-Pedersen and Gani, 2004; Bek-Pedersen et al., 2000; Gani and Bek-Pedersen, 2000; Sánchez-Daza et al., 2003) and process control (Alvarado-Morales et al., 2010; Hamid et al., 2010; Mansouri et al., 2015) applications. This approach is very well established as a powerful and simple method for design of separation operations, with or without reactions, that results in optimal/near optimal separation designs both in terms of energy consumption, control and operation when the process is designed at the maximum driving force.

The driving force is defined as the difference in composition of a specific element (equivalent element or compound) between two co-existing phases. Note however, although the driving-force diagram is plotted for a binary pair of elements or compounds, since all separation tasks are performed for specific binary pairs of compounds (or elements or equivalent elements), this concept can be applied also to multi-compound mixtures as well. Also, the separation of a mixture of *NC* compounds would need *NC*-1 separation tasks and therefore, *NC*-1 binary pairs of driving forces are involved for each separation task (Gani and Bek-Pedersen, 2000). Note that the element-based reactive driving-force diagram fully considers the extent of reaction on an element basis, and in this work it is applied in the design of reactive distillation columns for chemical equilibrium or kinetically controlled reactions (Michelsen, 1994).

This approach provides the basis for the determination of important reactive distillation column design variables in terms of two parameters, the location and the size of the maximum driving force, D_x and D_y, respectively. The feed stage location (N_F) and the minimum reflux ratio, *RR* (and/or the reboil ratio, *RB*) are determined from these two parameters for a given feed and product specification. A driving force diagram together with the distillation design parameters is given in Figure 3.2.

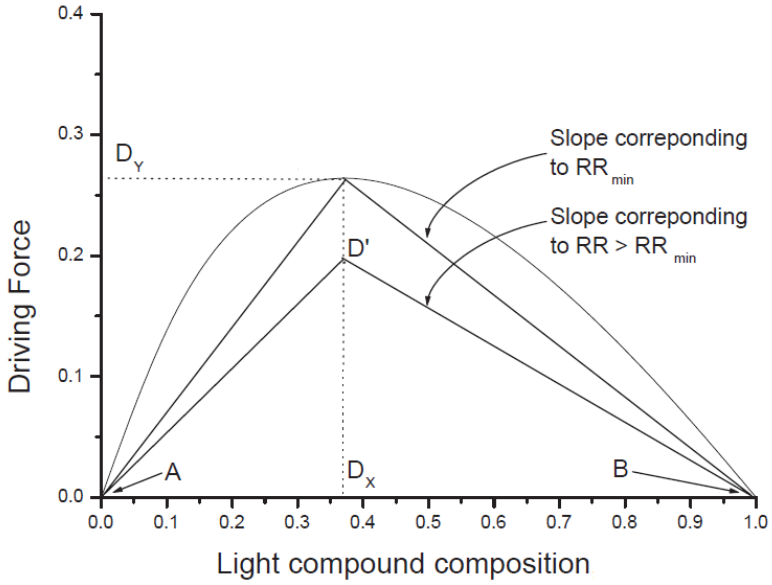

Figure 3.2 A Driving force diagram with the important distillation design parameters (Bek-Pedersen and Gani, 2004).

In this work, first principle thermodynamics are employed to demonstrate that the driving force, *DF*, has concrete thermodynamic basis and to this end it is shown how it is obtained with thorough mathematical and thermodynamic analysis for both non-reactive and reactive driving force (based on elements).

3.2.1 Driving force definition from a thermodynamic perspective

The internal energy of a system is defined by the following equation:

$$U = TS - PV + \sigma\wp + \sum_i \mu_i n_i + \psi q \tag{3.23}$$

The term *TS* represents the heat and all the other terms are the ones that represent various forms of the internal energy associated with work done on the system. The term $\sigma\wp$ is important in small systems where the ratio of the surface area to the volume becomes large. The next term, contributes to the potential of a nucleus; and the last term, contributes to chemical potential of a charged molecule.

Eq. (3.23) is fundamental and it is the sum of the products of an extensive property and its conjugated intensive property. The conjugated intensive property is the partial derivative of the internal energy with respect to the extensive variable. Extensive and conjugated intensive variables of the internal energy are given Table 3.1.

Table 3.1 Extensive and conjugated intensive variables of the internal energy

Extensive property		**Conjugated intensive property**	
S	Entropy	T	Temperature
V	Volume	$-P$	Pressure
$\wp$	Surface area	σ	Surface tension
$\boldsymbol{n_i}$	Number of moles	μ_i	Chemical potential
q	charge	ψ	Electrical potential

If a homogeneous system is not at equilibrium, gradients in the intensive variables exist. These gradients will give rise to transport of extensive properties because a gradient in an intensive property is a driving force of flow of its conjugated extensive property. That is, diffusion is not caused by gradients in the compositions but by gradients in the chemical potentials. When the surface area energy contributes little to the internal energy and the system carries no charges, one can simplify eq. (3.23) to the form given by eq. (3.24):

$$U = TS - PV + \sum_i \mu_i n_i \tag{3.24}$$

3.2.2 Driving force and equilibrium

Equilibrium is a consequence of the second law of thermodynamics and it corresponds to a condition that an isolated system will approach equilibrium by increasing its entropy and that the equilibrium state is a stationary point of maximum entropy. Given that the isolated system consists of several phases (reactive or not), and that the individual phases are considered as open systems that can exchange energy, work and matter with one another; then the extensive independent properties *U*, *V* and *n* at equilibrium are subject to the following constraints:

$$\sum_{j}^{NP} dU^{j} = 0 \tag{3.25}$$

$$\sum_{j}^{NP} dV^{j} = 0 \tag{3.26}$$

$$\sum_{j}^{NP} dn_{i}^{j} = 0 \qquad i = 1, \ldots, NC \tag{3.27}$$

Where i denotes to the individual components i = 1, ... , NC and j the individual phases j = 1 , … , NP. There are thus NP (NC + 2) independent variables and NC + 2 constraints. The following differential equation relates changes taking place between equilibrium states in an isolated system. This is obtained by solving eq. (3.24) for gradients of extensive variables of the internal energy.

$$dS = \frac{1}{T} dU + \frac{P}{T} dV - \frac{1}{T} \sum_{i} \mu_{i} dn_{i} \tag{3.28}$$

Now, one can express the condition of equilibrium as follows:

$$dS = \sum_{j}^{NP} \frac{dU^{j}}{T^{j}} + \sum_{j}^{NP} \frac{P^{j}}{T^{j}} dV^{j} - \sum_{j}^{NP} \sum_{i}^{NC} \frac{\mu_{i}^{j}}{T^{j}} dn_{i}^{j} = 0 \tag{3.29}$$

In the above equations, the independent variables are subject to the constraints given by eqs. (3.25)-(3.27). These constraints can be removed by considering the independent variables of one of the phases, given phase β, as dependent variables. When the sum of the changes of the extensive variables is zero, one can express the changes of the extensive properties of phase α in this way:

$$dU^{\beta} = -\sum_{\beta \neq j}^{NP} dU^{j} \tag{3.30}$$

$$dV^{\beta} = \sum_{\beta \neq j}^{NP} dV^{j} \tag{3.31}$$

$$dn_{i}^{\beta} = \sum_{\beta \neq j}^{NP} dn_{i}^{j} \qquad i = 1, \ldots, NC \tag{3.32}$$

One can now replace the changes of the dependent variables, the extensive properties of phase β, in Eq. (3.29) with the expressions in Eqs. (3.30)-(3.32). Therefore, an equation where all extensive variables are independent variables is obtained as follows:

$$\sum_{\beta \neq j}^{NP} \left(\frac{1}{T^{j}} - \frac{1}{T^{\beta}} \right) dU^{j} + \sum_{\beta \neq j}^{NP} \left(\frac{P^{j}}{T^{j}} - \frac{P^{\beta}}{T^{\beta}} \right) dV^{j} - \sum_{\beta \neq j}^{NP} \sum_{i}^{NC} \left(\frac{\mu_{i}^{j}}{T^{j}} - \frac{\mu_{i}^{\beta}}{T^{\beta}} \right) dn_{i}^{j} = 0 \tag{3.33}$$

In a separation system which is modeled at equilibrium the third term of Eq. (3.33) resembles that chemical potential of the phases are equal, that is $\mu_{i}^{j} = \mu_{i}^{\alpha}$ and $\beta \neq j$ for i = 1, … , NC.

3.2.3 Driving for designing separation operations

In this section, the driving force definition given by Gani and Bek-Pedersen (2000) is derived using equilibrium assumption by first principle thermodynamics.

3.2.3.1 Non-reactive systems

Theorem:

The driving force is defined as the difference in composition of two co-existing phases according to Gani and Bek-Pedersen (2000). Here given the two phases are vapor (*v*) and liquid (*l*) at equilibrium for a binary non-reactive ideal system. The driving force equation is given as follows (Gani and Bek-Pedersen, 2000):

$$DF = y_i - x_i \tag{3.34}$$

Proof:

As it was relayed in the previous section, at equilibrium, the chemical potential of all phases are equal. Therefore the following condition applies:

$$\mu_i^v = \mu_i^l \tag{3.35}$$

This means that the chemical potential at the vapor phase is equal to the chemical potential at liquid phase. Now we write the equations of the chemical potential at each phase based on Gamma-Phi approach:

$$\mu_i^v = \mu_i^\circ + RT\ln\left(y_i\varphi_i\right) + RT\ln\left(P\right) \tag{3.36}$$

$$\mu_i^l = \mu_i^\circ + RT\ln\left(x_i\gamma_i\right) + RT\ln\left(P^{sat}\right) \tag{3.37}$$

Therefore, further simplification of the above equations gives the following:

$$y_i\varphi_i P = x_i\gamma_i P_i^{sat} \tag{3.38}$$

Thus,

$$\ln\left(y_i\varphi_i P\right) = \ln\left(x_i\gamma_i P_i^{sat}\right) \tag{3.39}$$

Also,

$$y_i = \left(\frac{P_i^{sat}}{P}\right)\left(\frac{\gamma_i}{\varphi_i}\right)x_i \tag{3.40}$$

and,

$$DF = y_i - x_i = \left(\frac{P_i^{sat}}{P}\frac{\gamma_i}{\varphi_i} - 1\right)x_i \tag{3.41}$$

or given that the relative volatility of a mixture is given as $\alpha_{ij} = \frac{y_i / x_i}{y_j / x_j} = \frac{y_i (1 - x_i)}{x_i (1 - y_i)}$; by isolating y_i and replacing that in the driving force definition, the following equation for driving force in terms of relative volatility is obtained.

$$DF = y_i - x_i = \frac{x_i \alpha_{ij}}{1 + x_i (\alpha_{ij} - 1)} - x_i \tag{3.42}$$

Therefore, from a process design point of view, the maximum driving force needs to be identified in (P, T, x) domain as it is discussed in the introduction of section 3.2.

3.2.3.2 Reactive systems

The driving force is defined as the difference in composition of two co-existing phases in a reactive system. Here given the two phases are element (or equivalent element) vapor (v) and liquid (l) phases at equilibrium for a binary element (or equivalent element) reactive ideal system. Therefore, the driving force equation is given as follows (Sánchez-Daza et al., 2003) for a reactive system:

$$DF = W_i^v - W_i^l = \frac{W_i^l \alpha_{ij}}{1 + W_i^l (\alpha_{ij} - 1)} - W_i^l \tag{3.43}$$

For a reactive system, similar to a non-reactive system, from a process design point of view, the maximum driving force needs to be identified in (P, T, W) domain as it is discussed in the introduction of section 3.2.

3.3 Driving force and Gibbs free energy

The driving force concepts have a distinct relationship with Gibbs free energy, that as the maximum value of the driving force, the excess Gibbs free energy is either maximized or minimized (depending on activity coefficients of a system). This depends on the properties of the system under consideration. In order to demonstrate this relationship the benzene-toluene binary system is considered. A gamma-phi approach is used, where the UNIFAC model is employed to calculate liquid phase behavior and Peng-Robinson EoS is for calculating vapor phase behavior.

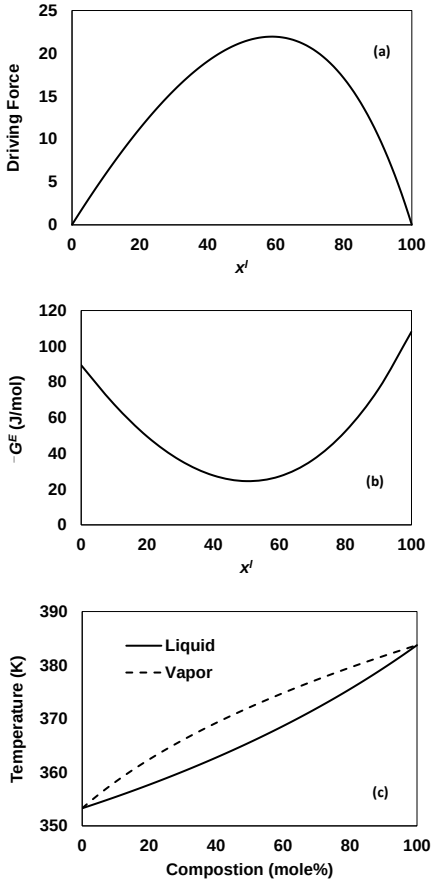

Figure 3.3 (a) driving froce diagram based on the light component – benzene; (b) corresponding excess Gibbs free energy diagram; and (c) *T-x-y* for benzene. All diagrams are isobaric and 1 atm.

In the benzene-toluene binary pair, benzene has the lower boiling point. Therefore, the driving force calculations are based on benzene. In order to calculate the excess Gibbs free energy (G^E) for each of the points on the *T-x-y* diagram that are at

equilibrium, the activity coefficient are obtained and G^E is calculated through the following equation (Reddy et al., 2012):

$$G^E = RT\left(x_1 \ln \gamma_1 + x_2 \ln \gamma_2\right) \tag{3.44}$$

Figure 3.3a shows the driving force diagram and Figure 3.3b shows the corresponding excess Gibbs free energy diagram while Figure 3.3c, shows the *T-x-y* diagram for the benzene-toluene system at 1 atm. It is well-known that every point on this driving force diagram or *T-x-y* diagram is at equilibrium and therefore, each equilibrium point at its minimum Gibbs free energy. Therefore, what Figure 3.3b reveals is that at the maximum driving force an optimal/near optimal point exists in terms of excess Gibbs free energy. Thus, the design obtained at the maximum driving force very well satisfies the conditions to guarantee an optimal and/or near optimal solution.

3.4 Driving force based integrated design and control

The integrated process design and control is explained conceptually through the use of a process model represented by balance equations (mass, energy and momentum), constitutive equations (phenomena models usually as a function of intensive variables) and conditional equations (equilibrium, controller and defined relations). In a generic form, the model equations are given by,

$$D = f\left(x, y, u, d, \theta, t\right) \tag{3.45}$$

Where $D = dx/dt$ for dynamic model and $D = 0$ for steady-state model.

Constitutive equations:

$$\theta = g_1\left(u, x, y\right) \tag{3.46}$$

Conditional equations:

$$0 = g_2\left(u, x, y, d, \delta\right) \tag{3.47}$$

In Eqs. (3.45)-(3.47), y is a vector of Ny output-controlled variables; d is a vector of Nd feed stream-disturbance variables, u is a vector of Nu design-manipulated variables; θ is a vector of constitutive variables; x is a vector of Nx process-state variables and δ is vector of $N\delta$ controller parameters (needed for example, in closed-loop simulation of the process).

From a driving force based process design point of view, for specified inputs of design variables (u) and disturbances in feed stream variables (d), values for process variables (x)and output variables (y) that satisfy a set of design specifications (process design objectives) are determined at the maximum driving force. In this case x and y also define some of the operational conditions for the process. That is, values of variables d and u should be such that the desired process specifications (targets) of x and y are obtained, giving a feasible design. From multiple sets of values for these variables, the optimal design is found.

From a driving force based controller design point of view, for any changes in *d* and/or set point values in *y*, values of *u* that restores the process to its optimal designed condition are determined corresponding to the maximum driving force. That is, to maintain *x* and *y* at their target values for a disturbance in *d*, *u* needs to be manipulated; or keeping *d* fixed for a change in set-point for *y*, *u* needs to be changed. Therefore, process design and control work with the same set of variables and the issue is how to select these variables (controller structure) and their values (design) (Russel et al., 2002). It should be noted that the solution for *x* and *y* is directly influenced by θ (the constitutive variables such as reaction rate, equilibrium constant or driving force). Consider the case where *y*, *u*, and *d* are vectors of size two, while θ and *x* are scalers. The sensitivities of the controlled variables with respect to disturbances is given by the following equation,

$$\frac{dy}{dd} = \begin{bmatrix} \frac{dy_1}{dd_1} & \frac{dy_2}{dd_1} \\ \frac{dy_1}{dd_2} & \frac{dy_2}{dd_2} \end{bmatrix} \tag{3.48a}$$

Similarly, the sensitivities of the controlled variables with respect to the manipulated variables is given by,

$$\frac{dy}{du} = \begin{bmatrix} \frac{dy_1}{du_1} & \frac{dy_2}{du_1} \\ \frac{dy_1}{du_2} & \frac{dy_2}{du_2} \end{bmatrix} \tag{3.48b}$$

Note that the constitutive Eq. (3.46), relates θ to *x* (and *y*) and therefore, by integrating design-control of the process through the characteristics of θ with respect to θ to *x* (and *y*) allows the calculation of the sensitivities of the controller sensitivity Eqs. (3.48a)-(3.48b) through the following:

$$\begin{bmatrix} \frac{dy_1}{dd_1} & \frac{dy_2}{dd_1} \\ \frac{dy_1}{dd_2} & \frac{dy_2}{dd_2} \end{bmatrix} = \begin{bmatrix} \left(\frac{dy_1}{d\theta}\right)\left(\frac{d\theta}{dx}\right)\left(\frac{dx}{dd_1}\right) & \left(\frac{dy_2}{d\theta}\right)\left(\frac{d\theta}{dx}\right)\left(\frac{dx}{dd_1}\right) \\ \left(\frac{dy_1}{d\theta}\right)\left(\frac{d\theta}{dx}\right)\left(\frac{dx}{dd_2}\right) & \left(\frac{dy_2}{d\theta}\right)\left(\frac{d\theta}{dx}\right)\left(\frac{dx}{dd_2}\right) \end{bmatrix} \tag{3.49a}$$

$$\begin{bmatrix} \frac{dy_1}{du_1} & \frac{dy_2}{du_1} \\ \frac{dy_1}{du_2} & \frac{dy_2}{du_2} \end{bmatrix} = \begin{bmatrix} \left(\frac{dy_1}{d\theta}\right)\left(\frac{d\theta}{dx}\right)\left(\frac{dx}{du_1}\right) & \left(\frac{dy_2}{d\theta}\right)\left(\frac{d\theta}{dx}\right)\left(\frac{dx}{du_1}\right) \\ \left(\frac{dy_1}{d\theta}\right)\left(\frac{d\theta}{dx}\right)\left(\frac{dx}{du_2}\right) & \left(\frac{dy_2}{d\theta}\right)\left(\frac{d\theta}{dx}\right)\left(\frac{dx}{du_2}\right) \end{bmatrix} \tag{3.49b}$$

Note that for the separation of a binary mixture, θ is the driving force (a scaler) and it is a concave function with respect to *x* (liquid composition of one compound of the binary pair and so also a scaler). A sample derivation of the terms of Eq. (3.49a)

corresponds to dy_1/dd_1 be given in Example 3.3, for a specific version of the process model and its corresponding constitutive model and conditional equation involving a binary separation. Note that the derivative of driving force as a function of liquid composition is obtained directly from the constitutive model; the derivatives of *y* with respect to driving force and *x* with respect to disturbance variable are obtained from the process model equations (two independent version of the model).

Example 3.3: A sample derivation of the terms of controller sensitivity

Let us consider a feed stream of flowrate F and composition z_f entering a binary distillation column operating at a fixed pressure P. At the top of the column, a liquid product x^D is obtained and at the bottom a liquid product x^B is obtained. Assuming that we have a binary mixture, z_f, x^D and x^B represent the mole fractions of compound 1 (light key compound) in the feed, the top and the bottom product streams, respectively. Note that the mole fractions of compound 2 in these streams can be calculated using the condition equation ($\sum_i^2 x_i = 1$) and therefore, are not independent variables. x^l and y^v are the liquid and vapor mole fractions leaving an equilibrium stage. The equation of the rectifying operating line is given by,

$$y^v = x^D\left[\frac{1}{RR+1}\right] + x^l\left[\frac{RR}{RR+1}\right] \tag{3.50}$$

Subtracting x^l from both sides, gives the following where DF is the driving force:

$$DF = y^v - x^l = x_d\left[\frac{1}{RR+1}\right] + x^l\left[\frac{RR}{RR+1}\right] - x^l \tag{3.51}$$

Rearranging the above equation gives Eq. (3.52):

$$x^D = (RR+1)DF + x^l \tag{3.52}$$

Derivation of dx^D/dDF and dx^l/dF_f :

The component mass balance can also be made for the total column, and inserting Eq. (3.52) into it, gives (F_f is the feed flowrate of compound 1 – it is a disturbance variable).

$$F_f = F \cdot z_f = (RR+1)DF \cdot D + D \cdot x^l + B \cdot x^B \tag{3.53}$$

Eq. (3.53) can be differentiated with respect to driving force (DF) to give:

$$\frac{dx^D}{dDF} = (RR+1) + \frac{dx^l}{dDF} \tag{3.54}$$

Eq. (3.53) can be differentiated with respect to driving force (F_f) to give:

$$1 = D(RR+1)\frac{dDF}{dF_f} + D\frac{dx^l}{dF_f} + B\frac{dx^B}{dF_f} \tag{3.55}$$

Rearranging, gives the following:

$$\frac{1}{B}=\left(\frac{dx^{l}}{dF_{f}}\right)\left(\frac{dDF}{dx^{l}}\right)\left[\frac{D\left(RR+1\right)}{B}\right]+\left(\frac{dx^{B}}{dDF}\right)\left(\frac{dDF}{dx^{l}}\right)+\frac{D}{B} \tag{3.56}$$

Derivation dx^{l}/dDF *:*

Note that Eqs. (3.54) – (3.56) need dx^{l}/d*DF*, which is obtained from the equilibrium relation such as,

$$y^{v}=\frac{x^{l}\alpha}{1+x^{l}\left(\alpha-1\right)} \tag{3.57}$$

Subtracting both sides by x^{l}, gives,

$$DF=y^{v}-x^{l}=\frac{x^{l}\alpha}{1+x^{l}\left(\alpha-1\right)}-x^{l} \tag{3.58}$$

Differentiating Eq. (3.58) with respect to x^{l}, gives d*DF*/dx^{l}. Given the measured/controlled variable vector $\mathbf{y} = [x^{D}, x^{B}]$, disturbance vector $\mathbf{d} = [F_f , z_f]$, $\mathbf{x} = [x^{l}]$ and $\theta = [DF]$, one by setting $y_1 = x^{D}$; $d_1 = F_f$; $x = x^{l}$ and $\theta = DF$, it is possible to use Eqs. (3.54) and (3.55) or (3.57) and the derivative of Eq. (3.58) to obtain the right hand side of Eq. (3.48a). Similarly, the right hand side of Eq. (3.48b) can also be obtained. Note that Eqs. (3.52), (3.53) and (3.54) are derived as a function of driving force, *DF*. The detailed derivation for a binary distillation system involving methanol-water is provided as an appendix.

It should be noted that at the maximum driving force, the largest difference between vapor phase and liquid phase compositions is achieved. As the driving force approaches zero, separation of the corresponding key component/element *i* from the mixture becomes difficult, while, as the driving force approaches a maximum, the energy necessary to maintain the two-phase system is a minimum and the separation is the easiest. This is because the driving force is inversely proportional to the energy added to the system to create and maintain the two-phase (vapor–liquid) system. Thus, the process design corresponding to the driving force at the location of its maximum, integrates design and control.

This concept is illustrated through representation of a dynamic process system in Figure 2. The optimal solution for *x* (states) and *y* (outputs can be obtained at the maximum point of the reactive driving force (see diagram which is based on θ (the constitutive variables), *t* is the independent variable (usually time) and δ is a controller parameter. The steady state model is obtained by setting $D = 0$ in Eq. (3.45). Otherwise, Equations (3.45)–(3.47) represent a dynamic model with a system of differential algebraic equations (DAEs). By using model analysis applied to these equations, the corresponding derivative information with respect to *x*, *y*, *u*, *d* and θ are obtained (to satisfy controller design objectives).

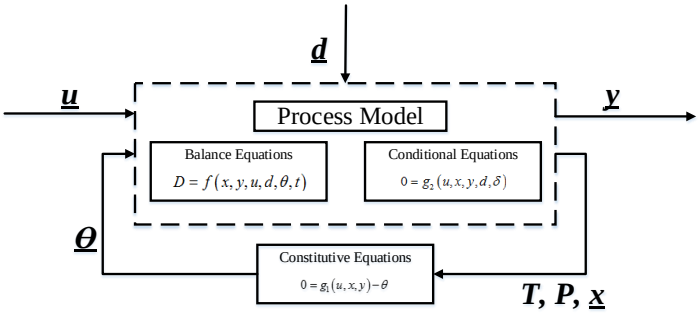

Figure 3.4 Dynamic process system representation

As stated above, solution of the balance equations for x and y is influenced by θ (the constitutive variables such as equilibrium constant or reaction rate). Also, since x and y are intensive variables, they may be used to formulate problems related to process synthesis, design and control. The analysis of the model equations, classifies the variables in terms of x, y, u, d and θ for integrated design and control problems. This helps the selection of controller structure. Therefore, $d\theta/dx$ indirectly influences the process operation and controller structure selection and/or design. The elements of Eq. (3.48a) or (3.49a) which have the minimum value that is the least sensitivity of controlled variables to disturbances; and the elements of Eq. (3.48b) or (3.49b) which have the highest values, that is the highest sensitivity of the controlled variables to manipulated variables will determine the control structure.

4
METHODOLOGY FOR INTEGRATED PROCESS DESIGN AND CONTROL

In this work, the case where the process flowsheet (reactive distillation process) is known together with the feed and process specifications is considered. The objective is to find the design variables, the operating conditions (including set-points for controlled variables) and controller structure that optimize the steady-state measures (energy consumption) and, simultaneously, a measure of the plant controllability, subject to a set of constraints, which ensure the desired dynamic behavior and satisfy the process specifications. Therefore, an integrated approach is employed where key variables together with their target values that have roles in process-controller design are identified; and, the resulting solution to the optimization problem addresses the trade-offs between conflicting design and control objectives.

The integrated process design and control problem is formulated as a generic mathematical optimization problem (see equations 4.1-4.11) in which a performance objective function in terms of design, control and cost is optimized subject to a set of constraints: process (dynamic and steady state), constitutive (thermodynamic states) and conditional (process-control specifications) models-equations. Eq. (4.1) represents the objective function which includes both the process design and controller design objectives, which can either be maximized or minimized. Eq. (4.2) and Eq. (4.3) define a system of linear and non-linear equations, for example, mass and energy balance (algebraic) equations representing a steady state and dynamic process model, respectively. Eq. (4.4) and Eq. (4.5) represent the physical constraints and design specifications, respectively; and Eq. (4.6), because integration of functions/operations is also included in the process design problem, represents a set of constraints that the reactive distillation process must satisfy. Eqs. (4.7) and (4.8) represent and define the bounds on the design variables, x (real) and decision variables M (binary-integer), respectively, while Eq. (4.9) and Eq. (4.10) represent the

conditional process control constraints whereas Eq. (4.11) defines the controller structure.

$$\min L = \sum_{i=1}^{m}\sum_{j=1}^{n} w_{i,j} J_{i,j} \tag{4.1}$$

s.t.

$$0 = g(x,u,\theta) \tag{4.2}$$

$$\frac{dx}{dt} = f(x,y,d,u,\theta,t) \tag{4.3}$$

$$b^l \le B_1 x + B_2 y \le b^u \tag{4.4}$$

$$h^l \le h(x,y) \le h^u \tag{4.5}$$

$$v^l \le v(x,y) \le v^u \tag{4.6}$$

$$w^l \le u(x,y) \le w^u \tag{4.7}$$

$$M_j \in \{0,1\},\ j = 1,2,...n_y,\ x \ge 0 \tag{4.8}$$

$$0 = h_1(u,x,y) \tag{4.9}$$

$$0 \le h_2(u,x,y,d) \tag{4.10}$$

$$CS = y + uY \tag{4.11}$$

In equations (4.1)-(4.11), x and y are regarded as the set of process variables in process design and as the set of state and/or controlled variables in controller design; they usually represent temperatures, pressures and compositions. u is the set of design variables (for process design) and/or the set of manipulated variables (for controller design). d is the set of disturbance variables, θ is the set of constitutive variables (physical properties, reaction rates), v is the set of chemical system variables (molecular structure, reaction stoichiometry, etc.) and t is the independent variable (usually time). The optimization problem given by equations (4.1)–(4.11) represents a MINLP problem. This problem can be difficult to solve if the process model consisting of balance, constitutive and process control equations is large and non-linear. In order to manage this complexity, a decomposition based solution approach

where the problem is decomposed into a set of sub-problems that are solved according to pre-defined calculation order has been used in this work. This method is referred to as the decomposition based solution method (Karunanithi et al., 2005b). Most of the sub-problems require bounded solution of a sub-set of equations. The final sub-problem is solved as a much reduced NLP or MINLP. The feasible alternatives are then evaluated using a set of performance related constraints (Eq. (4.5)). For the remaining process alternatives, the objective function (Eq. (4.1)) is calculated and ordered. Thereby, the highest or the lowest values of objective function can be easily identified. If the number of feasible alternatives is too large, the MINLP problem for a reduced size of the vector *y* is solved. Alternatively, a set of NLPs for a fixed set of y can also be solved. This solution could be regarded as the best for specific problem definitions, the selected performance criteria, constraints, and, availability of data, parameters and models. A global optimal solution cannot be guaranteed with this method. In the context of this solution strategy, the solution from the decomposition based method may be used as a very good starting point for the solution of the MINLP problem for the direct solution strategy (solve all equations simultaneously).

The decomposition-based framework proposed in this work consists of five steps: (1) the problem is formulated and the objective function is defined, (2) the number of elements representing the reaction mixture is determined, (3) key light and heavy key elements are identified (4) the reactive distillation column is designed based on key elements using driving force approach, and in the last step (5) dynamic verification of the design is performed. Also, in principle, it should be applicable to any non-reactive distillation process separating a binary or multicomponent mixture. The framework utilizes a number of algorithms for design and control in different steps. The design methods and tools, which are similar in concept to non-reactive distillation design have been derived and implemented in the framework. These methods are based on the element concept. Note that the process design and control objectives are tied together at the maximum driving force. These objectives are evaluated and calculated as the multi-objective performance function. Therefore, if a maximum of the driving force is identified, the design-control goals will always be satisfied. If the system does not have a maximum of the driving force, then the proposed algorithm cannot be applied. The simulations in steps 4 and 5 are carried out to get the quantitative values but the concept of integration guarantees achievement of the design-control goals (as confirmed by the numerical and analytical results). The developed methodology is implemented through a computer-aided decomposition based framework. A set of algorithms have either been developed or employed in order to successfully solve each sub-problem in the framework. By solving each sub-problem, a large number of the infeasible alternatives within the search space are identified and eliminated. This leads to a final sub-problem that is much smaller and can be solved more easily. The concept of driving force (Bek-Pedersen and Gani, 2004; Bek-Pedersen et al., 2000) is used, reactive or non-reactive, to locate the optimal solution for the integrated process design and control, being the optimal operating point for an intensified process from both design and control points of view. Figure 4.1 illustrates the work-flow implemented in the computer-aided framework for integrated process design and control of reactive distillation processes. The detailed description of each step of the framework is given in the rest of this chapter.

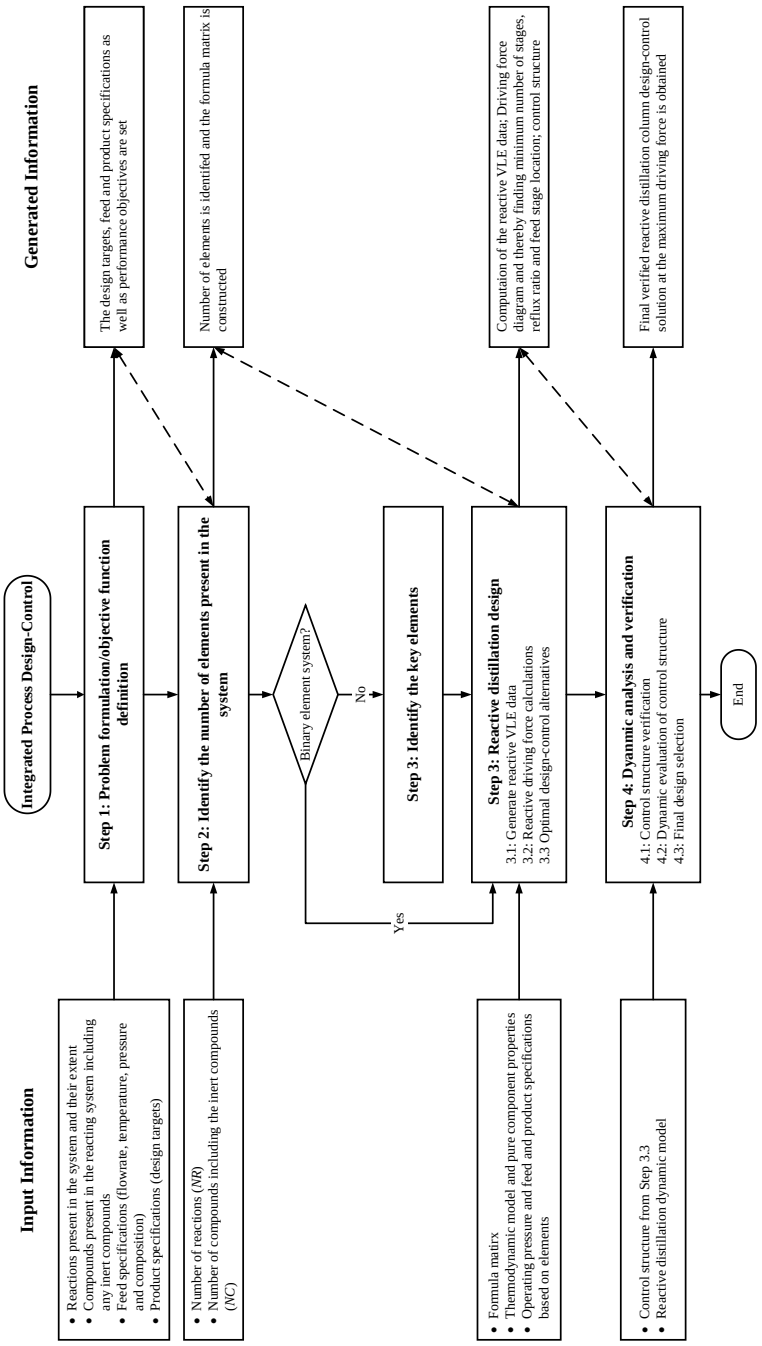

Figure 4.1 Framework for integrated process design and control of reactive distillation processes

4.1 Step 1: Problem formulation/objective function definition

The data/information on raw materials, products, catalysts, reaction conversions, and feed conditions (temperature, pressure, and composition) is collected in this step. Note that, this step starts after a decision to use a RDC has been made. Here, design targets and product specifications are given. Furthermore, the objective function which is to be maximized or minimized from both design and control perspectives is defined in this step. The objective function may be in the form of a weighted multi-objective function or a set of process design and control performance metrics which are to be maximized or minimized. Examples of such multi-objective performance functions are given in Example 4.1.

Example 4.1: Multi-objective performance functions

Different forms of optimization scenarios can be considered to address the integrated process design and control problem. Some of these potential scenarios are given below:

Scenario 1:
Given a set of economic, process design and control/operation objectives, select a set of performance metrics to be maximized or minimum and/or satisfied. Examples of such performance metrics are: (i) operating costs of a process, inverse of profit, energy and sustainability indices for a process, for example reboiler and condenser duties for a distillation column, CO_2 eq. emission from a process, water consumption, etc. From a process design, economic and sustainability point of view it is desired that these metrics are minimized (ii) controller performance metrics that evaluate the performance of a given controller structure. For example, integral of absolute errors or total variation of inputs, etc. From a control point of view these metrics need to be minimized for a given controller structure. (iii) There can be also some metrics and or conditions which need to be satisfied. For example the relative gain arraye (RGA) for rearranged 2×2 system must have the values closest to unity on diagonal to ensure the least interactions between control loops.
Therefore, for a process design and corresponding controller structure that is identified as optimal/feasible these metrics must have the minimum values compared to any other sub-optimal design-control solution.

Scenario 2:
The design-control multi-objective performance function may be also written in form of a weighted objective function. Each performance criteria either from a process design, economic and sustainability point of view, or from a control point of view is assigned a weight. In some cases different criteria have different significance. For example, in some cases the process economics are more important than other criteria. Therefore, this specific criterion is assigned a higher weight compared to the rest. An example of such performance objective function is as follows:

$$f_{Obj} = \min\left(w_1 P_1 + w_2 P_2 + w_3 \frac{1}{P_3} \right) \tag{4.12}$$

In equation (4.12), P_1 represents costs associated to the reboiler and condenser duties in a distillation column. P_2 is the sensitivity of the controlled variables to disturbances in the feed (dy/dd). P_3 is the sensitivity of manipulated variables u with respect to controlled variables y (dy/du). Note that in equation (4.12), w_1, w_2 and w_3 are weight factors.

4.2 Step 2: Identify the number of elements present in the system

In this step, the number of elements present in the reactive system is identified through algorithm 2.1.

Algorithm 2.1: Identification of number of elements

Objective: To identify the number of elements present in the system

Step (i): Calculate the number of elements using Eq. (3.15) where *NC* is the number of compounds, and *NR*, is the number of reactions: $NE = NC - NR$

Step (ii): If the number of elements (*NE*) is equal to two go to *Step* (iii), otherwise, stop and return to Step (i). More than two elements will require selection of reactive key binary pairs according to developed rules (Jantharasuk et al., 2011; Mansouri et al., 2016) – see Step 3.

Step (iii): Write the formula matrix (A_e) from the formula coefficients a_{ji} with the constituent elements (j=1,2,...,*NE*) as rows and the species (i=1,2,..,*NC*) as columns (Pérez-Cisneros et al., 1997).

If a binary element system was encountered, go to Step 4,

Else, if a multi-element system (more than two elements) was identified, go to Step 3 to identify the key pair of elements.

4.3 Step 3: Identify the key elements

The equivalent binary elements, that is light key and heavy key elements, are selected according to the rules of key element selection for a multi-element system (Jantharasuk et al., 2011) and they are as follows:

Rule I: The mixture on component basis is arbitrarily considered as attaining the expected reaction conversion. The corresponding compositions are later applied with the 'Rule of key element selection' in the next steps.

Rule II: The element that is contained by the remaining lightest component should not be specified as heavy key and/or heavy non-key element.

Rule III: The element that is contained by the remaining heaviest component should not be specified as light key and/or light non-key element.

Rule IV: The key element should be presented along the whole column (should be contained in both distillate and bottom products).

4.4 Step 4: Reactive distillation column design

The objective of this step is to find the design-control option for the reactive distillation column using the driving force approach.

4.4.1 Step 4.1: Generate reactive vapor-liquid equilibrium (VLE) data

The reactive equilibrium data are obtained either through availability of data or computation of reactive bubble points or dew points. If the data is not available, the reactive bubble point algorithm is used (Sánchez-Daza et al., 2003). Below the algorithm to construct the reactive phase VLE diagram using the reactive bubble point algorithm is given for binary (algorithm 4.1a) and multi-element systems (4.1b).

Algorithm 4.1a: Construction of reactive phase VLE diagram for binary element systems

Objective: To calculate the vapor-liquid equilibrium data at given temperature or pressure and element feed composition

Step (i)*:* Give element composition in the feed (W_j^l , j = 1, 2) and pressure (P)

Step (ii)*:* Assume a temperature (T) – This can be a temperature between bubble point and dew point.

Step (iii)*:* Solve for component moles n_i^l in the liquid phase (chemical equilibrium). Note NE=2 in this work.

$$W_j^l \sum_{k=1}^{NE}\sum_{i=1}^{NC} A_{ki} n_i^l - \sum_{i=1}^{NC} A_{ji} n_i^l = 0 \quad \text{for } j = 1, 2, ..., NE \tag{4.13}$$

$$\sum_{i=1}^{NC} Z_{i,k} \mu_i^l = 0 \quad \text{for } k = 1, 2, ..., NR \tag{4.14}$$

where $Z_{i,k}$ is the stoichiometric coefficient of the compounds in the reaction mixture

Step (iv)*:* Compute vapor mole fractions y_i at equilibrium implicitly.

$$y_i \phi_i^v = x_i \phi_i^l \quad \text{for } i = 1, 2, ..., NC \tag{4.15}$$

Note that activity coefficient models can be also used for fugacity balances.

Step (v)*:* Calculate a correction for temperature using the check equation ($\sum_{i=1}^{NC} y_i - 1 = 0$). If not converged, return to *Step* (iii), else, go to *Step* (vi)

Step (vi)*:* Compute element mole fractions for the vapor phase using below equation

(Pérez-Cisneros et al., 1997):

$$W_j^v = \frac{\sum_{i=1}^{NC} A_{ji} y_i}{\sum_{k=1}^{NE} \sum_{i=1}^{NC} A_{ki} y_i} \tag{4.16}$$

The element composition in the liquid phase is calculated using the below equation:

$$W_j^l = \frac{\sum_{i=1}^{NC} A_{ji} x_i}{\sum_{k=1}^{NE} \sum_{i=1}^{NC} A_{ki} x_i} \tag{4.17}$$

It should be noted that with the element mole fractions there is not any chance for obtaining negative values for composition variables.

Step (vii): Repeat *Steps* (i)-(vi) for new values of W_j^l to obtain the reactive phase diagram for the entire composition domain (0-1). For systems without miscibility gaps, a constant discretization step of 0.05 in the x-axis composition is used and recommended. Note that this phase diagram needs to be generated only once and it is not computationally expensive.

Step (viii): If more than two elements are encountered, calculate the equivalent binary composition for the entire composition domain using the key elements identified in Step 3. The light key equivalent element composition is given by Eq. (3.24) and is as follows:

$$W_{LK,eq}^{\beta} = \frac{W_{LK}^{\beta}}{W_{LK}^{\beta} + W_{HK}^{\beta}}$$

Algorithm 4.1b: Construction of reactive phase VLE diagram for multi-element systems

Objective: To calculate the vapor-liquid equilibrium data at given temperature or pressure and element feed composition

Step (i)*:* Give element composition in the feed (W_j^l , j = 1, 2, …, *NE*) and pressure (P)

Step (ii)*:* Assume a temperature (T) – This can be a temperature between bubble point and dew point.

Step (iii)*:* Solve for component moles n_i^l in the liquid phase (chemical equilibrium). Note *NE*=2 in this work.

$$W_j^l \sum_{k=1}^{NE} \sum_{i=1}^{NC} A_{ki} n_i^l - \sum_{i=1}^{NC} A_{ji} n_i^l = 0 \quad \text{for } j = 1, 2, ..., NE \tag{4.13}$$

$$\sum_{i=1}^{NC} Z_{i,k} \mu_i^l = 0 \quad \text{for } k = 1, 2, ..., NR \tag{4.14}$$

where $Z_{i,k}$ is the stoichiometric coefficient of the compounds in the reaction mixture

Step (iv)*:* Compute vapor mole fractions y_i at equilibrium implicitly.

$$y_i \phi_i^v = x_i \phi_i^l \quad \text{for} \quad i = 1, 2, ..., NC \tag{4.15}$$

Note that activity coefficient models can be also used for fugacity balances.

Step (v)*:* Calculate a correction for temperature using the check equation ($\sum_{i=1}^{NC} y_i - 1 = 0$). If not converged, return to *Step* (iii), else, go to *Step* (vi)

Step (vi)*:* Compute element mole fractions for the vapor phase using below equation (Pérez-Cisneros et al., 1997):

$$W_j^v = \frac{\sum_{i=1}^{NC} A_{ji} y_i}{\sum_{k=1}^{NE} \sum_{i=1}^{NC} A_{ki} y_i} \tag{4.16}$$

The element composition in the liquid phase is calculated using the below equation:

$$W_j^l = \frac{\sum_{i=1}^{NC} A_{ji} x_i}{\sum_{k=1}^{NE} \sum_{i=1}^{NC} A_{ki} x_i} \tag{4.17}$$

It should be noted that with the element mole fractions there is not any chance for obtaining negative values for composition variables.

Step (vii): In case of more than two elements are encountered, calculate the equivalent binary composition for the entire composition domain using the key elements (LK and HK) identified in Step 3. The light key equivalent element composition is given by Eq. (3.21) and is as follows:

$$W_{LK,eq}^l = \frac{W_{LK}^l}{W_{LK}^l + W_{HK}^l}$$

$$W_{LK,eq}^v = \frac{W_{LK}^v}{W_{LK}^v + W_{HK}^v}$$

Step (vii): Repeat *Steps* (i)-(vii) for new values of W_j^l to obtain the reactive phase diagram for the entire composition domain (0-1). For systems without miscibility gaps, a constant discretization step of 0.05 in the x-axis composition is used and recommended. Note that this phase diagram needs to be generated only once and it is not computationally expensive.

4.4.2 Step 4.2: Reactive driving force calculations

In order to obtain the reactive distillation design at the maximum driving force, algorithm 4.2 is applied. In this step, the reactive distillation column design at the maximum driving force is obtained. The reactive driving-force based on elements (or binary equivalent elements) is calculated using equation (3.50) as described by Sanchez-Daza *et al*. (Sánchez-Daza et al., 2003), or in case of equivalent binary elements, light key equivalent compositions are used to calculate the driving force.

$$DF = W_i^v - W_i^l = \frac{W_i^l \alpha_{ij}}{1 + W_i^l \left(\alpha_{ij} - 1\right)} - W_i^l$$

Here two algorithms are presented. Algorithm 4.2 is for the case for designing a reactive distillation column with a single feed. In course of this algorithm, reactive McCabe-Thiele algorithm is also given as a sub-algorithm. Reactive McCabe–Thiele method is to calculate the minimum number of stages to obtain the desired product specifications (targets) in top and bottom of a binary element reactive distillation column. The method is based on the method proposed by McCabe and Thiele (McCabe and Thiele, 1925) for non-reactive distillation design. Daza et al. (Sánchez-Daza et al., 2003) have extended this method to also include reactive binary distillation columns and can be also used for equivalent binary element columns as well (systems which can be represented by two elements, A and B).

Algorithm 4.2: Reactive distillation design using driving force approach
Single feed reactive distillation column

Objective: To find the reactive distillation column design (number of stages, reflux ratio, feed location) at the maximum driving force using the specified design targets

Step (i): Retrieve vapor-liquid element data (binary or equivalent binary) from algorithm 4.1.

Step (ii): Calculate the corresponding driving force for the entire composition domain using equation (3.50), then plot $|DF|$ versus W_i^l based on the light key element.

Step (iii): Identify the area of operation of the driving force diagram, which is feed, distillate and bottom compositions based on the light key element (or the light key equivalent element) using the design targets set in Step 1.

Step (iv): Determine the reflux ratio and reboil ratio. To do this, determine the slopes of lines AD_y and BD_y (see Figure 3.2). Determine the corresponding minimum reflux ratio (RR_{min}) and reboil ratio (RB_{min}). Next, Determine the real reflux ratio (RR) and reboil ratio (RB) from $RR = 1.2(RR_{min})$ and $RB = 1.2(RB_{min})$.

Step (v): If the number of stages, N, are given go to *Step* (vi),
Else, use reactive McCabe-Thiele algorithm to obtain minimum number of stages as follows:

Sub-Algorithm 4.1:

Sub-Step (i): Retrieve information form Step 3.1 and draw reactive equilibrium curve (W^v_A-W^l_A diagram – for the light element)

Sub-Step (ii): Draw the angle bi-sector line (45° line), locate $W^l_{A,D}$ (composition of element A in distillate), $W^l_{A,B}$ (composition of product AB in the bottom) and W^F_A (composition of element A in the feed) on the 45° line.

Sub-Step (iii): Use the reflux ratio and reboil ratio obtained at the maximum driving force (algorithm 3.2) to calculate the slopes of the operating lines.

Sub-Step (iv): Draw the rectifying and stripping operating lines from $W^{l}_{A,D}$ and $W^{l}_{A,B}$ on the 45° line. Find the minimum number of stages by drawing the steps.
End of Sub-Algorithm 4.1

Step (vi): Identify the feed stage location, N_F, from $N_F = N\,(1 - D_x)$.

Step (vii): Check the design targets in terms of low key and heavy key elements in the feed, distillate and bottom as well as the location of maximum driving force on the *x*-axis (D_x) with the following additional conditions (Bek-Pedersen and Gani, 2004; Bek-Pedersen et al., 2000). If one or more conditions apply, use the guidelines to further retrofit the design.

If condition 1a is satisfied, then relocate NF between 5% and 10% up in the column.
Else, if condition 1b is satisfied, then relocate NF between 5% and 10% down in the column.
If condition 2a is satisfied then relocate NF 10% down.
Else, if condition 2b is satisfied, then relocate NF 5% down.
Else, if condition 2c is satisfied, then relocate NF 5% up.
Else, if condition 2d is satisfied, then relocate NF 10% up.

Condition 1	
a)	$W_{HK,z} < 0.8$ and $D_x < 0.7$
b)	$W_{HK,z} < 0.8$ and $D_x > 0.3$
Condition 2	
a)	$\frac{1-W_{LK,D}}{1-W_{HK,B}} < 0.01$ and $D_x < 0.7$
b)	$\frac{1-W_{LK,D}}{1-W_{HK,B}} < 0.1$ and $D_x < 0.7$
c)	$\frac{1-W_{HK,B}}{1-W_{LK,D}} < 0.1$ and $D_x > 0.3$
d)	$\frac{1-W_{HK,B}}{1-W_{LK,D}} < 0.01$ and $D_x > 0.3$

Step (viii): Perform steady-state simulation to confirm that the design targets are satisfied. These steady-state values are the nominal values for control.

If it is supposed to have a reactive distillation column with the mixtures of the same feed in two different streams and different compositions; then a reactive distillation column with two feeds is encountered. The feeds have the flowrates *H* and *K*. Therefore, Algorithm 4.3 is proposed to design a two feed reactive distillation column at the maximum driving force. Note that this algorithm is adapted from the original McCabe-Thiele method (McCabe and Thiele, 1925) for designing distillation columns with two feeds.

Algorithm 4.3: Reactive distillation design using driving force approach
Two feed reactive distillation column

Objective: To find the reactive distillation column design (number of stages, reflux ratio, feed location) with two feeds at the maximum driving force using the specified design targets

Step (i): Retrieve vapor-liquid element data (binary – algorithm 4.1a or equivalent binary – algorithm 4.1b)

Step (ii): Calculate the corresponding driving force for the entire composition domain using equation (3.50), then plot $|DF|$ versus W_i^l based on the light key element (or equivalent light key element).

Step (iii): Identify the area of operation of the driving force diagram (reactive zone information), which are feed compositions (feed one and two), distillate (W^D) and bottom (W^B) compositions based on the light key element (or the equivalent light key element) using the design targets set in Step 1.

> **Definition 1:** Let W_k and W_h be the compositions of the feeds
> **Definition 2:** Let W_g be the amount of the composition if the mixture if the two feeds were mixed – This corresponds to the value corresponding to the maximum driving force on the *x*-axis of the driving force diagram (D_x).
> **Condition 1:** Let $W_h > W_k$ so that the *H* feed is indeed placed higher in the column.

If the area of operation is not between 0 and 1, re-scale the *x*-axis between 0-1

Step (iv): Determine the reflux ratio and reboil ratio. To do this, determine the slopes of lines AD_y and BD_y (see Figure 3.2). Determine the corresponding minimum reflux ratio (RR_{min}) and reboil ratio (RB_{min}). Next, Determine the real reflux ratio (RR) and reboil ratio (RB) from $RR = 1.2(RR_{min})$ and $RB = 1.2(RB_{min})$.

Step (v): Construct the XY diagram using the vapor liquid element data (binary or equivalent binary) from Algorithm 4.1a or 4.1b.

Step (vi): Draw the angle bi-sector line (45° line), locate W^D, W^B, W_k, W_h and W_g on the *x*-axis of the XY diagram.

Step (vii): The rectifying and striping lines from *Step* (iv) are exactly the same as the case if there was a single feed (see Algorithm 4.2). That is they start from the product compositions. The enrichment line for the middle of the column is found by joining the points where enrichment lines for rectifying and stripping sections intersect the lines $x = W_k$ and $x = W_h$.

Step (viii): Find the minimum number of reactive stages by drawing the steps.

Step (ix): Perform steady-state simulation, and if further purification is required by the problem formulation, then add non-reactive reactive stages one-at-the-time to the top and bottom of the reactive section until desired purification of products is achieved.

Algorithm 4.3 is illustrated in Figure 4.2. After applying Algorithm 4.2 or 4.3 for reactive driving force approach calculations, the optimal reactive distillation design configuration at the maximum driving force is obtained.

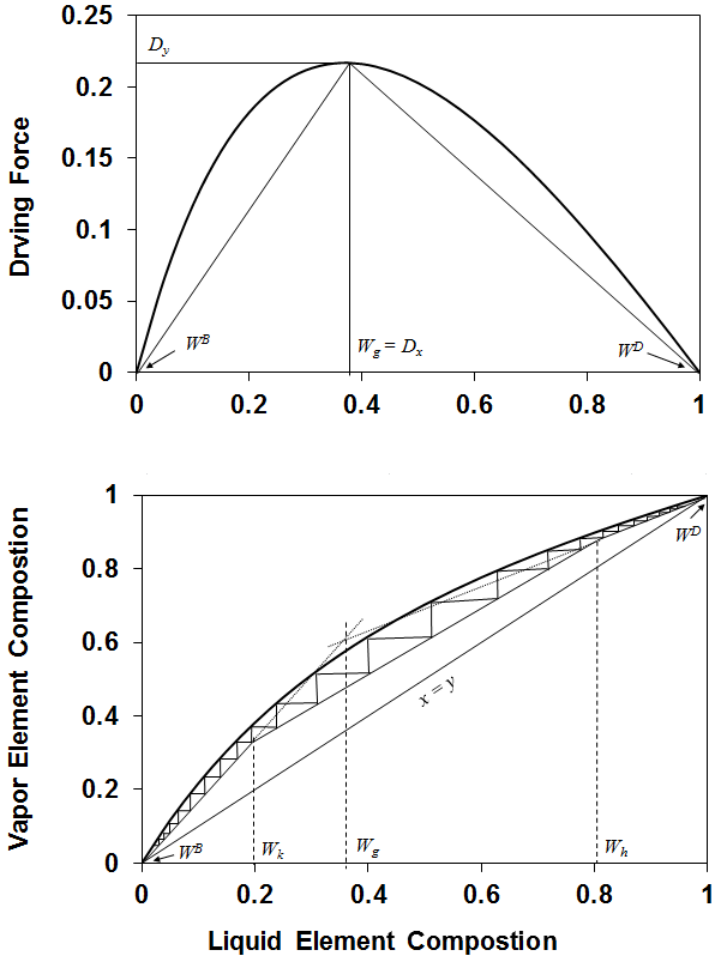

Figure 4.2 Illustrative example of the instructions given in Algorithm 4.3.

4.4.3 Step 4.3: Optimal design-control structure determination

The optimal design control structure determination is obtained analytically through the application of Algorithm 4.4.

Algorithm 4.4: Optimal design-control structure determination

Objective: The best controller structure at the maximum driving force is analytically identified by applying this algorithm.

Step (i): Selection of controlled variables – In this algorithm, the primary controlled variable is $W_i^{l,\max}$ (D_x), which is the *x*-axis value corresponding to the maximum driving force (D_y) . The secondary controlled variables are the product composition (design targets), which are measurable variables and they are the distillate and bottom product purities of the light key element, $W_A{}^D$ and $W_A{}^B$ (or $W_{LK,eq}^D$ and $W_{LK,eq}^B$ for a multi-element system), respectively. The reason behind this selection is that conceptual variables (that is driving force, *DF*) cannot be measured directly. Note that in this algorithm, it is presented for a binary element system. For a multi-element system all the equations are the same except that the light key element is replaced by the equivalent light key element for a multi-element system.

Step (ii): Sensitivity of controlled variables to disturbances – In order to calculate the sensitivity, apply a chain rule to relate the derivatives of primary controlled variable to the derivatives of the secondary controlled variables. In order to apply the chain rule, use the following key concepts:

The desired element product at the top and the bottom is $W_A{}^D$ and $W_A{}^B$ (or $W_{LK,eq}^D$ and $W_{LK,eq}^B$ for a multi-element system), the distillate and bottom composition of light key element (element A), respectively. At the maximum point of the driving force diagram, $W_A{}^D$ and $W_A{}^B$ (controlled variables) are the least sensitive to the imposed disturbances in the feed. The design variables vector is $y = [W_A{}^D \quad W_A{}^B]$, $x = W_A{}^l$ and θ = DF is selected on the y-axis of the driving force diagram. The disturbance vector is, $d = [F_f \quad z_{WAf}]$ (feed flowrate and feed composition of element *A*). Therefore, the chain rule is expressed as in Eq. (4.18) using Eq. (3.48a) and (3.49a):

$$\frac{dy}{dd} = \begin{bmatrix} \frac{dW_A^D}{dF_f} & \frac{dW_A^D}{dz_{W_{Af}}} \\ \frac{dW_A^B}{dF_f} & \frac{dW_A^B}{dz_{W_{Af}}} \end{bmatrix} = \begin{bmatrix} \left(\frac{dW_A^D}{dDF}\right)\left(\frac{dDF}{dW_A^l}\right)\left(\frac{dW_A^l}{dF_f}\right) & \left(\frac{dW_A^D}{dDF}\right)\left(\frac{dDF}{dW_A^l}\right)\left(\frac{dW_A^l}{dz_{W_{Af}}}\right) \\ \left(\frac{dW_A^B}{dDF}\right)\left(\frac{dDF}{dW_A^l}\right)\left(\frac{dW_A^l}{dF_f}\right) & \left(\frac{dW_A^B}{dDF}\right)\left(\frac{dDF}{dW_A^l}\right)\left(\frac{dW_A^l}{dz_{W_{Af}}}\right) \end{bmatrix} \quad (4.18)$$

The value of Eq. (4.18) at the maximum driving force is obtained after some mathematical derivations are performed (see Appendix A for details). Having the derivatives in Eq. (4.18) derived analytically. The solution to Eq. (4.18) is expressed by Eq. (4.19).

$$\begin{bmatrix} \frac{dW_A^D}{dF_f} \\ \frac{dW_A^B}{dF_f} \\ \frac{dW_A^D}{dz_{W_{Af}}} \\ \frac{dW_A^B}{dz_{W_{Af}}} \end{bmatrix} = \begin{bmatrix} \left((RR+1)+\left(\frac{dDF}{dW_A^l}\right)^{-1}\right)\left(\frac{dDF}{dW_A^l}\right)\left(\frac{a_1}{\left[a_2\frac{dDF}{dW_A^l}+a_3+\left(\frac{dW_A^D}{dDF}\right)\left(\frac{dDF}{dW_A^l}\right)\right]}\right) \\ \left(\left(\frac{dDF}{dW_A^l}\right)^{-1}-RB\right)\left(\frac{dDF}{dW_A^l}\right)\left(\frac{a_4}{\left[a_5\frac{dDF}{dW_A^l}+a_6+\left(\frac{dW_A^B}{dDF}\right)\left(\frac{dDF}{dW_A^l}\right)\right]}\right) \\ \left((RR+1)+\left(\frac{dDF}{dW_A^l}\right)^{-1}\right)\left(\frac{dDF}{dW_A^l}\right)\left(\frac{a_7}{\left[a_2\frac{dDF}{dW_A^l}+a_3+\left(\frac{dW_A^D}{dDF}\right)\left(\frac{dDF}{dW_A^l}\right)\right]}\right) \\ \left(\left(\frac{dDF}{dW_A^l}\right)^{-1}-RB\right)\left(\frac{dDF}{dW_A^l}\right)\left(\frac{a_8}{\left[a_5\frac{dDF}{dW_A^l}+a_6+\left(\frac{dW_A^B}{dDF}\right)\left(\frac{dDF}{dW_A^l}\right)\right]}\right) \end{bmatrix} \quad (4.19)$$

It is noted that the driving force diagram is always concave with a unique maximum for non-azeotropic systems. It is also noted that the expressions for $\left(dW_A^D/dDF\right)\left(dDF/dW_A^l\right)$ and $\left(dW_A^B/dDF\right)\left(dDF/dW_A^l\right)$ in Eq. (4.19) are equal to 1 (note Eqs. (A.5) and (A.6) in Appendix A) at the maximum driving force and greater than 1 in any other point. Furthermore, at the maximum value of driving force diagram value of dDF/dW_A^l is equal to zero. Therefore, Eq. (4.19) at the maximum driving force is expressed as:

$$\frac{dy}{dd} = \begin{bmatrix} \frac{dW_A^D}{dF_f} & \frac{dW_A^B}{dF_f} \\ \frac{dW_A^D}{dz_{W_{Af}}} & \frac{dW_A^B}{dz_{W_{Af}}} \end{bmatrix} \approx \begin{bmatrix} (0)\left(\frac{a_1}{a_3+1}\right) & (0)\left(\frac{a_4}{a_6+1}\right) \\ (0)\left(\frac{a_7}{a_3+1}\right) & (0)\left(\frac{a_8}{a_6+1}\right) \end{bmatrix} \approx \begin{bmatrix} 0 & 0 \\ 0 & 0 \end{bmatrix} \quad (4.20)$$

Note that in Eq. (4.19) and (4.20), a_1,.., a_8 are constants. Eq. (4.20) reveals that the sensitivity of controlled variables to disturbances in the feed is minimized at the maximum driving force.

Step (iii): Selection of the Controller Structure – The potential manipulated variables vector is u = [L V], which are represented by reflux ratio (RR) and reboil ratio (RB). Hence, the sensitivity of the secondary controlled variables to the manipulated variables is calculated by Eq. (4.21) (see Appendix B for derivation details).

$$\frac{dy}{du}=\begin{bmatrix}\frac{dW_A^D}{dRR} & \frac{dW_A^D}{dRB}\\ \frac{dW_A^B}{dRR} & \frac{dW_A^B}{dRB}\end{bmatrix}= \begin{bmatrix} DF+(RR+1)\left(\frac{dDF}{dW_A^l}\right)\left(\frac{dW_A^l}{dRR}\right)+\frac{dW_A^l}{dRR} & (RR+1)\left(\frac{dDF}{dW_A^l}\right)\left(\frac{dW_A^l}{dRB}\right)+\frac{dW_A^l}{dRB}\\ \frac{dW_A^l}{dRR}-\left(\frac{dDF}{dW_A^l}\right)\left(\frac{dW_A^l}{dRR}\right)RB & \frac{dW_A^l}{dRB}-DF\end{bmatrix} \tag{4.21}$$

One can see from the driving force diagram that there is a well-defined maximum of *DF* for a value of W_A^l. Since the process is designed at this point and the controller should maintain this set-point, thus the derivatives are evaluated at this point of W_A^l. Therefore, the value of dDF/dW_A^l at the maximum driving force is equal to zero. Furthermore, assuming that $dW_A^l/dRR = dW_A^l/dRB = 0$ (W_A^l at the maximum driving force corresponds to $W_A^{l,\max}$ which is a number. Thus, the derivative of the dependent variable that has a fixed value is zero), Eq. (4.21) is obtained (this corresponds to a system with no or little cross interactions between *y* and *u* since changes in *u* cannot propagate through column). The best controller structure is easily determined by looking at the value of d*y*/d*u*. It is noted from Eq. (4.22) that since the values of dW_A^D/dRR and dW_A^B/dRB are bigger, controlling W_A^D by manipulating *RR* and controlling W_A^B by manipulating *RB* will require less control action. This is because only small changes in *RR* and *RB* are required to move W_A^D and W_A^B in a bigger direction. Therefore, for the optimal design obtained at the maximum driving force from Algorithm 4.2 or 4.3, the control structure is always given by Eq. (4.22) and it is verified by analytical analysis that it is the optimal-design control structure.

$$\frac{dy}{du}=\begin{bmatrix}\frac{dW_A^D}{dRR} & \frac{dW_A^D}{dRB}\\ \frac{dW_A^B}{dRR} & \frac{dW_A^B}{dRB}\end{bmatrix}=\begin{bmatrix} DF & 0\\ 0 & -DF\end{bmatrix} \tag{4.22}$$

or the following for a multi-element system:

$$\frac{dy}{du}=\begin{bmatrix}\frac{dW_{LK,eq}^d}{dRR} & \frac{dW_{LK,eq}^d}{dRB}\\ \frac{dW_{LK,eq}^B}{dRR} & \frac{dW_{LK,eq}^B}{dRB}\end{bmatrix}=\begin{bmatrix} DF_{LK,eq} & 0\\ 0 & -DF_{LK,eq}\end{bmatrix} \tag{4.23}$$

4.5 Step 5: Dynamic analysis and verification

The objective of this step is to verify the design-control solution that was obtained at the maximum driving force. This verification is first performed by verifying the appropriateness of the controller structure and next, by performing rigorous dynamic closed-loop simulation or by performing experiment. Note however, using a rigorous

simulation will be easier for this verification since appropriate values of *y* and *u* are obtained through the previous steps of this framework.

4.5.1 Step 5.1: Controller structure verification

In order to verify the appropriateness of the control structure obtained at the maximum equivalent binary element driving force (see Eq. 4.22), Algorithm 5.1 is applied.

Algorithm 5.1: Control structure verification

Objective: To verify the control structure obtained at the maximum driving force using a rigorous dynamic model.

Step (i): Obtain the linear representation of the optimal design control option at the maximum driving force; either by using the transfer functions from step test between each manipulated (*u*) and control variable (*y*) or linearizing the model and obtaining state-space matrices (A; B; C; D).

Step (ii): Construct the steady-state gain matrix (*G*) from the transfer functions.

Step (iii): Verify that the gain matrix *G* has non-zero determinant.

Step (iv): Calculate the relative gain matrix (RGA) using Eq. (4.23) as follows (Bristol, 1966):

$$RGA(G) = G \otimes \left(G^{-1}\right)^{T} \tag{4.23}$$

Step (v): Verify that pairings such that the rearranged system, with the selected pairings along the diagonal, has an RGA matrix element close to unity, and off-diagonal elements close to zero (for a 2×2 system); therefore, control structure at the maximum driving force has least interactions with each other for the pairing given by Eq. (4.22).

Step (vi) – *Optional*: Calculate Niederlinski Index using Eq. (4.24) as follows (Chiu and Arkun, 1991; Corriou, 2004):

$$N_I = \frac{\det|G|}{\prod_i G_{ii}} \tag{4.24}$$

If this index is negative the system is unstable whatever the tuning of the controllers are.

Else,

If it is positive, it is impossible to conclude. Thus, it is a sufficient condition, except for multivariable systems of size lower than or equal to 2, where it is also necessary.

4.5.2 Step 5.2: Dynamic evaluation of control structure

The objective of this step is evaluate the close-loop performance of the control structure identified and verified in Step 4 and Step 5.1, respectively; in the presence of disturbances in the feed. Therefore, to this end Algorithm 5.2 is applied. Figure 4.3, depicts the closed-loop implementation concept in this framework.

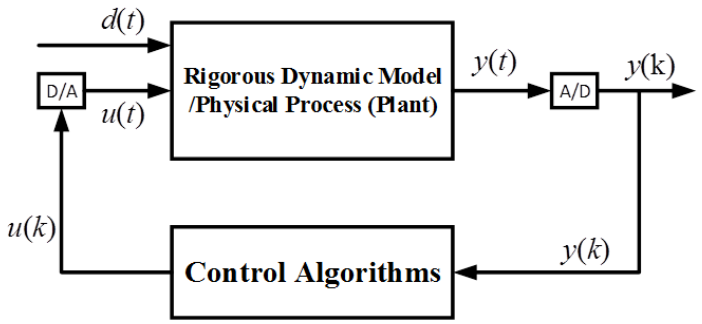

Figure 4.3 Schematic drawing of the communication network in a control system.

Algorithm 5.2: Control structure evaluation

Objective: To evaluate the performance of the control structure at the maximum driving force through closed-loop simulation

Step (i): Select a disturbance scenario in the feed.

Step (ii): Perform open-loop analysis in the presence of the disturbances (using a specified maximum in the disturbance size) to evaluate resulting transient responses. If the deviation is less than 2% return to *Step* (i) and select another disturbance scenario.

Step (iii): Select an appropriate control algorithm at regulatory level.

Step (iv): Retrieve nominal steady-state values for the control variables from Step 4.2.

Step (v): Select an appropriate tuning method (IMC rules (Rivera et al., 1986) or SIMC rules (Skogestad, 2003)) to obtain tuned controller parameters.

Step (vi): Perform closed-loop simulation and verify that the disturbance is rejected and the system is recovered to its original set-points.

4.5.3 Step 5.3: Final selection

In this step the value of the performance objective function or controller performance metrics (defined in Step 1) is calculated for the design-control option at the maximum driving force.

5
APPLICATION EXAMPLES

This chapter outlines several applications of the computer-aided framework. The objective of these case studies is to highlight the application of integrated process design and control framework with its associated algorithms and computer-aided tools. The design based on the driving force concept and the corresponding controller structure is to be determined and evaluated against candidates corresponding to process designs that do not use the largest available driving force. The analysis results are also confirmed with closed-loop and open-loop simulations.

Conceptual examples: This chapter starts with two conceptual examples that are not the direct application of the framework. However, these motivating examples are useful to show the interactions between process design decisions and operation. The first motivating example is designing a reactor-separator-recycle (RSR) process. Here, the decisions regarding the reactor design and the anticipated recovery and recycle of unreacted raw materials affect the controllability and operation of the process. The second conceptual example is an intensified process option for production of methyl-acetate. The flowsheet consists of a membrane-based reactor and a purification section. The process is originally designed using the concepts elaborated in motivating example 1, for reactor-separator-recycle process, and for the purification step, the driving force concept is used to design the distillation columns. Here, the design steps will not be shown as the case has been originally designed by Babi et al., (2014) using the concepts outlined also in this work. This example is an intensified process flowsheet. Therefore, here only dynamic analysis on the case is performed to verify that the process design by Babi et al., (2014) is actually an integrated process design-control solution.

Application Examples: Three case studies are carried out to demonstrate the application of the framework for integrated process design and control of reactive distillation processes following a step by step demonstration of the framework. The first case study presents the integrated process design and control of a single feed

reactive distillation column where the reaction mixture is represented by binary elements. The second case study is a single feed reactive distillation column where a multi-element (more than two elements) is encountered. Finally, the third case study is a two feed reactive distillation column with multi-elements that consists of both reactive and non-reactive sections.

5.1 Conceptual example 1: MTBE synthesis via a RSR system

In chemical industry the existence of recycle streams is very common to recycle unreacted raw material after the product purification. However, it is well-known that the presence of the recycle streams poses challenges in process design and operation where "snowball" effect may happen in presence of disturbances. Therefore, the design-control interactions and the ability to address them in the early stages of process design are important. The present conceptual example is production of Methyl-tertiary-Butyl-Ether (MTBE) represented by a simple reactor-separator-recycle process. The reactor-recycle-separator (RSR) system is given in Figure 5.1.

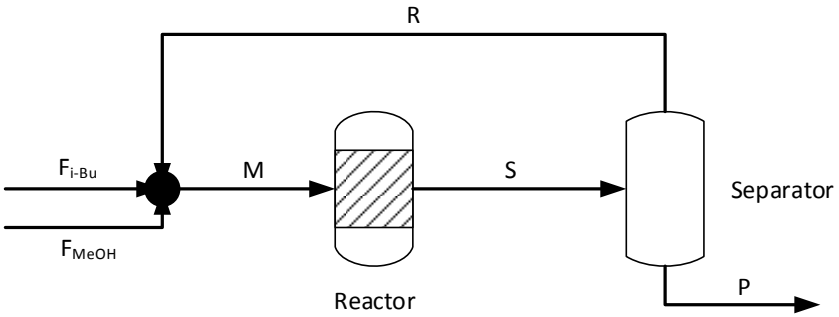

Figure 5.1 Simple schematic of MTBE production process without an inert compound

MTBE reaction kinetics catalyzed by sulphuric acid has been described by Al-jarallah et al. (1988) as follows:

$$i-Butene + Methanol \underset{k_2}{\overset{k_1}{\rightleftarrows}} MTBE \tag{5.1}$$

The rate expression for formation of MTBE is expressed by the following equation:

$$\frac{d[MTBE]}{dt} = k_1[MeOH]^{0.5}[i-Bu]^{0.5} - k_2[MTBE] \tag{5.2}$$

Where the constants k_1 and k_2 are given as:

$$k_1 = 16.43\times10^8 \exp\left(-\frac{12600}{RT}\right)[H_2SO_4]^{1.5} \tag{5.3}$$

$$k_2 = 1.22\times10^{20} \exp\left(-\frac{31100}{RT}\right)[H_2SO_4]^{1.5} \tag{5.4}$$

In the above equations, $R = 1.987\, cal\cdot mol^{-1}K^{-1}$ and T is in K. In the rate constant equations (Eqs. 5.3 and 5.4) concentration of H_2SO_4 (homogeneous catalyst) is fixed. The methanol/isobutene ratio on a molar basis is 1:2.

In order to address the design-control interactions, dimensionless mole-balance equations are parameterized by the plant Damköhler number (Da) and the separation specifications. This conceptual example demonstrates how the decisions in course of designing reactor-separator-recycle (RSR) systems parametrized by *Da* number affect process control and operation. In this example, we consider the separation unit as a black box and consider a kinetic model for the reactor, complete recovery of product and isothermal process. Based on this simplified flowsheet for MTBE production process without inert compound, the mass balance equations are as follows:

$F_{i\text{-}Bu,F}$ (isobutene flowrate in the feed), k_1 (forward reaction kinetic constant) and $C_{i\text{-}Bu,F}$ (isobutene concentration in the reactor), are selected as reference variables. Therefore, the corresponding mass balances in terms of dimensionless variables can be written. It should be noted that in this case, it is assumed that the reaction is n^{th} order (n = 0.5) with respect to limiting reactant (isobutene) in the forward direction. Note that the dimensionless variables are:

$$Da = k_1 C^{-0.5}_{i-Bu,F} V_r / F_{i-Bu,F} \qquad s_i = F_{i,S} / F_{i-Bu,F}$$
$$z_i = C_i / C_{i-Bu,F} \qquad m_i = F_{i,M} / F_{i-Bu,F}$$
$$f_i = F_{i,F} / F_{i-Bu,F} \qquad r_i = F_{i,R} / F_{i-Bu,F}$$

Note that *Da* for an n^{th} order reaction is given as $Da = kC^{n-1}_{i,F}V/F_{i,F}$ given by Bildea et al. (2000).

Mixer:

$$0 = f_{MeOH} + r_{MeOH} - m_{MeOH} \tag{5.5}$$
$$0 = 1 + r_{i-Bu} - m_{i-Bu} \tag{5.6}$$
$$0 = f_{MTBE} + r_{MTBE} - m_{MTBE} \tag{5.7}$$

Note that since complete recovery of MTBE (product) is assumed, the terms f_{MTBE} and r_{MTBE} in Eq. (5.7) are equal to zero.

Separator:

$$0 = s_{MeOH} - \beta_{MeOH,S} s_{MeOH} - \left(1 - \beta_{MeOH,S}\right) s_{MeOH,S} \tag{5.8}$$
$$0 = s_{i-Bu} - \beta_{i-Bu,S} s_{i-Bu} - \left(1 - \beta_{i-Bu,S}\right) s_{i-Bu} \tag{5.9}$$
$$0 = s_{MTBE} - \beta_{MTBE,S} s_{MTBE} - \left(1 - \beta_{MTBE,S}\right) p_{MTBE} \tag{5.10}$$

Where $\beta_{MeOH,S}$ and $\beta_{i-Bu,S}$ are recovery factors of methanol and isobutene which their values can be between 0 and 1. Note that since complete recovery of MTBE is assumed ($\beta_{MTBE,S} = 0$); therefor, Eq. (5.10) is reduced to: $0 = s_{MTBE} - p_{MTBE}$.

Reactor:

$$0 = m_{MeOH} - s_{MeOH} - Da\left(z_{MeOH,S} z_{i-Bu,S}\right) \tag{5.11}$$

$$0 = m_{i-Bu} - s_{i-Bu} - Da\left(z_{MeOH,S} z_{i-Bu,S}\right) \tag{5.12}$$

$$0 = m_{MTBE} - s_{MTBE} + Da\left(z_{MeOH,S} z_{i-Bu,S}\right) \tag{5.13}$$

Note that the reaction rate equation is given by Eq. (5.2). The extent of the reaction is defined as (ξ) in order to take into account the change in the number of moles. In reacting systems, extent of reaction is used as means to take into account the change in the number of moles due to the reaction. Table 5.1 gives, the change in the number of moles and the corresponding mole fractions, $z_{i,S}$, for the reacting system at the reactor outlet (stream S – see Figure 5.1).

Table 5.1 Mole fractions of MTBE production reaction.

Component	**Initial**	**Final (at stream S)**	**Mole fraction, $z_{i,S}$**
Methanol	$F_{MeOH,M}$	$F_{MeOH,M} - \xi$	$(F_{MeOH,M} - \xi)/(F_M - \xi)$
Isobutene	$F_{i\text{-}Bu,M}$	$F_{i\text{-}Bu,M} - \xi$	$(F_{i\text{-}Bu,M} - \xi)/(F_M - \xi)$
MTBE	0	ξ	$\xi/(F_M - \xi)$
Total	F_M	$F_M - \xi$	1

Note that ξ has unit of mole flow (kmol/h). Therefore, given that the fresh flowrate of isobutene has been taken as a reference variable, therefore,

$$\xi_v = \frac{\xi}{F_{i-Bu,F}} \tag{5.14}$$

Moreover, Table 5.1 lists the flowrate of methanol and isobutene leaving the reactor in terms of dimensionless variables:

$$s_{i-Bu} = m_{i-Bu} - \xi_v \tag{5.15}$$

$$s_{MeOH} = m_{MeOH} - \xi_v \tag{5.16}$$

Knowing that: $r_{i-Bu} = \beta_{i-Bu,S} s_{i-Bu,S}$; therefore, isobutene flowrate on the dimensionless basis in the reactor outlet stream (S) is obtained considering equation (5.6):

$$s_{i-Bu} = 1 + r_{i-Bu} - \xi_v = 1 + \beta_{i-Bu} s_{i-Bu} - \xi_v \tag{5.17}$$

Thus,

$$s_{i-Bu} = \frac{1 - \xi_v}{1 - \beta_{i-Bu}} \tag{5.18}$$

and the flowrate of isobutene into the reactor is:

$$m_{i-Bu} = 1 + \beta_{i-Bu}\left(\frac{1 - \xi_v}{1 - \beta_{i-Bu}}\right) = \frac{1 - \xi_v \beta_{i-Bu}}{1 - \beta_{i-Bu}} \tag{5.19}$$

Similarly, the dimensionless inlet and outlet flowrate of methanol to the reactor can be written as follows:

$$s_{MeOH} = \frac{f_{MeOH} - \xi_v}{1 - \beta_{MeOH}} \tag{5.20}$$

$$m_{MeOH} = \frac{f_{MeOH} - \xi_v \beta_{MeOH}}{1 - \beta_{MeOH}} \tag{5.21}$$

Therefore, the total dimensionless outlet flowrate of the reactor (at stream S) is:

$$s = m_{i-Bu} + m_{MeOH} - \xi_v = \frac{1 - \xi_v \beta_{i-Bu}}{1 - \beta_{i-Bu}} + \frac{f_{MeOH} - \xi_v \beta_{MeOH}}{1 - \beta_{MeOH}} - \xi_v \tag{5.22}$$

Thus, the dimensionless mole fractions of the reactor effluent are as follows:

$$z_{i-Bu,S} = \frac{1 + r_{i-Bu} - \xi_v}{s} \tag{5.23}$$

$$z_{MeOH,S} = \frac{\left(f_{MeOH} - \xi_v\right)/\left(1 - \beta_{MeOH}\right)}{s} \tag{5.24}$$

$$z_{MTBE,S} = \frac{\xi_v}{s} \tag{5.25}$$

Substituting equations (5.23) – (5.25) into equations (5.11) – (5.13) gives the following set of equations:

$$0 = m_{MeOH} - s_{MeOH} - Da\left(\left(\frac{\left(f_{MeOH} - \xi_v\right)/\left(1 - \beta_{MeOH}\right)}{s}\right)\left(\frac{1 + r_{i-Bu} - \xi_v}{s}\right)\right) \tag{5.26}$$

$$0 = m_{i-Bu} - s_{i-Bu} - Da\left(\left(\frac{\left(f_{MeOH} - \xi_v\right)/\left(1 - \beta_{MeOH}\right)}{s}\right)\left(\frac{1 + r_{i-Bu} - \xi_v}{s}\right)\right) \tag{5.27}$$

$$0 = m_{MTBE} - s_{MTBE} + Da\left(\left(\frac{\left(f_{MeOH} - \xi_v\right)/\left(1 - \beta_{MeOH}\right)}{s}\right)\left(\frac{1 + r_{i-Bu} - \xi_v}{s}\right)\right) \tag{5.28}$$

Solving the above equations at different *Da* numbers can give a full understanding of the non-linear behavior of MTBE reaction-separation-recycle system. In order to better analyze the system, Damköhler number (*Da*) is plotted versus limiting reactant conversion (*X*) and reactor outlet flowrate in different recovery factors ($\beta_{i\text{-}Bu}$, β_{MeOH}). Note that conversion (with respect to isobutene) is calculated, that is:

$$X = 1 - \frac{s_{i-Bu,s}}{m_{i-Bu}} \tag{5.29}$$

Now, substituting Eq. (5.18) for $s_{i-Bu,s}$ and Eq. (5.19) for m_{i-Bu} in Eq. (5.29) gives the following expressions:

$$X = 1 - \left(\frac{1 - \xi_v / 1 - \beta_{i-Bu}}{1 - \xi_v \beta_{i-Bu} / 1 - \beta_{i-Bu}}\right) = 1 - \left(\frac{1 - \xi_v}{1 - \xi_v \beta_{i-Bu}}\right) \tag{5.30}$$

Figure 5.2 and Figure 5.3 show the results of the dimensionless analysis of the system with respect to Damköhler number (*Da*).

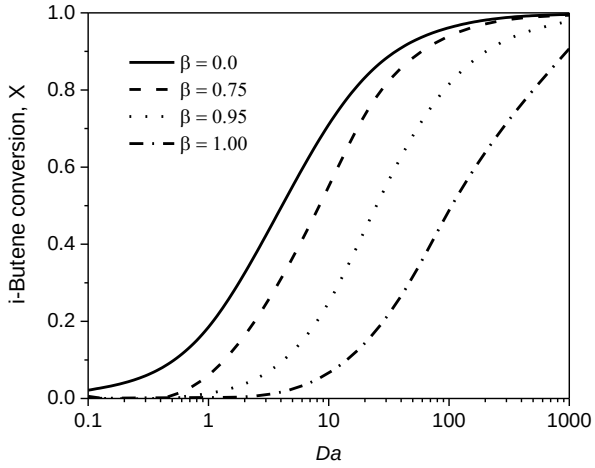

Figure 5.2 Dimensionless analysis of the system: Da versus isobutene conversion ($\beta = \beta_{MeOH} = \beta_{i\text{-}Bu}$)

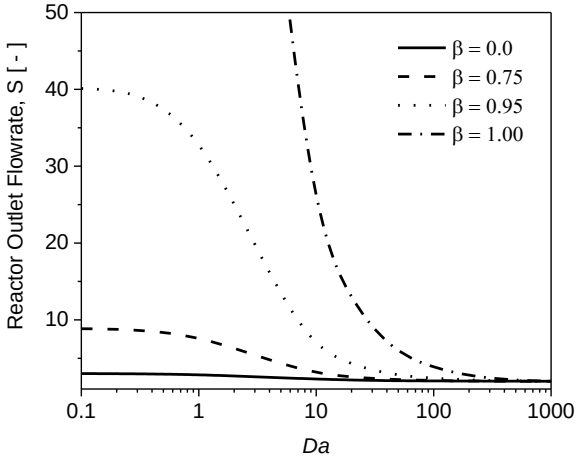

Figure 5.3 Dimensionless analysis of the system: Da versus reactor outlet flowrate ($\beta = \beta_{MeOH} = \beta_{i\text{-}Bu}$).

The conversion of isobutene ($X_{i\text{-}Bu}$) decreases because of a larger amount of isobutene that has to be reacted within the same reactor volume (assuming V_r is kept constant). On the other hand, it is important to highlight the combined effect of the Da number and the recovery factor β. That is, a steeper slope is observed in the conversion profile as β decreases, especially at lower Da numbers (Da < 50). This effect indicates that a faster rate of reaction is most likely taking place due to the stoichiometric

consumption of reactant (isobutene). Nonetheless, larger β values means that a higher residence time in the reactor is required for isobutene. As β approaches 1 with $X_{i\text{-}Bu}$ relatively low, the reactor outlet increases considerably which implies an increased "snowball" effect likelihood. On the contrary, operating for high conversion values implies either low feeds to the system or the use of large equipment. Therefore a tradeoff might arise and appropriate criteria should be established through the formulation and solution of an optimization. In order to verify the aforementioned discussion, rigorous dynamic simulation was performed in two scenarios which on is operating at low *Da* number and the other one is at high *Da* number. Note that from a process design point of view, a fixed reactor volume and recovery factor has been considered for both designs. Thus, *Da* number has been moved by changing the feed flowrate. Table 5.2 describes the two designs that are selected for verification purposes.

Table 5.2 Design alternatives for rigorous dynamic simulation

Design	*Da*	$\%X_{i\text{-}Bu}$	$F_{i\text{-}Butene}$ [lit/hr]	Volume [lit]	Height [m]	T [K]	β	Set-point	CV	MV
A	150	33.2	0.1	50	5	353	0.99	Level (50%)	Level	Outlet Flowrate
B	0.1	0. 1	200	50	5	353	0.99	Level (50%)	Level	Outlet Flowrate

* $\beta = \beta_{MeOH} = \beta_{i\text{-}Bu}$

Figure 5.4, presents the closed-loop performance of Design A and B in presence of a disturbance in the methanol feed flowrate. It can be observed from the closed-loop performance of the two designs that the design at high *Da* number (design A) is less sensitive to the disturbances in the feed than a design at low *Da* number (design B). That is the *Da* number defines the sensitivity of the process to the disturbances in the feed and this sensitivity determines the controller performance in closed-loop operation. Note however, in this example a perfect temperature control is assumed since the process was assumed initially to be isothermal. Note that in the closed-loop simulations the reactor level is the controlled variable (CV) and the reactor outlet flowrate is the manipulated variable (MV). The PI-type controller was used to perform the closed-loop simulations. Therefore, as it can be seen from this analysis at higher *Da* number the possibility for the presence of "snow-ball" effect is less than lower *Da* numbers. Thus, this analysis shows the interactions between design and control of the chemical processes with recycle loops.

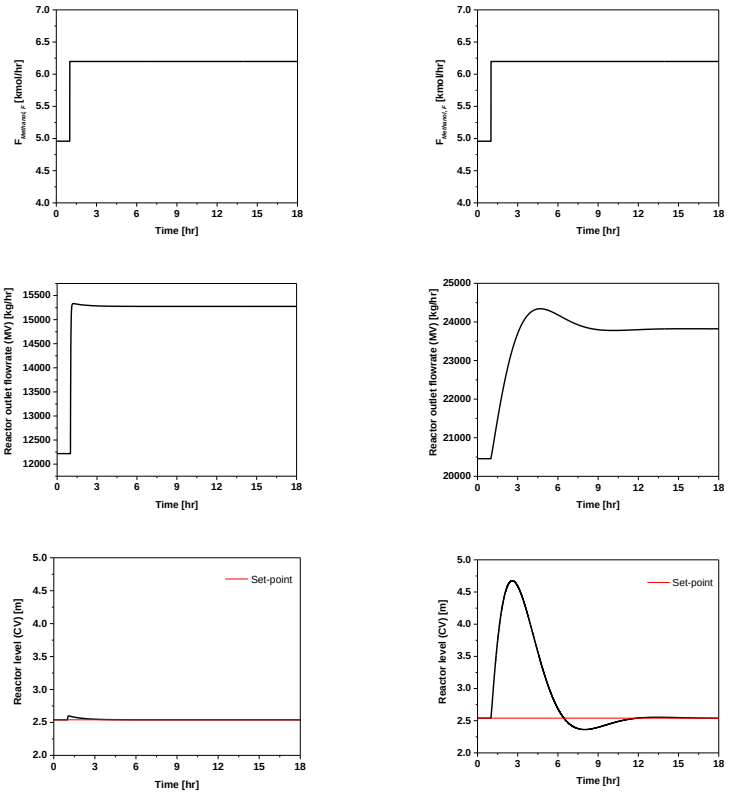

Design (A), *Da* = 150 Design (B), *Da* = 0.1

Figure 5.4 Dynamic closed-loop performance of the RSR system for MTBE synthesis at two different *Da* numbers.

5.2 Conceptual example 2: Methyl-acetate membrane-assisted intensified process

Babi et al. (2014) proposed a framework to synthesize intensified process. Their framework is well-developed at the operations level and the task level, and it includes the basic (general) concepts at the phenomena level. In their work, they have elaborated on the concept of phenomena-based synthesis. They also present the concept of phenomena building blocks involved in chemical processes. They have presented their framework in great detail with a step by step explanation of the work-flow. The application of their framework is illustrated through a case study involving the production of methyl-acetate, where it is shown that sustainable membrane-based processing options can be determined. Amongst the methods that they use in their framework, is the driving force concept to design reactive and non-reactive distillation operations. Furthermore, they have performed a detailed membrane reactor analysis including modeling and RSR behavior using *Da* number.

In this example, their detailed design of a membrane-based process intensification flowsheet option is obtained. The dynamic behavior of the process in presence of disturbances will be elaborated. The purpose of this motivating example is that the driving force concept (explained in detail in Chapters 3 and 4) can also be applied to other process intensification options. Furthermore, its combination with other design tools such as *Da* analysis for RSR systems will result in feasible control structures.

Here, the detailed design of process flowsheet will not be discussed as it has been published by Babi et al. (2014) and the interested reader may refer to their publication to obtain the design details. Instead, the focus is given on the dynamic analysis and showing that the design obtained from their framework, using concepts such as driving force, has inherently integrated design and control features. This will be illustrated by dynamic simulations.

5.2.1 Process description

The production of methyl-acetate (MeOAc) is important mainly due to its application as a solvent for various usages such as glues and paints. The product purity must be equal or greater than 99%. The reaction between methanol (MeOH) and acetic acid (HOAc) yields methyl acetate (MeOAc) and water (H_2O). The reaction takes place in liquid phase over a catalyst. It is exothermic with a heat of reaction pf -5.42 kJ/mol and is given as follows:

$$MeOH + HOAc \leftrightarrow MeOAc + H_2O \tag{5.31}$$

Note that here, the raw materials are assumed to be at their pure state. The membrane-based intensified process flowsheet for production of methyl-acetate is given in Figure 5.5. In the process flowsheet, methanol and acetic acid are fed with a 1:1 ratio since with a membrane assisted reactor, removal of water is possible and equilibrium is achieved faster. As it was relayed before, Babi et al. (2014) have done a detailed analysis of the membrane reactor. The membrane used in this case a PVA membrane produced by Sulzer Chemtech, PERVAP 2201.

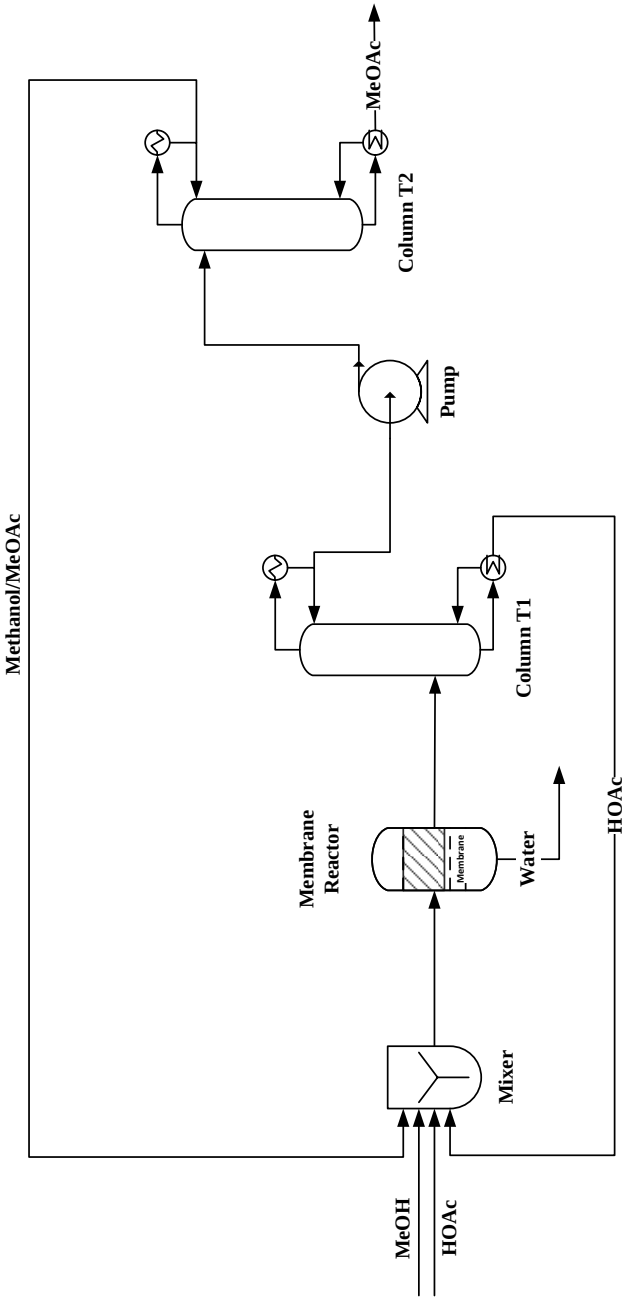

Figure 5.5 Membrane-based process flowsheet developed (Babi et al., 2014).

5.2.2 Dynamic analysis

Hamid et al. (2010), proposed a methodology for integrated process design and control of chemical processes. They have employed the same design concepts as being used by Babi et al. (2014) to design their intensified process flowsheet. Here, the control strategy of Hamid et al. (2010) is used to demonstrate the dynamic appropriateness of the flowsheet designed by Babi et al. (2014) – see Figure 5.5.

It is readily known, that the process presented in Figure 5.5 has been designed in a feasible *Da* number range and the distillation columns are designed at the maximum driving force. These design decisions ensure an integrated process design-control solution. Therefore, the nominal steady-state values of the process are optimal set-points for control. Here, in order to perform the closed-loop simulations the control strategy proposed by Hamid (2010) is employed. The controllers on the reactor are to control the level by manipulating the outlet flowrate of the reactor; and temperature control by manipulating the heat added/removed from the reactor. The latter control structure must be as tight as possible since any change in the reactor temperature affects the reaction dynamics, thereby moving the process to another *Da* number. The distillation controllers are to control top and bottom product stream temperatures by manipulating reboiler duty and reflux rate. Note however that there are also level controllers to maintain the level set-point of condenser drum and reboiler sump. All the controllers are selected to be PI-type controllers. Figure 5.6, shows the controller structure implementation on the process flowsheet presented in Figure 5.5.

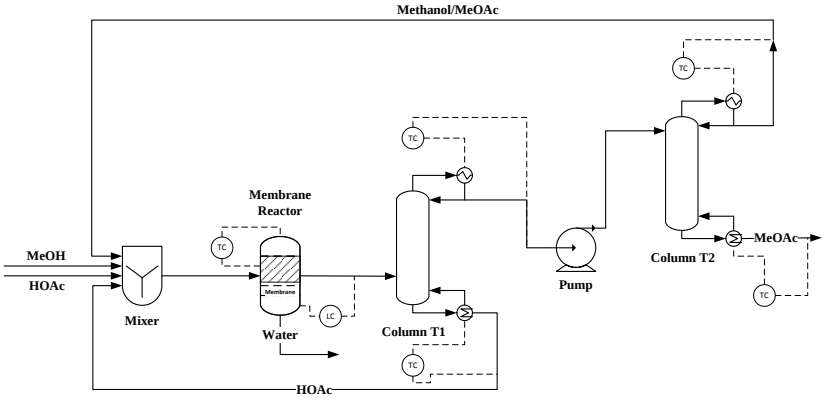

Figure 5.6 Control structure implementation for membrane-assisted process flowsheet.

In order to demonstrate the inherent abilities of the process design, dynamic closed-loop simulation of the process in presence of a disturbance in the feed is carried. The disturbance scenario is +10% step change in the feed temperature. Figure 5.7, shows the dynamic closed-loop performance of the reactor.

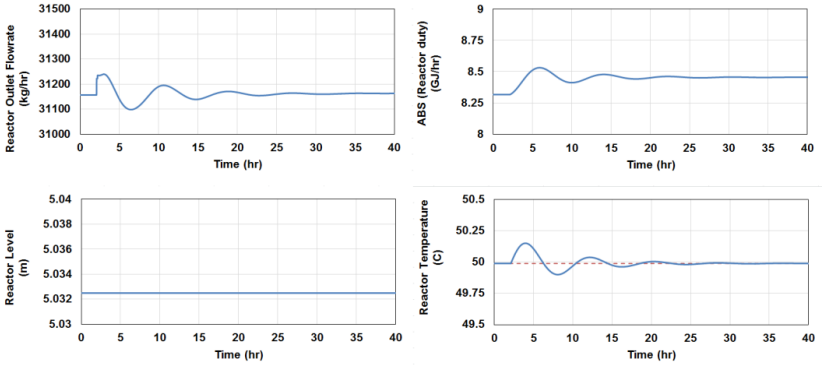

Figure 5.7 Closed-loop performance of the membrance reactor in presence of a disturbance in the feed.

As it can be seen in Figure 5.7, the level has mainly remained unchanged, which can be also due to the nature of the disturbance (feed temperature) that has not disturbed it significantly. However, the reactor temperature is disturbed and the controller is able to reject the disturbance with a relatively small over shoot. Figure 5.8, shows the closed-loop performance of column T1 in the presence of the same disturbance in the feed. Similarly, it is observed that the process is restored to its original set-point with a very small effort in the manipulated variables.

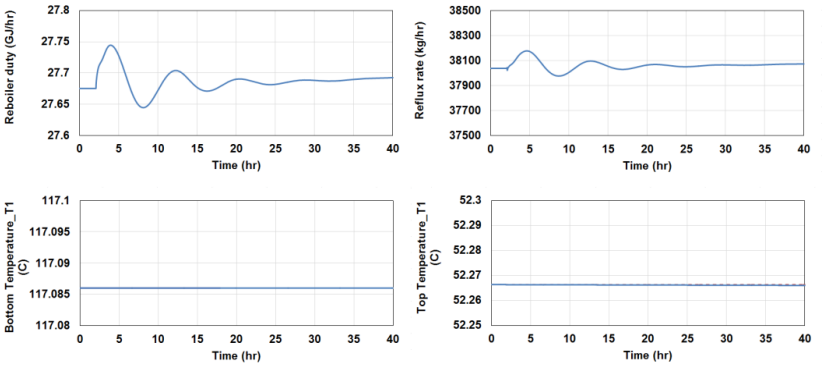

Figure 5.8 Closed-loop performance of the column T1 in presence of a disturbance in the feed.

Figure 5.9, shows the closed-loop performance of column T2 in presence of the same disturbance in the feed. As it can be seen, again the disturbance is rejected fairly fast and a large overshoot is not observed in the controlled variables. Nonetheless, the effort in the manipulated variables is also very small in order to reject the disturbance.

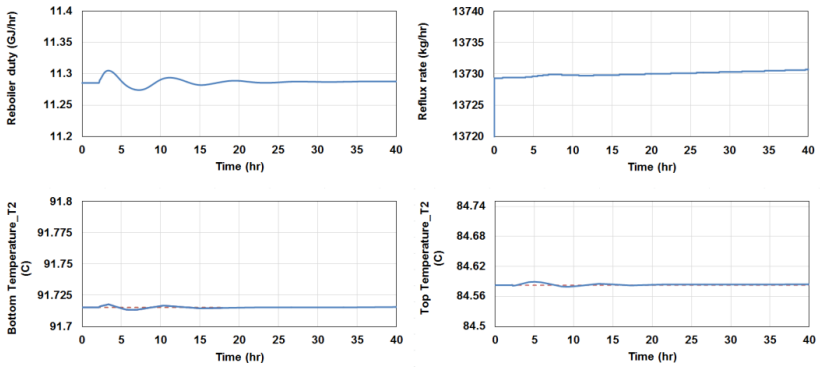

Figure 5.9 Closed-loop performance of the column T2 in presence of a disturbance in the feed.

In order to demonstrate the no snow-ball effect is observed in the recycle loops as well as showing that final product composition (MeOAc) composition in at the bottom of column T2 is maintained at its desired purity, the dynamics of theses uncontrolled variables is given in Figure 5.10 to Figure 5.12.

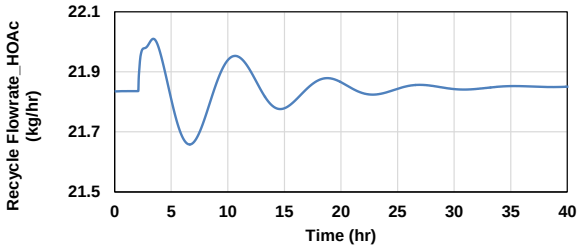

Figure 5.10 The dynamics of HOAc recycle stream – uncontrolled variable.

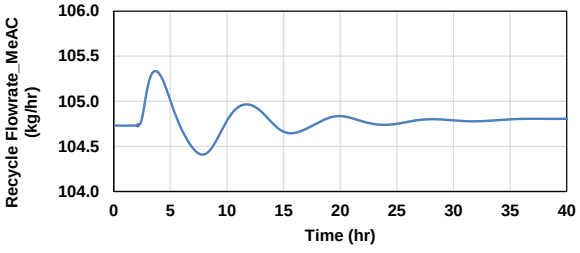

Figure 5.11 The dynamics of Methanol/MeOAc recycle stream – uncontrolled variable.

As it can be seen in Figure 5.11 and Figure 5.10, the recycle flowrate exhibits a stable response and does not show any snow-ball effect or accumulation of material in the recycle streams. Furthermore, Figure 5.11 shows the dynamic response of the MeOAc composition in the product stream (bottom of column T2). It is readily observed, that by controlling the temperature, the composition set-point is also maintained.

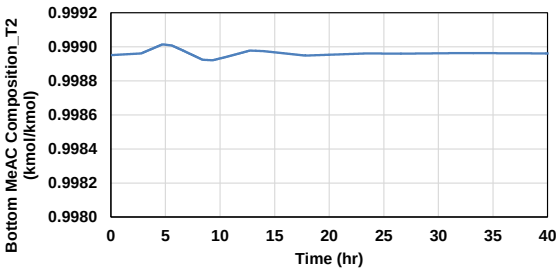

Figure 5.12 The dynamic response of MeOAc composition in the product stream (bottom of column T2) – uncontrolled variable.

Therefore, this motivating example demonstrates that using the *Da* analysis for designing the reactor and the driving force approach to design the distillation columns results in an operable process where the product specifications are maintained in presence of disturbances in the feed. Furthermore, it also shows that the so called "snow-ball" effect is also not present in the recycle loops in presence of the disturbances in the feed.

5.3 Application example 1: Single feed binary element reactive distillation column

The objective of this case study is to highlight the application of integrated process design and control framework with its associated algorithms and computer-aided tools. The design based on the driving force concept and the corresponding controller structure is to be determined and evaluated against two other controller structures corresponding to process designs that do not use the largest available driving force. The analysis results are also confirmed with closed-loop and open-loop simulations.

The process selected in this study to highlight the application of the integrated process design and control framework is the well-known production of Methyl Tert Butyl Ether (MTBE) by reactive distillation. The reactive distillation technology for MTBE production has been studied (Grosser et al., 1987; Schrans et al., 1996; Sharma and Singh, 2010) and advantages of reactive distillation has been well established in the case of MTBE.

When chemical reactions take place very fast so that equilibrium is reached almost instantaneously, as it is the case for MTBE synthesis, the chemical equilibrium condition can be implicitly incorporated in element mass balances through the relationship between the phase compositions and the element chemical potentials (Pérez-Cisneros et al., 1996). A dynamic model (Pérez-Cisneros, 1997) for the reactive distillation column is used in this case study. ICAS dynamic simulator is used to perform the simulations (Gani, 2015).

5.3.1 Step 1: Problem formulation/objective function definition

The reaction of methanol with isobutene that yields MTBE takes place in presence of an acidic catalyst. The reaction is reversible and exothermic, with a heat of reaction of -37.2 kJ/mol in the liquid phase at 25°C (Al-Jarallah et al., 1988).

$$isobutene\left(C_4H_8\right)+methanol\left(CH_4O\right)\leftrightarrow MTBE\left(C_5H_{12}O\right) \tag{5.33}$$

Note however, it is assumed that there is no inert compound present in the system. The pure component properties (critical properties, molecular weights, boiling and melting points) are retrieved from ICAS-Database (Nielsen et al., 2001). The feed conditions for production of MTBE are taken from Sánchez-Daza et al. (Sánchez-Daza et al., 2003) and they are summarized in Table 5.3.

Table 5.3 Design targets and product specifications for MTBE system.

Component	**Molar composition**		
	Feed	Distillate	Bottom
Isobutene (C_4H_8)	0.7	0.98	–
Methanol (CH_4O)	0.3	–	–
MTBE ($C_5H_{12}O$)	0.0	–	more than 0.8
Methanol conversion: more than 80%; Feed flowrate: 100 kmol/h; Feed temperature and pressure: 300K and 101.3 kPa; degree of vaporization (q): 0.795			

The design-control multi-objective performance function is defined as below:

$$f_{Obj} = \min\left(J_1, J_2, J_3, J_4\right) \tag{5.34}$$

In the above equation, a set of metrics are selected to the evaluate controller performance. They are: J_1 the sensitivity of the controlled variables to disturbances in the feed (dy/dd); J_2 the sensitivity of manipulated variables with respect to controlled variables (du/dy); J_3 measures the performance of the controller in terms of the integral of the absolute error (see Eq. 5.35); and J_4 measures the performance of the controller in terms of total variation of inputs (see Eq. 5.36).

$$J_3 = IAE = \int_0^{\infty} \left| y - y_{sp} \right| dt \tag{5.35}$$

$$J_4 = TV = \sum_{i=1}^{\infty} \left| u_{i+1} - u_i \right| \tag{5.36}$$

5.3.2 Step 2: Identify the number of elements present in the system

In this step, algorithm 2.1 is applied. The number of elements present in the system is two with one reaction. The element matrix, choice of elements and element reaction are given in Table 5.4.

Table 5.4 The element matrix and element reaction for MTBE reactive system (without inert).

Isobutene (C_4H_8) + Methanol (CH_3OH) ↔ MTBE ($C_5H_{12}O$) Element definition: $A = C_4H_8$ $B = CH_3OH$ Element reaction: $A + B \leftrightarrow \boldsymbol{C}$			
	Formula Matrix		
	C_4H_8 (1)	CH_3OH (2)	$C_5H_{12}O$
A	1	0	1
B	0	1	1

5.3.3 Step 3: Identify the key elements

Since a binary element system was encountered in Step 2, the key elements are already identified. Therefore, Step 4 must be carried out.

5.3.4 Step 4: Reactive distillation column design

5.3.4.1 Step 4.1: Generate reactive vapor-liquid equilibrium (VLE) data

The reactive VLE data for the MTBE reactive system is calculated by applying algorithm 4.1a and using the Wilson model for liquid phase activity coefficients and SRK equation of state for vapor phase fugacity coefficients. The calculated reactive bubble point for entire composition space is given in Figure 5.13 which presents the $T - W_A^l - W_A^v$ phase diagram for MTBE reactive system.

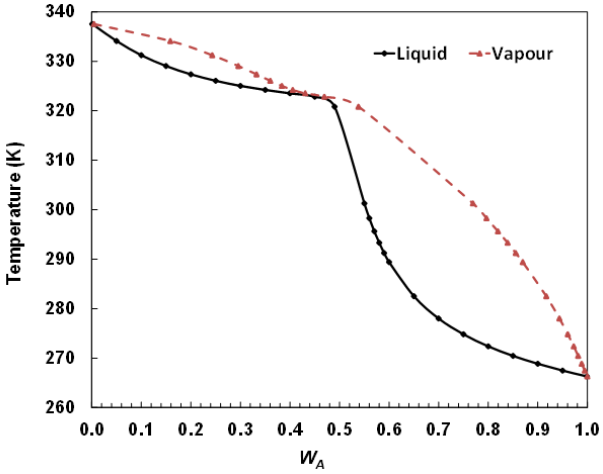

Figure 5.13 $T - W_A^l - W_A^v$ phase diagram for MTBE reactive system (P = 101.3 kPa).

5.3.4.2 Step 4.2: Reactive distillation column design

In this step, algorithm 4.2 is applied. The VLE data are retrieved from algorithm 4.1 and the reactive driving force diagram is constructed as illustrated in Figure 5.14.

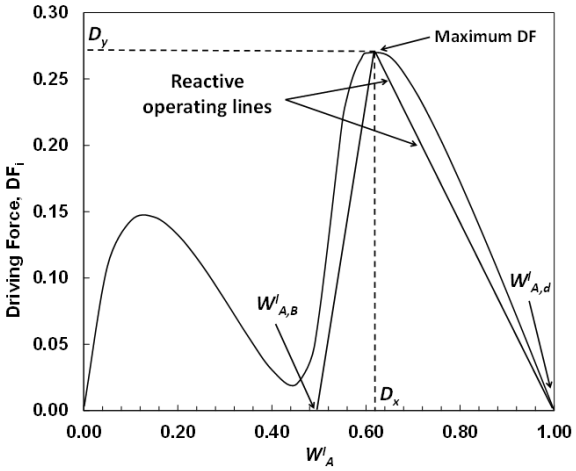

Figure 5.14 Reactive driving force diagram for MTBE reactive system (P = 101.3 kPa) (Sánchez-Daza et al., 2003).

The area of operation is identified on the x-axis of the reactive driving force diagram in terms of light key element as follows:

In order to define the operating area to satisfy design objectives, consider the light key element liquid mole fraction obtained by Eq. (21). When x_1=1 (pure isobutene),

and x_2=x_3=0, then, w_A^l = 1 and w_B^l = 0; and when x_2=1 (pure methanol), and x_1=x_2=0, then, w_A^l = 0 and w_B^l = 1. Therefore, when x_3=1 (pure MTBE), and x_1=x_2=0, then: w_A^l = 0.5 and w_B^l = 0.5. Having this simple evaluation performed, distillate (w_A^D) and bottom (w_A^B) are selected to be 0.99 and 0.5 on the *x*-axis of the reactive driving force diagram based on w_A^l element composition. This selection is to ensure that the design targets can be satisfied.

The point D_x and D_y corresponding to the maximum driving force are also identified and consequently slopes of operating lines are calculated which are used to determine *RR* and *RB*. In this case study, the number of stages (N) is not given; therefore, reactive McCabe-Thiele method is applied. The results of application of reactive McCabe-Thiele method are given in Figure 5.15.

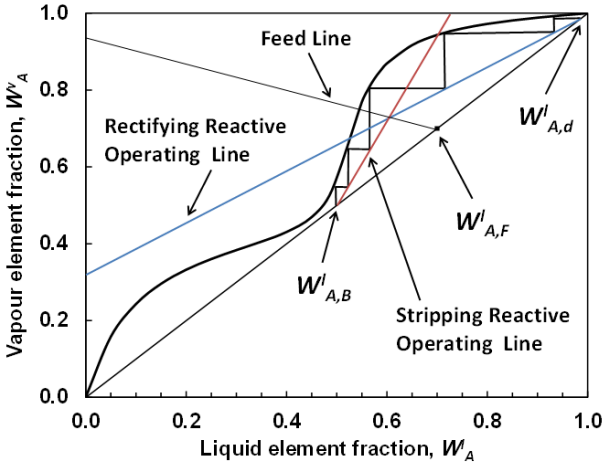

Figure 5.15 Reactive McCabe-Thiele method for designing MTBE reactive distillation column (Sánchez-Daza et al., 2003).

Note that from a practical point of view, presence of reaction in reboiler and condenser is infeasible and has not been reported in the literature to the best of authors' knowledge. Therefore, two non-reactive stages (i.e. partial reboiler and total condenser) are considered as stages. Thus, the total number of stages including reboiler and condenser is seven. Element feed, distillate and bottom compositions are checked against conditions given in algorithm 4.2 and it is found that condition 1(a) applies to the design specifications considered in this case study; therefore, the optimal feed location for the reactive distillation column design is at stage two from the top of the column. The final reactive distillation column design configuration at the maximum driving force is presented in Figure 5.16.

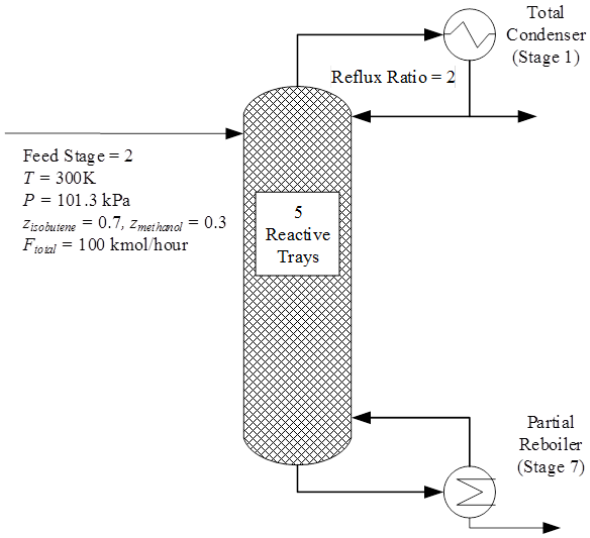

Figure 5.16 Reactive distillation column design configuration for design-control solution

In order to confirm that the design targets are satisfied, steady-state simulation of the design is performed. It is readily observed from steady-state results (see Table 5.5) that the isobutene composition in the distillate is 98 mole% and MTBE composition in the bottom is more than 84 mole% and the overall methanol conversion of 83.15% which match the design targets specified in Step 1.

Table 5.5 Nominal operating point of the optimal design-control solution.

Variable	**Optimal design-control solution**
Feed Temperature (K)	300
Distillate Temperature (K)	265.62
Bottom Temperature (K)	319.85
Feed flowrate (kmol/h)	100
Distillate flowrate (kmol/h)	45.543
Bottom flowrate	29.473
Feed composition (kmol/kmol)	$z^F_{isobutene} = 0.7; z^F_{methanol} = 0.3; z^F_{MTBE} = 0.0$
Distillate composition (kmol/kmol)	$x^D_{isobutene} = 0.9795; x^D_{methanol} = 0.0201; x^D_{MTBE} = 0.314E-03$
Bottom composition (kmol/kmol)	$x^B_{isobutene} = 0.0143; x^B_{methanol} = 0.1405; x^B_{MTBE} = 0.8451$
Overall methanol conversion	83.15%
Reboiler duty (MJ/h)	294.935
Condenser duty (MJ/h)	46.196
Reflux ratio	2
Heat addition to Reboiler (kJ/h)	0
Number of stages	7
Feed location	Stage 2

5.3.4.3 Step 4.3: Optimal design-control structure determination

The controlled variables (y) are top and bottom compositions, manipulated variables (u) are reflux ratio and reboiler duty (see Eq. 4.21). Moreover, the values of dDF/dW^l_A are calculated and plotted versus W^l_A (primary controlled variable) in Figure 5.17. It can be seen that the design at the maximum driving force has the least sensitivity of the controlled variables to the disturbances, and, the highest sensitivity to the manipulated variables. Since the reactive distillation column design is at the maximum driving force, the controller structure is given by Eq. (4.22).

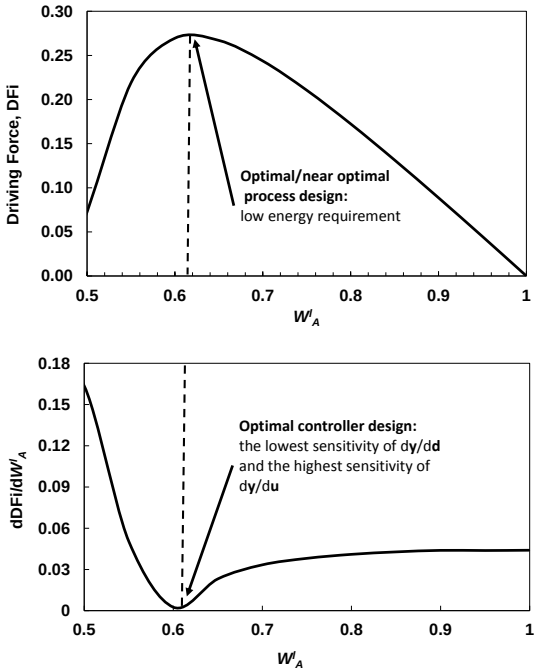

Figure 5.17 Driving force diagram for W_A–W_B separation (reactive zone only – top figure) and its corresponding derivative of DF with respect to W_A^l (bottom figure).

5.3.5 Step 5: Dynamic analysis and verification

5.3.5.1 Step 5.1: Control structure verification

In this step, algorithm 5.1 is applied. The transfer functions between each manipulated variable and controlled variable given by Eq. (4.22) are obtained by a step test and regressing the transfer function parameters (Pernebo and Silverman, 1982). The transfer functions have the form as Eq. (5.37):

$$G(s) = K\frac{1+\tau_z s}{(1+\tau_{p1}s)(1+\tau_{p2}s)} \tag{5.37}$$

The transfer function parameters for the design-control solution are given in Table 5.6. Note that manipulated variables (u) are reflux ratio (RR) and reboiler duty (Q_R) while control variables (y) are MTBE composition in the distillate (x^D_{MTBE}) and bottom (x^B_{MTBE}).

Table 5.6 Transfer function parameters for design-control alternatives

Manipulated variable/ Controlled variable	K	τ_{p_1}	τ_{p_2}	τ_z
$RR(s)/x^B_{MTBE}(s)$	0.32211 [-]	6.2527	2.324	–1.8092
$RR(s)/x^D_{MTBE}(s)$	–4.96E–05 [-]	2.0042	2.004	5.3828
$Q_R(s)/x^B_{MTBE}(s)$	–1.23E-06 [kJ/h]	3.6963	3.6821	–0.64004
$Q_R(s)/x^D_{MTBE}(s)$	–1.47E–11 [kJ/h]	0.017038	0.017038	–601749

Figure 5.18 shows the transfer function prediction of RR/x^B_{MTBE} pair for the optimal design control-solution. The steady-state gain matrix G is calculated and its corresponding determinant had a non-zero value.

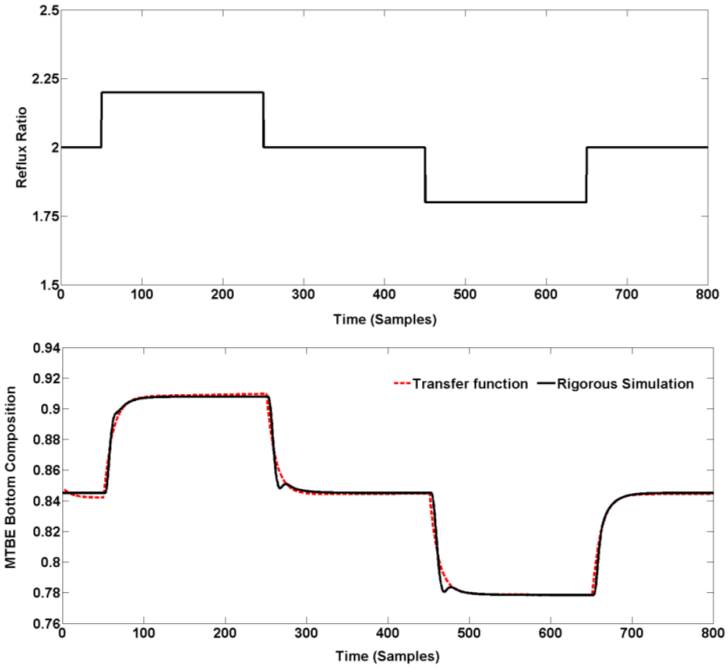

Figure 5.18 Transfer function prediction of RR/x^B_{MTBE} pair for the optimal design-control solution (each time sample is 5s)

The relative gain matrix is constructed using equation (4.23). The RGA values are then calculated given the potential control structures as in equation (4.22). The RGA matrix for optimal design-control solution is as follows:

$$RGA_{DC-Solution} = \begin{bmatrix} 0.93 & 0.07 \\ 0.07 & 0.93 \end{bmatrix}$$

It is seen from the calculated RGA matrix, that the design-control solution has values close to unity on the diagonal (the control structure at the maximum driving force) and off-diagonal values close to zero. This verifies the analytical solution obtained at the maximum driving force for the determined optimal control structure.

5.3.5.2 Step 5.2: Dynamic evaluation of control structure

Figure 5.19 shows the dynamic open-loop response of the control variables to a +15 kmol/h step change in the isobutene flowrate (from 70 kmole/h to 85 kmole/h) after 15 samples (each time sample is 5 seconds). This disturbance results in a change in total feed flowrate and at the same time a change in the feed composition.

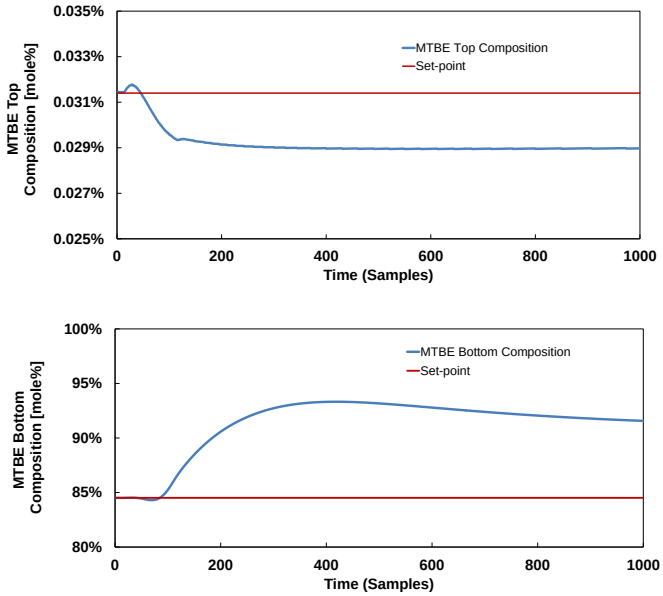

Figure 5.19 Open-loop response of optimal design-control solution to a disturbance in the feed (each time sample is 5s).

A proportional-integral (PI) controller is selected and its tuning parameters were calculated using the transfer functions in Table 5.6 (for selected control structure) and SIMC rules (Skogestad, 2003). The control structure implementation on the reactive distillation column is depicted in **Figure 5.20**.

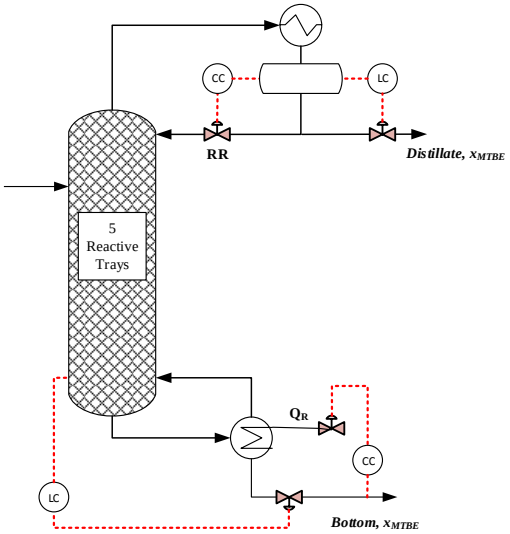

Figure 5.20 Simple schematic of control structure implementation.

In Figure 5.20, control configuration in which the purities of both the top and the bottom products are measured and controlled is presented. This control structure implementation is in compliance with the relative gain array (RGA) analysis by which the composition of the MTBE in distillate is controlled by manipulating the reflux flow rate in the top control loop. In the bottom control loop, the composition of the MTBE in bottom is controlled by manipulating the heat duty of the reboiler. The levels of the reflux drum and the reboiler are controlled by the distillate and bottom-product flow rates, respectively. Note however, in this case study, the level controllers are proportional (P) type and they are included in the model equations for dynamic model consistency and stability. Furthermore, it is assumed that there is a perfect pressure control on the column and thus, the pressure changes in the column are neglected. Figure 5.21 shows the closed-loop performance of optimal design-control solution under the presence of the previously defined disturbance scenario. It is verified in Figure 5.21 that the optimal design-control solution which is operating at the maximum driving force is able to reject the disturbance and restoring the control variables to their original set-points with a relatively small effort in the manipulated variables in both top and bottom loops. It was, however, also expected from the RGA matrix since the values close to unity resemble the least interactions between the control loops, thereby, an easier disturbance rejection is facilitated.

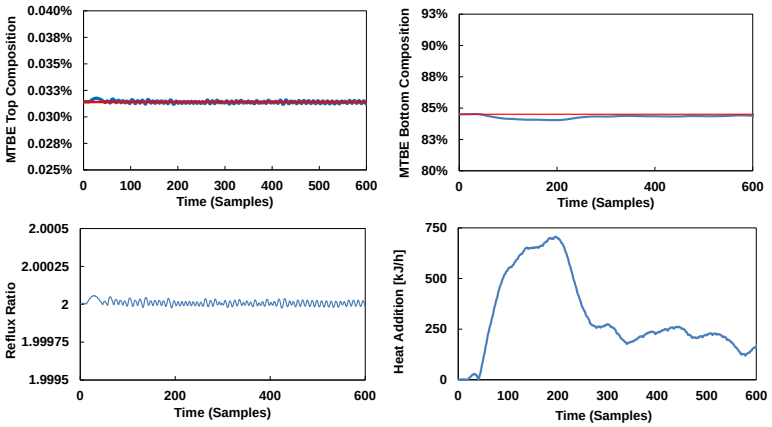

Figure 5.21 Closed-loop performance of optimal design-control solution, operating at the maximum driving to a disturbance in the feed (each time sample is 5s).

5.3.5.3 Step 5.3: Final selection

In the last step of the framework, the values of the controller performance metrics for the design-control solution are calculated and they are given in Table 5.7.

Table 5.7 The values of the controller performance metrics in application example 1.

Design	**Feed location**	J_1	J_2	$J_{3,D}$ (x^D_{MTBE} by RR)	$J_{3,B}$ (x^B_{MTBE} by Q_R)	$J_{4,D}$ (x^D_{MTBE} by RR)	$J_{4,B}$ (x^B_{MTBE} by Q_R)
Design-control solution	Stage 2	0.0	0.00313	0.00037	0.98647	0.00277	1527.51

*Note that J_3 and J_4 are calculated for both the controlled loops (controlled and manipulated variables pairings). They are the x^D_{MTBE} by RR (controlling the top composition of MTBE by reflux ratio) in the top control loop and x^B_{MTBE} by Q_R (controlling the bottom MTBE composition by reboiler duty) in the bottom control loop of the reactive distillation column (see Figure 5.20)

Further verification of design control solution

As extra analysis and to further verify that the optimal design-control solution has been obtained, two candidate design alternatives which are not at the maximum driving force are selected. This selection is only to show that by going away from the maximum driving force the control of the reactive distillation process becomes more difficult. Therefore, in this comparison only the feed location is altered and the same controller structure and controlled variables as the ones at the maximum driving force are used for the consistency of the comparisons. These design candidates are summarized in Table 5.8.

Table 5.8 Design alternatives (not at maximum driving force) for verification.

Design alternative	Feed location	Number of stages	Reflux ratio
1	Stage 3	7	2
2	Stage 4	7	2

The dynamic analysis is performed for the design alternatives (1) and (2) following Steps 5.1 – 5.2 of the framework. The candidate design alternatives both satisfied the design target and product specifications. Next, algorithm 5.1 was applied. The transfer functions were calculated and the corresponding RGA matrices were obtained as follows:

$$RGA_{Alternative(1)} = \begin{bmatrix} 9.06 & -8.06 \\ -8.06 & 9.06 \end{bmatrix}$$

$$RGA_{Alternative(2)} = \begin{bmatrix} -0.28 & 1.28 \\ 1.28 & -0.28 \end{bmatrix}$$

Design alternative (1) has a very large RGA element values for the selected pairing (diagonal) which means that the design is inherently difficult to control (Large RGA elements; typically, 5 − 10 or larger) for control indicate that the plant is fundamentally difficult to control due to strong input-output interactions (Skogestad and Morari, 1987)). In case of Design alternative (2), the values on diagonal are negative in which case the pairing is not recommended (Skogestad and Morari, 1987). For the other potential structure in Design alternative (2), although the values are close to unity, the control structure is infeasible from a practical and physical point of view. Next, algorithm 5.2 was applied. Figure 5.22 shows the closed-loop performance of Design alternative (1) to a disturbance in the feed.

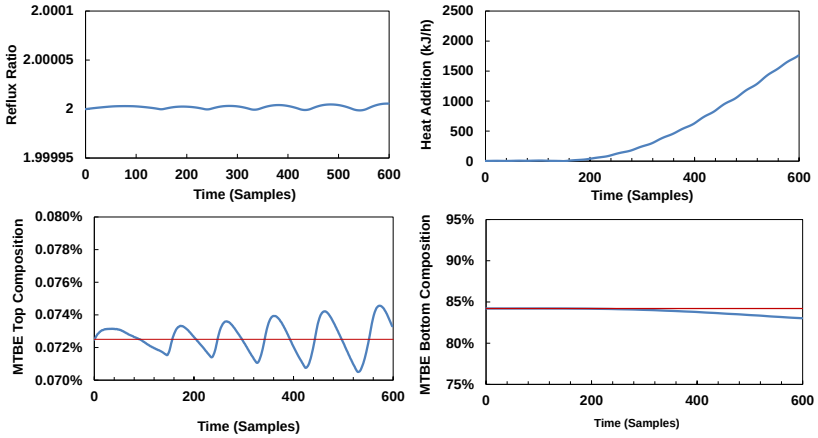

Figure 5.22 Closed-loop performance of Design alternative (1) (each time sample is 5s).

As it can be seen, the top composition loop is oscillating with a diverging trend, whereas for the bottom control loop it may take a significantly long time to reject the disturbance. With respect to Design alternative (2), in Figure 5.23, one can observe

how the large change in the bottom loop composition will eventually affect the top composition loop which again affects the bottom composition. The simulation results of Design alternative (2) reveal that this system appears to be unstable.

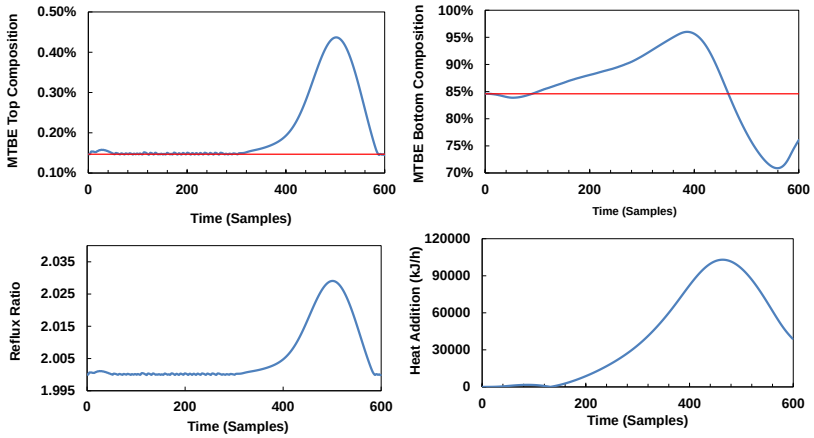

Figure 5.23 Closed-loop performance of Design alternative (2) (each time sample is 5s).

Finally, the values of the performance metrics for the design-control alternatives are calculated and compared with the design-control solution at the maximum driving force. These values are given in Table 5.9. It confirms that the reactive distillation design at the maximum driving force has the minimum value of the performance metrics.

Table 5.9 The values of the controller performance metrics for the design-control solution and alternatives (1) and (2)

Design	J_1	J_2	$J_{3,D}$ (x^D_{MTBE} by RR)	$J_{3,B}$ (x^B_{MTBE} by Q_R)	$J_{4,D}$ (x^D_{MTBE} by RR)	$J_{4,B}$ (x^B_{MTBE} by Q_R)
Design-control solution	0.0	0.00313	0.00037	0.98647	0.00277	1527.51
Design alternative (1)	0.03	0.04375	0.02411	3.79181	0.00025	6562.67
Design alternative (2)	0.15	1.00000	0.60871	353.784	0.02442	85006.39

*Note that J_3 and J_4 are calculated for both the controlled loops (controlled and manipulated variables pairings). They are the x^D_{MTBE} by RR (controlling the top composition of MTBE by reflux ratio) in the top control loop and x^B_{MTBE} by Q_R (controlling the bottom MTBE composition by reboiler duty) in the bottom control loop of the reactive distillation column (see Figure 5.20)

5.4 Application example 2: Single feed multi-element reactive distillation column

In order to demonstrate the application of the framework for integrated process design and controller design of multi-element systems, the synthesis of methyl-tert-butyl-ether (MTBE) with an inert compound and its well-known production via reactive distillation is selected (similar to application example 1). Furthermore, it is assumed in this case (since chemical reaction takes fast) that the equilibrium is achieved.

5.4.1 Step 1: Problem formulation/objective function definition

For the case of MTBE synthesis the advantages of using a reactive distillation are very well established. The reaction of methanol and isobutene yields MTBE. However, normally pure isobutene is not fed to the process and it also contains some 1-butene as impurity (inert). The MTBE reaction is exothermic and reversible and it takes place in presence of an acidic catalyst (Al-Jarallah et al., 1988). The reaction is therefore expressed as follows:

$$\begin{aligned} &isobutene\left(C_4H_8\right)+methanol\left(CH_4O\right)+1-butene\left(C_4H_8\right)\leftrightarrow \\ &MTBE\left(C_5H_{12}O\right)+1-butene\left(C_4H_8\right) \end{aligned} \tag{5.38}$$

The design feed compositions and product specifications are obtained (Pérez-Cisneros, 1997) and summarized in Table 5.10. Note however, the main target to be satisfied is the MTBE bottom composition.

Table 5.10 Design targets and product specifications (Pérez-Cisneros, 1997)

Component	Structure	Feed	Distillate	Bottom
i-butene	C_4H_8	0.590	0.773	0.061
Methanol	CH_4O	0.343	0.000	0.012
1-butene	C_4H_8	0.067	0.196	0.024
MTBE	$C_5H_{12}O$	0	0.031	0.907
Feed flowrate: 100 kmol/h; Feed temperature and pressure: 320K and 11 atm				

The design-control multi-objective performance function is defined as below:

$$f_{Obj}=\min\left(J_1,J_2,J_3,J_4,J_5\right) \tag{5.39}$$

In the above equation, a set of metrics are selected to the evaluate controller performance. They are: J_1 is the energy consumption associated with the process; J_2 is integral of the absolute error (IAE), and J_3 is total variation (TV) of inputs. These are a set of performance metrics selected to characterize the closed-loop performance of controller (see Eqs. 5.39 and 5.40).

$$J_2=IAE=\int_0^{\infty}\left|y-y_{sp}\right|dt \tag{5.35}$$

$$J_3=TV=\sum_{i=1}^{\infty}\left|u_{i+1}-u_i\right| \tag{5.36}$$

J_4 and J_5 are set of metrics to evaluate the appropriateness of the control structure and they are RGA which for the design at the maximum driving force should propose the structure with the least interactions between the loops, and N_I which is a measure of system stability, respectively.

5.4.2 Step 2: Identify the number of elements present in the system

The number of elements present in the system is identified by applying Eq. (3.17). In this case there are four compounds and one reaction. Therefore, the reaction mixture is represented by three elements and the formula matrix is given in Table 5.11.

Table 5.11 Elements representing the system and formula matrix

Isobutene (C_4H_8) + Methanol (CH_3OH) + 1-Butene ↔ MTBE ($C_5H_{12}O$) + 1-Butene				
Element definition: $A = C_4H_8$ $B = CH_3OH$ $C = C_4H_8$ (*isomer*)				
Element reaction: $A + B + C \leftrightarrow AB + C$				
Formula Matrix				
	Isobutene	Methanol	MTBE	1-Butene
A	1	0	1	0
B	0	1	1	0
C	0	0	0	1

5.4.3 Step 3: Identify the key elements

Following the rules given in Step 3 of the framework and its corresponding rules for selection of key element, the light key and heavy key elements are identified as B and A to be light key (LK) and heavy key (HK) elements, respectively.

5.4.4 Step 4: Reactive distillation column design

5.4.4.1 Step 4.1: Generate vapor-liquid equilibrium data

In this step, Algorithm 4.1b is applied to generate the vapor-liquid equilibrium data. SRK equation of state has been used for vapor phase fugacity coefficients and Wilson model for liquid phase activity coefficients. The phase diagram for the MTBE multi-element system based on equivalent binary elements is presented in Figure 5.24.

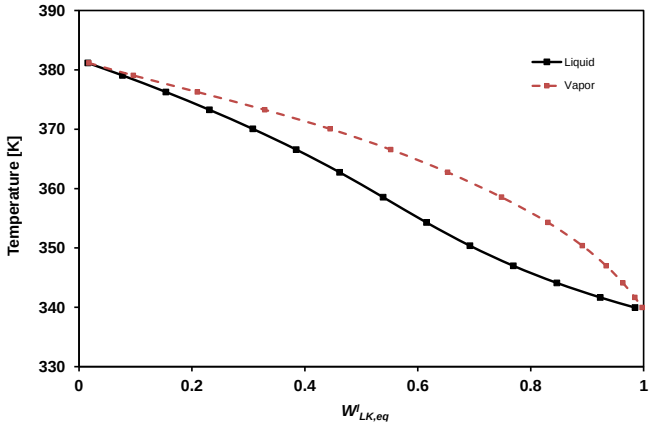

Figure 5.24 Phase diagram for MTBE multi-element system at 11 atm

5.4.4.2 Step 4.2: Reactive distillation design based on equivalent binary elements

In this step, the reactive distillation column is designed at the maximum equivalent binary driving force by applying Algorithm 4.2. The area of operation is identified on the *x*-axis of the driving force diagram given in Figure 5.25. That is the feed and design target composition on converted to element basis and then based on the key elements, they are translated to equivalent element compositions.

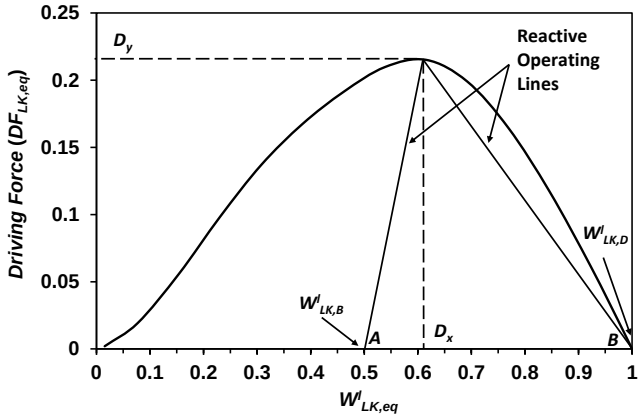

Figure 5.25 Reactive binary equivalent element driving force diagram for MTBE multi-element system.

The slopes of the lines corresponding to minimum reflux and boilup ratios are determined. Note however, in this case study since the number of stages is not given, these slopes are used in a McCabe-Thiele method to find the minimum number of stages. The equivalent binary element reactive McCabe-Thiele diagram is given in Figure 5.26. The minimum number of stages are found to be five reactive stages

plus non-reactive condenser and reboiler (from a practical point of view presence of reaction in reboiler and condenser has not been reported, therefore these two stages are added). The feed and product specifications are checked against additional conditions given in algorithm 4.1 and the feed location is identified to be at stage 4 from the top of the column.

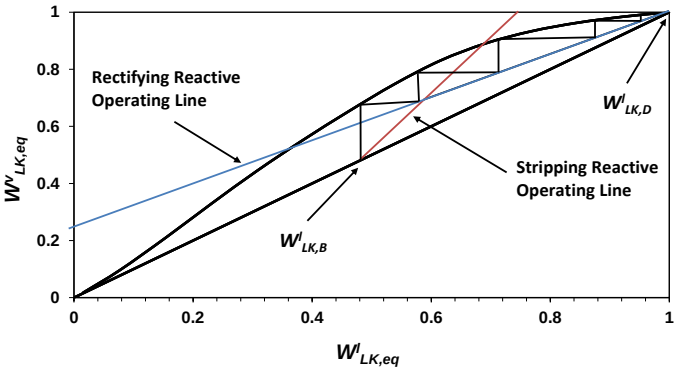

Figure 5.26 Reactive McCabe-Thiele diagram and calculations for MTBE multi-element system.

In order to verify that the design objectives in terms of product specifications are satisfied, rigorous steady-state simulation of the reactive distillation column at the maximum driving force is performed. Figure 5.27 shows the composition profile of the compounds present in the system across the column.

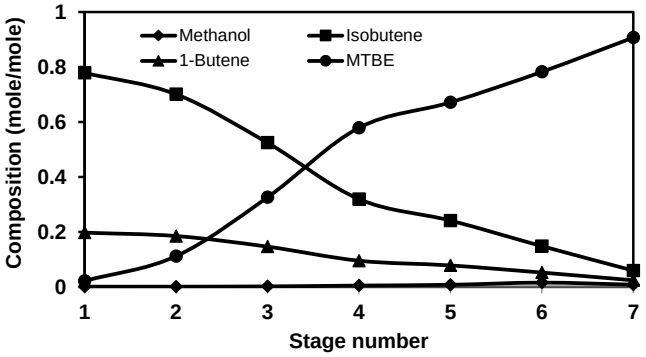

Figure 5.27 Composition profile across the reactive distillation column.

As it is shown in Figure 5.27, the design objectives set in Step 1 (see Table 1) are satisfied. It must be noted that the last step of the framework, which is dynamic validation, is to showcase that the design specifications are matched and system is sufficiently well restored to its original set-points in the presence of disturbances in the feed (load change is also a disturbance in the feed). Table 5.12, presents the reactive distillation column design parameters.

Table 5.12 Reactive distillation design parameters at the maximum driving force.

Number of stages	Feed location	Reflux ratio	Boilup ratio	Reboiler duty (kW)	Condenser duty (kW)
7	4	2.83	1.27	323.3	533.3

5.4.4.3 Step 4.3: Optimal design-control solution

The controlled variables and manipulated variables are determined according to algorithm 4.4 since the reactive distillation column is designed at the maximum equivalent binary element driving force. They are top and bottom compositions for controlled variables and, reflux rate and reboiler duty for manipulated variables. Furthermore, the values of $dDF_{LK,eq}/dW^{l}_{LK,eq}$ are calculated and plotted against $W^{l}_{LK,eq}$. As it is shown in Figure 5.28, at the maximum driving force there is the least sensitivity of the controlled variables to the disturbances, and, the highest sensitivity to the manipulated variables. The control structure is therefore determined by Eq. (4.23). Note that $dDF_{LK,eq}/dW^{l}_{LK,eq}$ on the *y*-axis of Figure 5.28 corresponds to the slope of the line between each two points on the driving force diagram (see Figure 5.25) which in turn corresponds to the derivative value the driving force with respect to $W^{l}_{LK,eq}$.

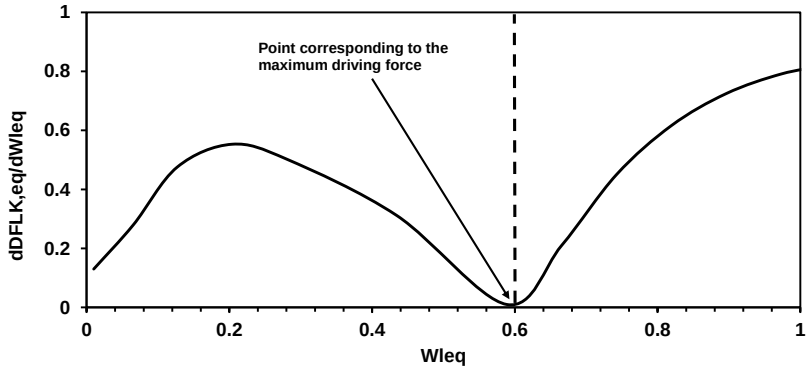

Figure 5.28 The values of $dDF_{LK,eq}/dW^{l}_{LK,eq}$ are calculated and plotted against $W^{l}_{LK,eq}$ for MTBE reactive system.

5.4.5 Step 5: Dynamic analysis and verification

5.4.5.1 Step 5.1: Control structure verification

In order to verify the control structure, algorithm 5.1 is applied. The linearized model of the process, i.e. state-space model is obtained and the steady-state gain matrix was constructed for a 2×2 system. The gain matrix had non-zero determinant and the RGA is obtained as follows:

$$RGA = \begin{bmatrix} 1.06 & -0.06 \\ -0.06 & 1.06 \end{bmatrix}$$

Therefore, it can be verified that selected controller pairing for the design corresponding to the maximum driving force has the least interactions between the loops as the diagonal values (for a 2×2 system) are close to unity. Furthermore, the Niederlinski index (N_I) is calculated and it is found to be N_I =0.0372 which is positive. This verifies that the system is not unstable.

5.4.5.2 Step 5.2: Control structure evaluation

In order to evaluate the performance of the control structure, algorithm 5.2 is applied. To this end, first open-loop simulation is performed in presence of a disturbance scenario which is a +16.5% step change in the methanol flowrate. The open-loop response of the system to this disturbance is shown in Figure 5.29. The controller structure is then implemented using Proportional-Integral (PI) type controllers on the reactive distillation according to Eq. (4.23). The controller tuning parameters are obtained using IMC rules. Furthermore, a perfect pressure control is assumed and the level controllers for reboiler and condenser are Proportional (P) type controllers.

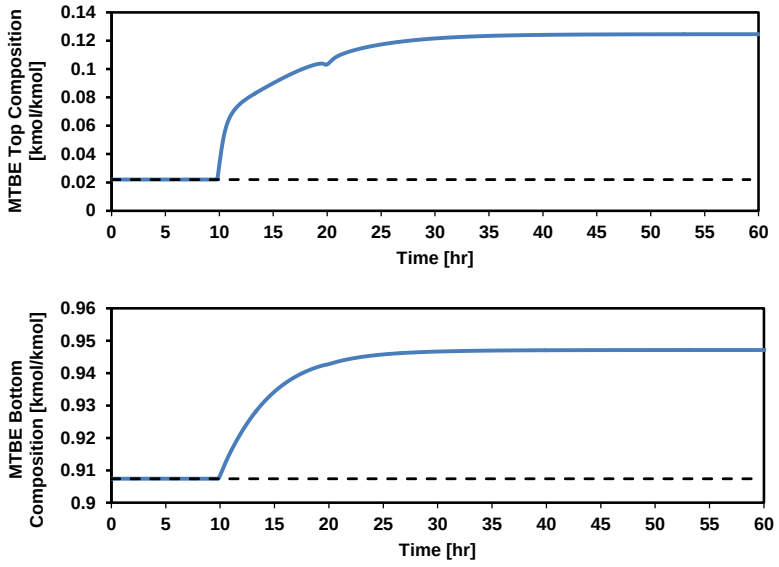

Figure 5.29 Open-loop response of the optimal design-control solution to a disturbance in the feed.

Figure 5.30, presents the closed-loop performance of the reactive distillation column design to +16.5% step change in methanol feed flowrate as a disturbance. As it can be seen in Figure 5.30, the control structure is able to reject the disturbance efficiently with a very small over shoot in controlled variables. Furthermore, this shows that the design is least sensitive to the disturbances and has the highest sensitivity to

manipulated variables. That is with a very small effort in the manipulated variables, the process is recovered back to its original set-point.

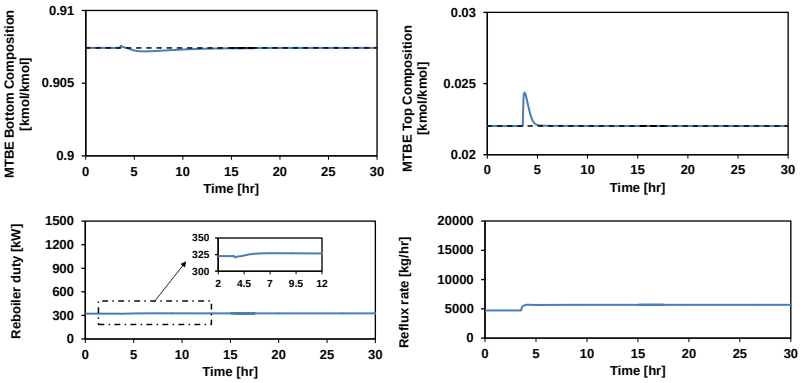

Figure 5.30 Closed-loop performance of design-control solution to a disturbance in the feed.

Note that, it can be readily observed from the output of this step of the framework that the process design does take into account the operational and product specifications. Also, the safety issues are not considered because none of the operating conditions correspond to extreme conditions of operation. The driving force based design is obtained to match the product specification and gives the easiest operation (defined by temperature and pressure since the driving force diagram is a function of these variables). Therefore, at the maximum driving force the operation should be safer than any other point.

5.4.5.3 Step 5.3: Final selection

In this step, the values of the terms included in the performance objective function are calculated and presented in Table 5.13.

Table 5.13 The values of the terms in performance objective objective function for design-control solution in application example 2.

J_1* [kW]	$J_{2,D}$ [hr]	$J_{2,B}$ [hr]	$J_{3,D}$ [-]	$J_{3,B}$ [-]	J_4 [-]	J_5 [-]
856.6	1.54E-03	1.47E-03	1026.22	2154.7	$\begin{bmatrix} 1.06 & -0.06 \\ -0.06 & 1.06 \end{bmatrix}$	0.0372

*The total energy consumption of the process, i.e. sum of reboiler and condenser duties.
** Note that J_2 and J_3 are calculated for both the controlled loops (controlled and manipulated variables pairings). They are the x^D_{MTBE} by RR (controlling the top composition of MTBE by reflux ratio) in the top control loop and x^B_{MTBE} by Q_R (controlling the bottom MTBE composition by reboiler duty) in the bottom control loop of the reactive distillation column.

5.4.5.3.1 Further verification of design-control solution using design alternatives which are not at the maximum driving force

In order to establish the appropriateness of the framework presented in this work, alternative reactive distillation column designs which are not at the maximum driving force are selected for comparison. For purpose of comparison the number of stages needs to be the same for all cases. It would be equivalent if the number of stages is allowed to change but the reflux is kept constant (separation would be feasible for the maximum driving force and infeasible for any other design not using the maximum driving force). Here, the objective is to show the operational cost, then the number of stages needs to be fixed – but the feed locations are changed. Also, for the comparison consistency, here we are using the same control structure as given in Eq. (4.23) for all the alternatives. The selected design alternatives are summarized in Table 5.14.

Table 5.14 Summary of alternative designs selected for verification as well as design-control solution (see Table 5.12).

Design	Number of stages	Feed location	Reflux ratio	Boilup ratio	Reboiler duty (kW)	Condenser duty (kW)
Design-Control Solution	7	4	2.83	1.27	323.3	533.3
Alter. 1	7	2	7.0	3.9	942.5	1162.7
Alter. 2	7	3	4.4	2.16	540.7	751.9
Alter. 3	7	5	5.65	2.61	663.1	873.1

The steady-state simulation of all the designs is performed and it is verified that they all satisfy the design targets. Furthermore, Algorithm 5.1 was applied and RGA and N_I are calculated for all the designs given in Table 5.14 (these are summarized in Table 5.15). Next, Algorithm 5.2 is applied and the closed-loop performance of all the alternatives is evaluated in presence of the same disturbance as for design-control solution. The results of the closed loop performance of the alternatives are given in Figures 5.31 – 5.33.

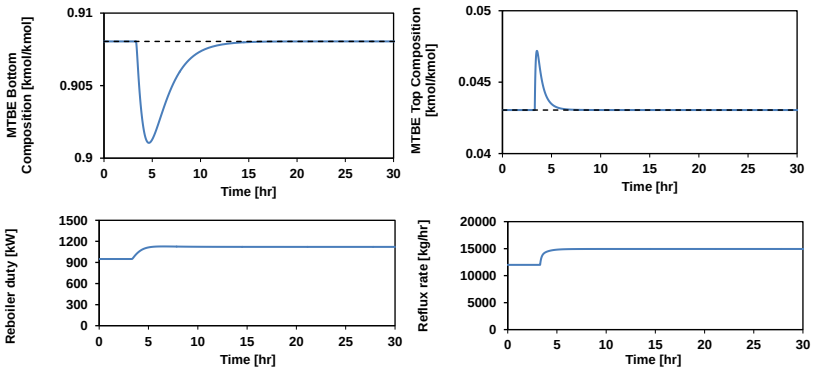

Figure 5.31 Closed-loop performance of design alternative 1 in presence of a disturbance in the feed.

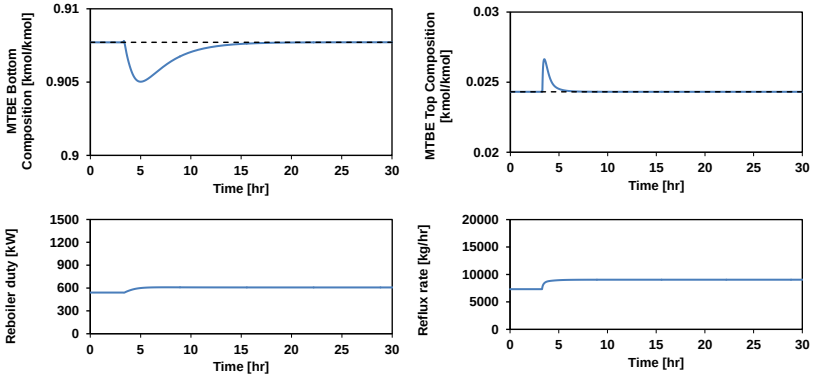

Figure 5.32 Closed-loop performance of design alternative 2 in presence of a disturbance in the feed.

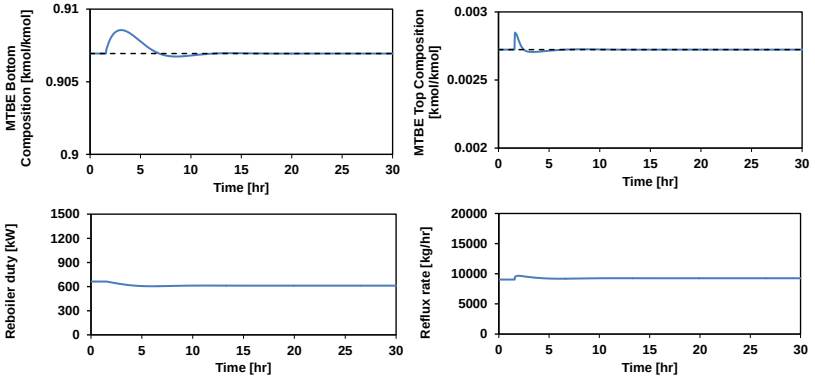

Figure 5.33 Closed-loop performance of design alternative 3 in presence of a disturbance in the feed.

Table 5.15, presents the values of the performance objective function for all designs including design-control solution. As it is given in Table 5.15, the design-control solution which corresponds to the reactive distillation column designed at the maximum driving force has the least values of the terms in the objective function both from a steady-state design point of view (nominal energy consumption) and from a control point of view.

Table 5.15 Summary of the comparison of performance objective function terms for design-control solution and alternative designs.

Obj. Function Parameter	Design-control solution	Alter. 1	Alter. 2	Alter. 3
J_1* [kW]	856.6	2112.2	1292.6	1536.3
$J_{2,D}$ [hr] (x^D_{MTBE} by RR)	1.54E–03	3.59E–03	1.30E–02	5.74E–03
$J_{2,B}$ [hr] (x^B_{MTBE} by Q_R)	1.47E–03	2.49E–02	1.95E–03	1.03E–04
$J_{3,D}$ [-] (x^D_{MTBE} by RR)	1026.2	2947.1	1725.14	1212.56
$J_{3,B}$ [-] (x^B_{MTBE} by Q_R)	2155	44309	17744	16264
J_4 [-]	$\begin{bmatrix} 1.06 & -0.06 \\ -0.06 & 1.06 \end{bmatrix}$	$\begin{bmatrix} -0.29 & 1.29 \\ 1.29 & -0.29 \end{bmatrix}$	$\begin{bmatrix} 1.34 & -0.34 \\ -0.34 & 1.34 \end{bmatrix}$	$\begin{bmatrix} -1.22 & 2.22 \\ 2.22 & -1.22 \end{bmatrix}$
J_5 [-]	0.0372	–3.447	0.7453	–0.8147

*The total energy consumption of the process, i.e. sum of reboiler and condenser duties.
** Note that J_2 and J_3 are calculated for both the controlled loops (controlled and manipulated variables pairings). They are the x^D_{MTBE} by RR (controlling the top composition of MTBE by reflux ratio) in the top control loop and x^B_{MTBE} by Q_R (controlling the bottom MTBE composition by reboiler duty) in the bottom control loop of the reactive distillation column.

5.4.5.3.2 Application of model predictive controller on the design-control solution

A model predictive controller (MPC) uses linear plant, disturbance, and noise models to estimate the controller state and predict future plant outputs. Using the predicted plant outputs, the controller solves a quadratic programming optimization problem to determine optimal manipulated variable adjustments. In this case, the A, B, and C matrices of a standard continuous-time state-space model are obtained in Algorithm 5.1-*Step* (i) for the design-control solution at the maximum driving force. D matrix is zero. Using the linear model of the process, a MPC-type controller is implemented to perform closed-loop simulations on the design-control solution at the maximum driving force. Here, the plant inputs are: condenser duty - Q_c (kW), reboiler duty – Q_R (kW), reflux mass flow rate – R (kg/h), distillate mass flow rate - D (kg/h), bottoms mass flow rate -B (kg/h) and the feed molar flow rate (kmol/h). The plant outputs are: column pressure - P (stage 1), reflux drum liquid level - RLev (m), sump liquid level - SLev (m), mole fraction of MTBE in the distillate - *x*D and mole fraction of MTBE in the bottoms - *x*B. Figure 16, presents the MPC implementation on design-control solution and comparison with the MPC implementation on design alternative 1. The disturbance scenario considered in Figure 16 is +10% step change in in the total feed flowrate. As it is shown in Figure 5.34(a), the MPC controller performance is better at the maximum driving force compared to the MPC performance of the design alternative 1. This is revealed by looking at the controlled variables (the time to reach the set-point) as well as the effort in manipulated variables.

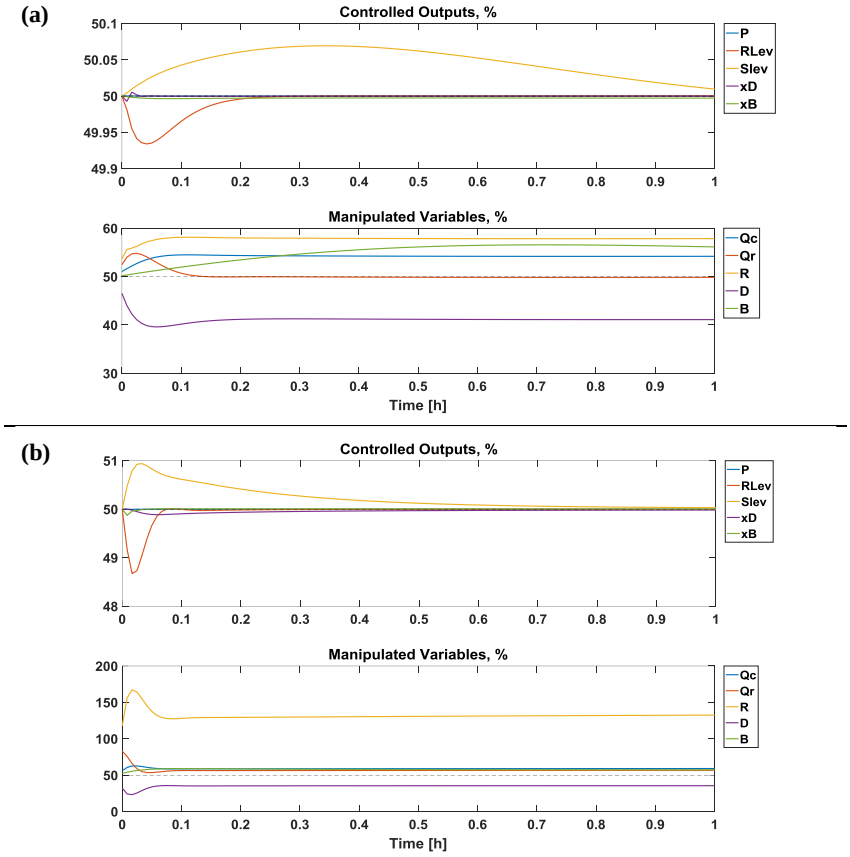

Figure 5.34 (a) closed-loop performance of the design-control solution, (b) closed-loop performance of design Alternative 1; using MPC implementation in presence of +10% step change in total feed flowrate.

Figure 5.35(a), shows the comparison of controlled outputs (*x*D and *x*B) using MPC implementation and PI controllers for the design-control solution at the maximum driving force to a +10% disturbance in total feed flowrate. It is readily observed from this figure, that the MPC has a better performance compared to the PI controller. However, Figure 5.35(b) shows the same comparison for an operating point which are not at the maximum driving force (design alternative 1). Looking at the comparison presented in Figure 5.35, it can be concluded that the design at the maximum driving force has a better controller performance, regardless of the choice of controller (MPC or PI), compared to any other operating point which is not at the maximum driving force. Therefore, it is verified that the design-control solution has a satisfactory performance not only using controllers at the regulatory level, but also advanced control algorithms such as MPC.

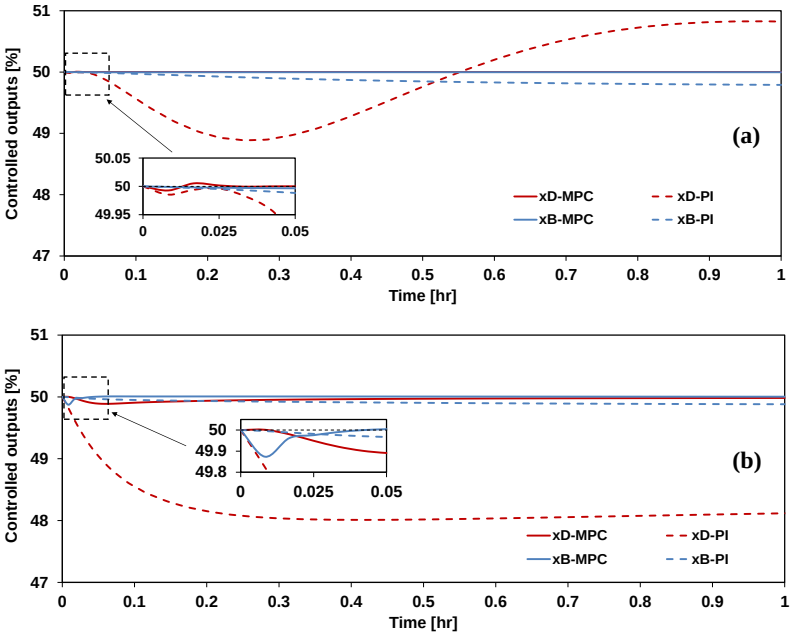

Figure 5.35 Comparison between controlled outputs (*x*D and *x*B) of model predictive controller (MPC) and proportional-integral (PI) controllers for (a) the design-control solution operating at the maximum driving force, and (b) the design Alternative 1 (not at the maximum driving force).

5.5 Application example 3: Two feed multi-element reactive distillation column

Babi et al. (2014) have demonstrated the advantages and feasibility of methyl-acetate production via intensified processes (in this case reactive distillation column). Through the rigorous simulation of several reactive distillation alternatives, they have found that reactive distillation columns with one feed will give methanol/methyl-acetate azeotrope in the top and water/acetic acid mixture at the bottom by analyzing reactive residue curve maps. However, based on their analysis reactive distillation columns with two feeds can give almost pure water at the bottom of the column and high purity methyl-acetate at the top. Nonetheless, reactive distillation columns with both reactive and non-reactive sections are preferred in this case given lower catalyst costs, assuming that the column specifications are the same. Therefore, in this example, the production of methyl-acetate via a reactive distillation column that has two feeds of the same flowrate of methanol and acetic acid; and both reactive and non-reactive sections are considered.

5.5.1 Step 1: Problem formulation/objective function definition

The design objective in this section is to obtain the reactive distillation column design operating at the maximum driving force to produce methyl-acetate with a purity of 99% ± 0.5% on a molar basis. The reaction between methanol (MeOH) and acetic acid (HOAc) yields methyl acetate (MeOAc) and water (H_2O). The reaction takes place in liquid phase over a catalyst. It is exothermic with a heat of reaction pf –5.42 kJ/mol and is given as follows:

$$MeOH\left(CH_4O\right) + HOAc\left(C_2H_4O_2\right) \leftrightarrow MeOAc\left(C_3H_6O_2\right) + Water\left(H_2O\right)$$

The design targets for a reactive distillation column with only reactive section is obtained from Jantharasuk et al. (2011) and is given as follows:

Table 5.16 Design targets and product specifications (Jantharasuk et al., 2011)

Component	Structure	Feed (1)	Feed (2)	Distillate	Bottom
Methanol	C_4H_8	1	0	0.0694	0
Acetic Acid	CH_4O	0	1	0.0089	0.3345
Methyl Acetate	C_4H_8	0	0	0.7612	0
Water	$C_5H_{12}O$	0	0	0.1606	0.6651
Feed (1): 230.28 kmol/h methanol; Feed temperature and pressure: 328K and 1 atm					
Feed (2): 230.28 kmol/h acetic acid; Feed temperature and pressure: 328K and 1 atm					

Note however, the design targets specified in Table 5.16 will be used in course of distillation column design. As it is mentioned previously, the final distillation column design target (including both reactive and non-reactive sections) is to obtain 99% pure methyl-acetate on a molar basis.

Likewise previous application examples, a similar objective function are also defined in this case. The design-control multi-objective performance function is defined as below (repeated from section 5.4):

$$f_{Obj} = \min\left(J_1, J_2, J_3, J_4, J_5\right) \tag{5.40}$$

In the above equation, a set of metrics are selected to the evaluate controller performance. They are: J_1 is the energy consumption associated with the process; J_2 is integral of the absolute error (IAE), and J_3 is total variation (TV) of inputs. These are a set of performance metrics selected to characterize the closed-loop performance of controller (see Eqs. 5.35 and 5.36 – repeated from section 5.3).

$$J_2 = IAE = \int_0^\infty \left| y - y_{sp} \right| dt \tag{5.35}$$

$$J_3 = TV = \sum_{i=1}^{\infty} \left| u_{i+1} - u_i \right| \tag{5.36}$$

J_4 and J_5 are set of metrics to evaluate the appropriateness of the control structure and they are RGA which for the design at the maximum driving force should propose the structure with the least interactions between the loops, and N_I which is a measure of system stability, respectively.

5.5.2 Step 2: Identify the number of elements present in the system

The number of elements present in the system is identified by applying Eq. (3.17). A discussion by Pöpken et al. (2001) specified that any side reaction is completely suppressed by using near-stoichiometric feeds (1:1 ration in this case – see Table 5.16). Therefore, in this case there are four compounds and one reaction, thereby the reaction mixture is represented by three elements and the formula matrix is given in Table 5.17.

Table 5.17 Elements representing the system and formula matrix

Methanol (CH_4O) + Acetic Acid ($C_2H_4O_2$) ↔ Methyl Acetate ($C_3H_6O_2$) + Water (H_2O)
Element definition: $A = CH_4O$ $B = C_2H_2O$ $C = H_2O$
Element reaction: $A + BC \leftrightarrow AB + C$

	Formula Matrix			
	Methanol	Acetic Acid	Methyl Acetate	Water
A	1	0	1	0
B	0	1	1	0
C	0	1	0	1

5.5.3 Step 3: Identify the key elements

In order to identify the key elements, the rules of key element selection are applied. Therefore, element C is selected as the non-key element, element A is the light key element (LK) and element B is the heavy key element (HK).

5.5.4 Step 4: Reactive distillation column design

5.5.4.1 Step 4.1: Generate vapor-liquid equilibrium data

In this step, algorithm 4.1b is applied. Like the previous application examples (see application examples 1 and 2 – sections 5.3 and 5.4), the SRK equation of state is

selected to calculate the vapor phase fugacity coefficients and Wilson model is used to calculate liquid phase activity coefficients. The phase diagram for this reactive system based on the equivalent binary elements is presented in **Figure 5.36**.

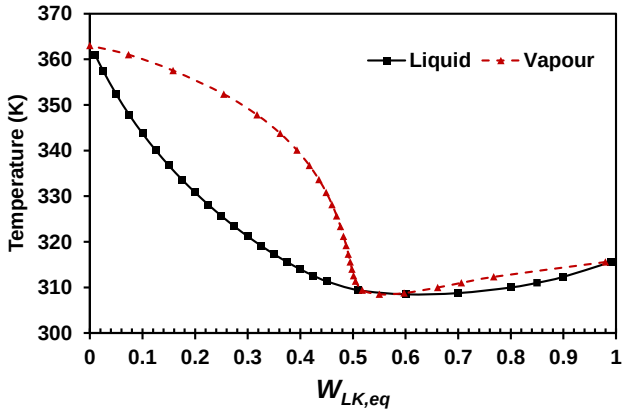

Figure 5.36 Phase diagram for methyl-acete multi-element system at 1 atm.

5.5.4.2 Step 4.2: Reactive distillation design based on equivalent binary elements

In this step, algorithm 4.3 for design of reactive distillation columns with two feeds involving multi-elements is applied. Therefore, the driving force diagram is constructed and the area of operation for the reactive distillation column without non-reactive stages is identified as depicted in Figure 5.37.

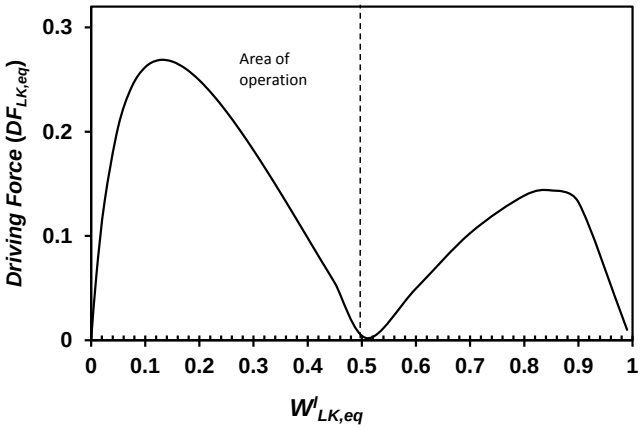

Figure 5.37 Reactive driving force diagram for methyl-acete multi-element system at 1 atm.

Following the guidelines in algorithm 4.3, the area of operation is rescaled between 0-1 in the composition domain on the *x*-axis of the driving force diagram and the corresponding McCabe-Thiele diagram is constructed. Note that in this particular case, the composition of the feeds (W_k , W_h) and the design targets in the distillate and bottom compositions (W^D , W^B). That is, the light key equivalent element composition is in pure state in one feed (W_k = 1) and does not exist in the other feed (W_h = 0). Figure 5.38 shows the result of application of algorithm 4.3 to design methyl-acetate multi-element reactive distillation column with two feeds.

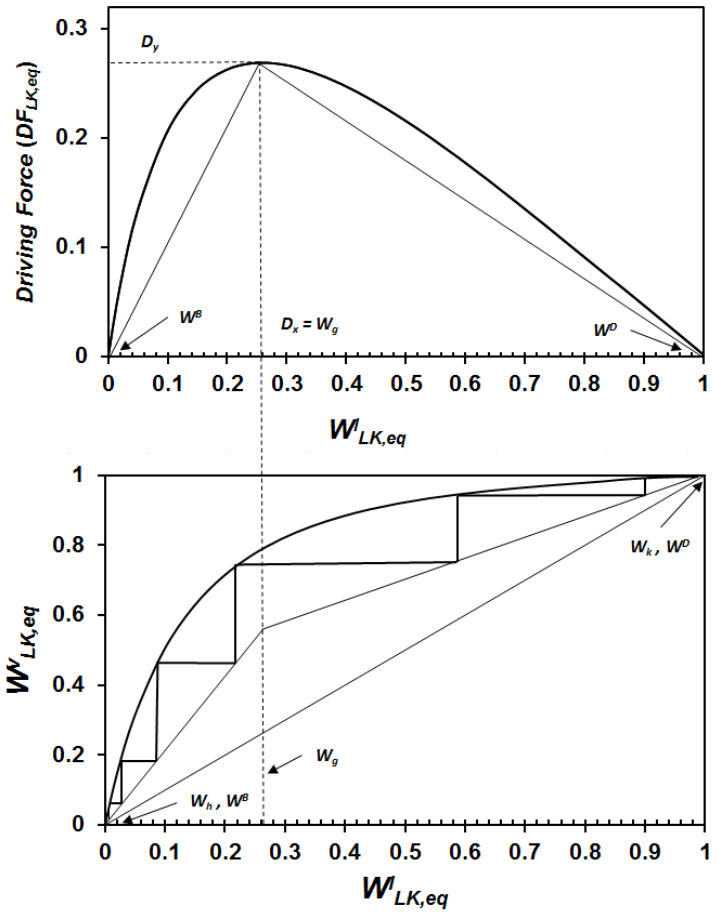

Figure 5.38 Reactive distillation column design for methyl-acetate multi-element system at 1 atm.

Therefore, the reactive distillation column without non-reactive stages and two feeds has six reactive stages plus non-reactive reboiler and condenser. Therefore, the reactive distillation column has eight stages. The feed that contains light key element (methanol) is introduced at the fist reactive stage and the other feed (which does not

contain the light key element – acetic aicd) is introduced at the last reactive stage. The reflux ratio is determined to be 2.2 according to the driving force method. Figure 5.39, presents composition profile across the column. It is seen from this figure that the design targets for the reactive distillation column with only reactive section has been satisfied (see Table 5.16).

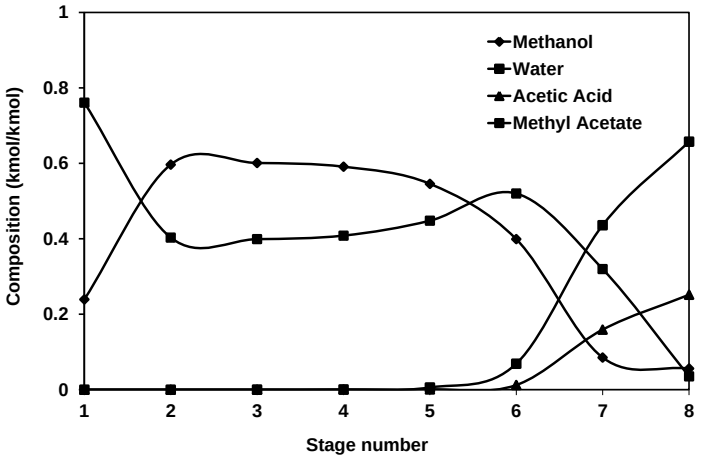

Figure 5.39 Composition profiles across the reactive distillation column with only reactive section and two feeds.

Note that according to the design objectives, the reactive distillation column with non-reactive stages capable of producing 99% ± 0.5% pure methyl acetate is desired. Therefore, non-reactive stages are added to the top and bottom of the reactive zone, one at the time, until the design targets are satisfied. Table 5.18, gives the nominal steady-state values for the final reactive distillation column design feed two feeds, reactive and non-reactive section, which is operating at the maximum driving force. The reactive distillation column has 45 stages where the feeds are introduced to the top and the bottom of reactive zone at stages 7 and 12, with $RR = 2.2$.

Table 5.18 Nominal steady-state values for multi-element reactive distillation column with two feeds and, reactive and non-reactive section.

Variable	Optimal design-control solution
Distillate Temperature (K)	305
Bottom Temperature (K)	357.9
Feed composition - MeOH (kmol/kmol)	$z_{Methanol}^{F_{methanol}} = 1; z_{MeOAc}^{F_{methanol}} = 0; z_{HOAc}^{F_{methanol}} = 0; z_{Water}^{F_{methanol}} = 0$
Feed composition - HOAc (kmol/kmol)	$z_{Methanol}^{F_{HOAc}} = 0; z_{MeOAc}^{F_{HOAc}} = 0; z_{HOAc}^{F_{HOAc}} = 1; z_{Water}^{F_{HOAc}} = 0$
Distillate composition (kmol/kmol)	$z_{Methanol}^{D} = 0.012; z_{MeOAc}^{D} = 0.985;$ $z_{HOAc}^{D} = 0; z_{Water}^{D} = 0.001$

Bottom composition (kmol/kmol)	$z^B_{Methanol} = 0.099; z^B_{MeOAc} = 0.007;$ $z^B_{HOAc} = 0.110; z^B_{Water} = 0.784$
Reboiler duty (GJ/h)	15.87
Condenser duty (GJ/h)	22.8
Reflux ratio	2.2
Number of reactive stages	6 (stage 7 – stage 12)
Number of stages	45
Feed location	Methanol feed = stage 7; Acetic acid feed = stage 12

5.5.4.3 Step 4.3: Optimal design-control solution

The controlled variables and manipulated variables are determined according to algorithm 4.4 given the reactive distillation column is designed at the maximum equivalent binary element driving force. They are top and bottom compositions for controlled variables and, reflux rate and reboiler duty for manipulated variables. Figure 5.40 shows the the values of $dDF_{LK,eq}/dW^l_{LK,eq}$ versus $W^l_{LK,eq}$. Therefore, at the maximum driving force there is the least sensitivity of the controlled variables to the disturbances, and, the highest sensitivity to the manipulated variables. The control structure is therefore determined by Eq. (4.22).

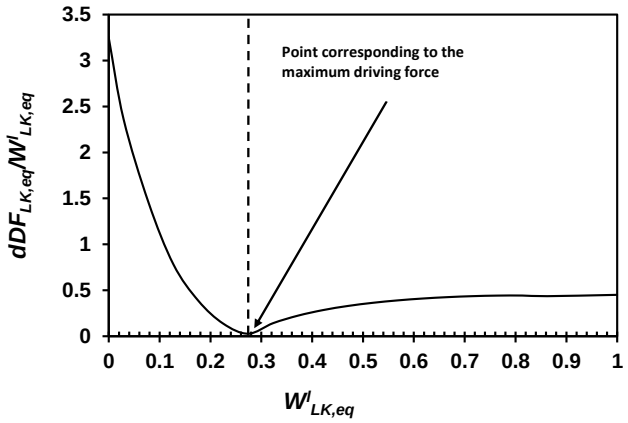

Figure 5.40 The values of $dDF_{LK,eq}/dW^l_{LK,eq}$ are calculated and plotted against $W^l_{LK,eq}$ for methyl acetate reactive system.

5.5.5 Step 5: Dynamic analysis and verification

5.5.5.1 Step 5.1: Control structure verification

The control structure obtained from algorithm 4.4 is verified by algorithm 5.1. To this end, the steady-state gain matrix for a 2×2 system is obtained. The gain matrix had non-zero determinant. The RGA for the rearranged system such that it represents the control structure by Eq. (4.23) is obtained as follows:

$$RGA = \begin{bmatrix} 1.10 & -0.10 \\ -0.10 & 1.10 \end{bmatrix}$$

Now it is verified that the control structure at corresponding to the maximum driving force is the feasible control structure as the diagonal values (for a 2×2 system) are close to unity. Since the other pairing has negative RGA element values, they are not recommended. Moreover, the Niederlinski index (N_I) is calculated and it is found to be N_I = 0.9048. This verifies that the system is not unstable.

5.5.5.2 Control structure evaluation

Here, algorithm 5.2 is applied. Therefore, two disturbance scenarios are considered: (1) +10% step change in the flowrate in feed stream 1 (methanol), and (2) +10% step change in the flowrate in the feed stream 2 (acetic acid). The transient response of the process in controlled variables in an open-loop is shown in

Figure **5.41** and

Figure **5.42** for disturbance scenario 1 and 2, respectively.

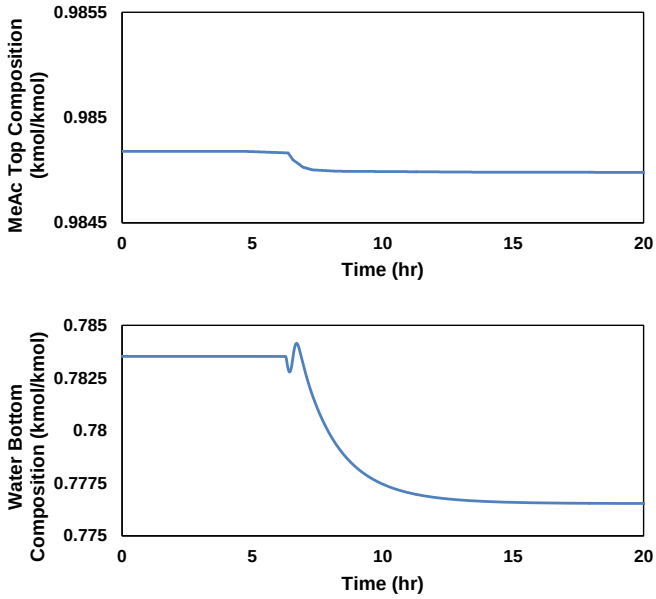

Figure 5.41 Open-loop response to a +10% step change in the flowrate of feed 1 (methanol)

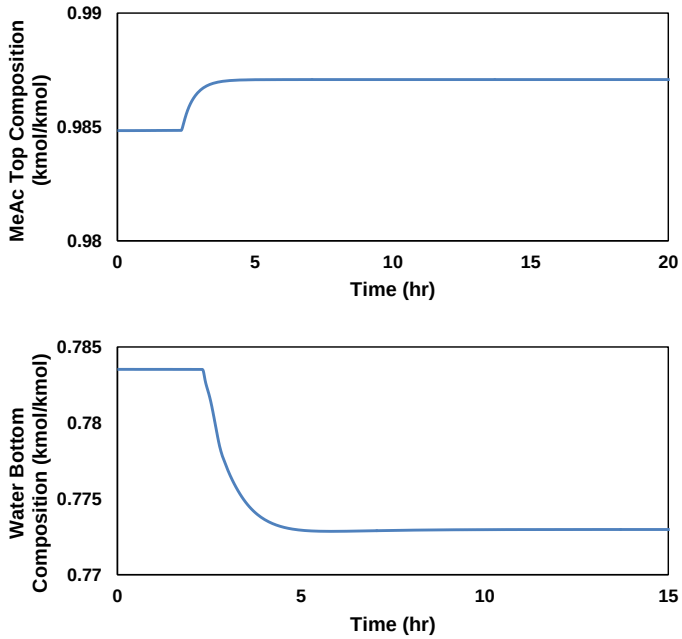

Figure 5.42 Open-loop response to a +10% step change in the flowrate of feed 2 (acetic acid)

Figure 5.43 and Figure 5.44 show the closed-loop response of the controller structure at the maximum driving force to the disturbance scenario 1 and 2, respectively.

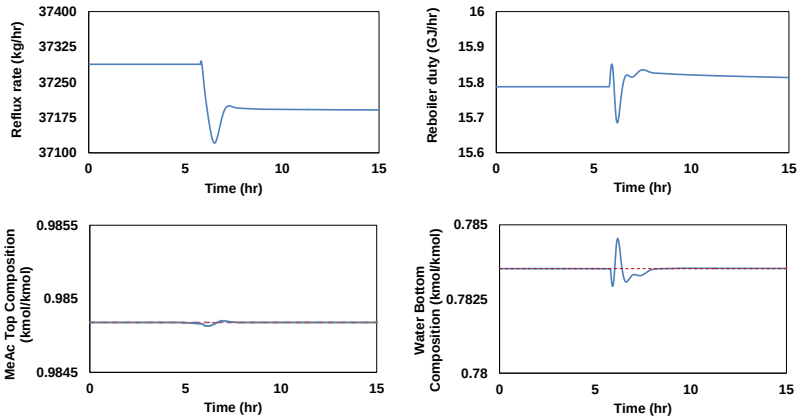

Figure 5.43 Closed-loop response of the process to a +10% step change in the flowrate of feed 1 (methanol)

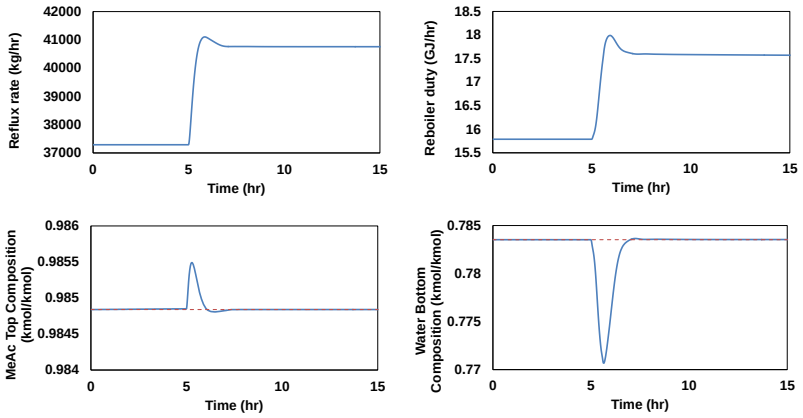

Figure 5.44 Closed-loop response of the process to a +10% step change in the flowrate of feed 2 (acetic acid)

As it is seen in these figures, the controller structure is able to reject the disturbance sufficiently well and restore the process back to its original set-points in case of both disturbances. Therefore, it is concluded, that the multi-element reactive distillation column with two feeds and, reactive and non-reactive sections which is operating at the maximum driving force has the ability to reject the disturbances in the feed using the controller structure that is also determined at the maximum driving force.

5.5.5.3 Final selection

Table 5.19, lists the terms of the performance objective function for the design control solution at the maximum driving force.

Table 5.19 The values of the terms in performance objective objective function for design-control solution in application example 3.

J_1* [GJ/hr]	$J_{2,D}$ [hr]	$J_{2,B}$ [hr]	$J_{3,D}$ [-]	$J_{3,B}$ [-]	J_4 [-]	J_5 [-]
38.67	0.0002	0.0081	269.2	16.23	$\begin{bmatrix} 1.10 & -0.10 \\ -0.10 & 1.10 \end{bmatrix}$	0.9048

* The total energy consumption of the process, i.e. sum of reboiler and condenser duties.
** Note that J_2 and J_3 are calculated for both the controlled loops (controlled and manipulated variables pairings). They are the x^{D}_{MeOAc} by RR (controlling the top composition of MeOAc by reflux ratio) in the top control loop and x^{B}_{Water} by Q_R (controlling the bottom water composition by reboiler duty) in the bottom control loop of the reactive distillation column.
*** J_2 and J_3 are only given for a +10% step disturbance in flowrate of feed 1 (methanol)

Further verification of design-control solution

Similar to the previous application examples, an alternative reactive distillation column design which is not operating at the maximum driving force is selected to demonstrate the appropriateness of the framework. For the purpose of comparison, the number of reactive and non-reactive stages as well as the location of the reactive section in the column is the same; and only the feed locations are altered in case of the alternative design. The alternative reactive distillation column for comparison is summarized in Table 5.20.

Table 5.20 Design parameters for alternative methyl acetate reactive distillation column not at the maximum driving force.

Design parameter	Value
Reboiler duty (GJ/h)	46.79
Condenser duty (GJ/h)	54.36
Reflux ratio	6.28
Number of reactive stages	6 (stage 7 – stage 12)
Number of total stages	45
Feed location	Methanol feed = stage 9 Acetic acid feed = stage 12

Next, algorithm 5.1 is applied and the RGA and N_I are calculated for the design alternative (see Table 5.21). Figure 5.45 and Figure 5.46 show the closed-loop performance of the design alternative in presence of disturbance scenario 1 and 2.

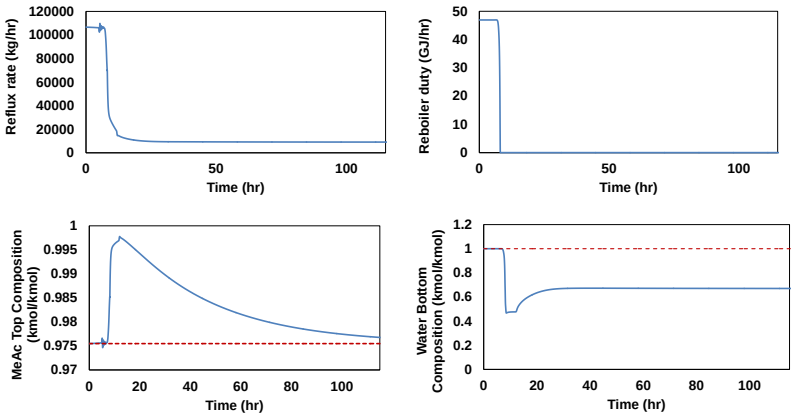

Figure 5.45 Closed-loop performance of design alternative for methyl-acetate reactive distillation to a +10% step change in flowrate of feed 1 (methanol)

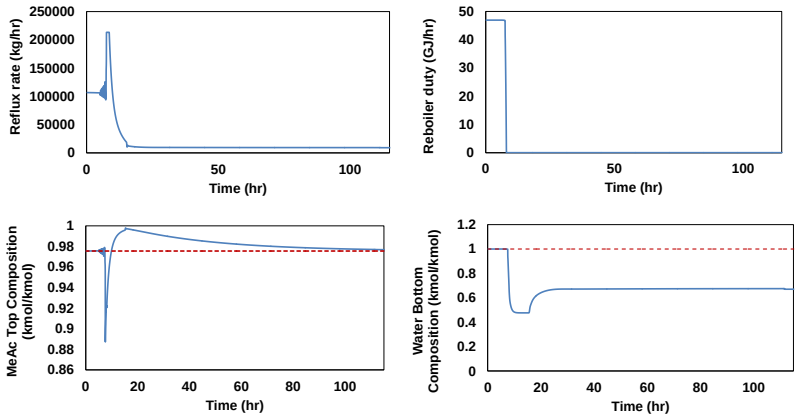

Figure 5.46 Closed-loop performance of design alternative for methyl-acetate reactive distillation to a +10% step change in flowrate of feed 2 (acetic acid)

As it is seen in Figure 5.45 and Figure 5.46, the controller is not able to sufficiently restore all controlled variables to their set-points. Furthermore, a very long settling time is observed in the controlled variables. Therefore, it further verifies that moving away from the maximum driving force will result in a more difficult control of the reactive distillation column. Table 5.21, lists the comparison between the design-control solution and the alternative reactive distillation column design in terms of performance objective function parameters.

Table 5.21 Summary of the comparison of performance objective function terms for design-control solution and alternative designs.

Obj. Function Parameter	Design-control solution	Alternative design
J_1* [GJ/hr]	38.67	101.15
$J_{2,D}$ [hr]	0.0002	8.716
$J_{2,B}$ [hr]	0.0081	369.9
$J_{3,D}$ [-]	269.2	126999.1
$J_{3,B}$ [-]	16.23	46.72
J_4 [-]	$\begin{bmatrix} 1.10 & -0.10 \\ -0.10 & 1.10 \end{bmatrix}$	$\begin{bmatrix} 1.23 & -0.23 \\ -0.23 & 1.23 \end{bmatrix}$
J_5 [-]	0.9048	0.8128

* The total energy consumption of the process, i.e. sum of reboiler and condenser duties.
** Note that J_2 and J_3 are calculated for both the controlled loops (controlled and manipulated variables pairings). They are the x^D_{MeOAc} by RR (controlling the top composition of MeOAc by reflux ratio) in the top control loop and x^B_{Water} by Q_R (controlling the bottom water composition by reboiler duty) in the bottom control loop of the reactive distillation column.
*** J_2 and J_3 are only given for a +10% step disturbance in flowrate of feed 1 (methanol)

Therefore, looking at Table 5.21, it si readily concluded that the design-control solution at the maximum driving force has a better performance compared to a design alternative which is not operating at the maximum driving force.

6
CONCLUSIONS AND FUTURE WORK

6.1 Conclusions

In this work, integrated design and control of reactive distillation processes that can be represented by two elements (binary elements) and multi-elements (more than two elements), has been considered through an integrated design-control method implemented in a computer-aided framework. Process design and controller design issues have been considered simultaneously to assure that design decisions give the optimal controllability and economic performance. The framework is generic and can be applied to any reactive distillation process that is represented as a binary or multi-element system. Also, in principle, it should be applicable to any non-reactive distillation process separating a binary mixture. The framework utilizes a number of algorithms for design and control in different steps. The design methods and tools, which are similar in concept to non-reactive distillation design have been derived and implemented in the framework. These methods are based on the element concept. The application of the framework has been highlighted through the MTBE reactive distillation process for binary and multi-element single feed reactive distillation columns. Also, its application for a two feed multi-element reactive distillation column with reactive and non-reactive sections has been demonstrated through a methyl-acetate reactive distillation process. The optimal design-control solution has been verified and confirms the design-control corresponding to the maximum driving force is less sensitive to the disturbances in the feed and has the ability to reject disturbances with minimum interaction between the control loops. The design-control solution has been compared with alternative designs which are not at the maximum driving force. It has been shown that the designs that are not at the maximum driving force are more difficult to control. It also highlights that process design can be identified that are easy to operate, control and needing low cost.

Furthermore, through analytical and closed-loop simulation it is also verified that the design-control solution has better performance compared to any other design

alternative within a fixed design space that is not at the maximum driving force in terms of control structure, disturbance rejection and controllability. Therefore, this approach shows that process design can be performed in an easier manner which results in better controllability, operation and energy requirement. It should be noted that the type of controller used does not matter for the integrated process design controller structure method based on the maximum driving force. This highlighted through the application examples.

Therefore, the achievements in this work are summarized as follows:

1. An integrated generic computer-aided framework for integrated process design and control of intensified process including reactive distillation processes is developed and the applicability of the method is demonstrated through different case studies for design-control of reactive distillation processes. This methodology is a hierarchical and a step-by-step procedure. Therefore, it provides the possibility for systematic analysis at every step of the framework. Every step of the design-control methodology is clearly explained in terms of calculations and analysis. Therefore, it is generic with respect to application and makes it favorable to be applied on various problems.

2. It is demonstrated the process design at the maximum available driving force results in better control and operation of reactive distillation processes. Thus, the control structure at the maximum driving force is determined for any reactive distillation process that operates at the maximum driving force. The application of the methodology is highlighted through several case studies and in every case the design at the maximum driving force had better performance compared to a design not operating at the maximum driving force.

3. The developed methodology is simple and easy to use in order to rapidly find an optimal design-control solution for an intensified operation – in this case reactive distillation.

6.2 Future works

The future work is to extend the application of the framework to other types of intensified processes, such as membrane-based operations, as well as to process flowsheets and plantwide control. Furthermore, the issues related to uncertainties associated with the model parameters are subject to future works. However, it must be noted that the qualitative results would not be affected – only the quantitative results would be affected in case of uncertainties in the model parameters. That is, the design at the maximum driving force would still be the best, but the steady state values for the controllers may be different.

Therefore, the following are the suggestions to further improve the methodology presented in this work:

1. *Alternative driving forces* and energy sources can be exploited for control, as new actuation possibilities. Therefore, although many process synthesis concepts have been proposed in the literature, yet there is not an effective method to combine process intensification fundamentals with rigorous optimization tools. Such method would be beneficial economically and would promote process innovation.

2. *Multiscale modelling* is and emerging field in process systems engineering. Although the idea of linking events occurring across time and length scales is not new, the numerical solution of these models is challenging because of computational limitations and the difficulty in coupling modelling methods with different characteristics; therefore, it will be beneficial to use methods such as the one developed in this work in course of formulating multiscale optimization algorithms. This is because the methodology developed in this work is not computationally expensive.

3. *Software implementation* of the proposed methodology in form of a simple tool that non-expert users can use is beneficial. Therefore, it is important the database of reactions (in terms of elements) is constructed so the user can very fast select the reaction without spending time on identifying elements. Furthermore, it is beneficial that such software is able to be connected to commercial process simulators so the optimal design at the maximum driving force is readily exported to process simulator.

4. The integrated process design-control solution obtained through the application the methodology presented in this work is guaranteed optimal (or near optimal if not optimal). However, it is beneficial that the results are compared with other solution approaches to identify their challenges and provide suggestions to improve their performance.

NOMENCLATURE

Latin symbols

A	Chemical element A
A_e	Formula matrix from the "natural" elements
$a_{j,i}$	Number of chemical elements j present in species i
B	Chemical element B
${b^d}_T$	Total Element moles in the distillate
${b^B}_T$	Total Element moles in the bottom
${b^F}_T$	Total Element moles
C	Chemical element C
d	Set of disturbance variables
DF	Driving force
D_x	Value on x-axis corresponding to maximum driving force
D_y	Value on y-axis corresponding to maximum driving force
f_{Obj}	Objective function
f	A vector of non-linear equations
F_f	Element flowrate in the feed
G	Gibbs free energy
G^E	Excess Gibbs free energy
h^l, h^u	Lower bounds and upper bounds of the linear and non-linear equations
K	Steady-state gain
M_j	The vector represents 0/1 binary variables
n_i	Number of moles for component i
N	Number of stages
N_F	Feed location
NC	Number of compounds
NE	Number of elements
NR	Number of reactions
P	Pressure
RR	Reflux ratio
RB	Reboil ratio

t	Independent variable, time
T	Temperature
u	Set of input variables
v^l, v^u	Lower bounds and upper bounds of chemical variables
W_j^k	Elemental mole fraction of element j in the phase k
W_{LK}^{β}	Light key element composition in phase β
W_{HK}^{β}	Heavy key element composition in phase β
$W_{LK,eq}^{\beta}$	Equivalent light key element composition in phase β
W_i^D	Element mole fraction of i in the distillate
W_i^B	Element mole fraction of i in the bottom
$W_{LK,D}$	Element mole fraction of light key element in the distillate
$W_{HK,D}$	Element mole fraction of heavy key element in the distillate
$W_{HK,B}$	Element mole fraction of heavy key element in the bottom
$W_{HK,z}$	Element mole fraction of heavy key element in the feed
x_i	Liquid mole fraction for component i
x^l	Liquid mole fraction
y_i	Vapor mole fraction for component i
y^v	Vapor mole fraction
y	Set of output variables
z_{WAf}	Element A feed composition

Greek symbols

θ	The constitutive variable
δ	Controller parameter
α	Relative volatility
γ_i	Activity coefficient of compound i
φ_i	Fugacity coefficient of compound i
μ_i	Chemical potential of compound i
λ_i	Chemical potential of element i
ζ	Dimensionless conversion

REFERENCES

Al-Arfaj, M., Luyben, W.L., 2000. Comparison of Alternative Control Structures for an Ideal Two-Product Reactive Distillation Column. Ind. Eng. Chem. Res. 39, 3298–3307. doi:10.1021/ie990886j

Albert, M., Hahnenstein, I., Hasse, H., Maurer, G., 1996. Vapor–liquid equilibrium of formaldehyde mixtures: New data and model revision. AIChE J. 42, 1741–1752. doi:10.1002/aic.690420625

Al-Jarallah, A.M., Lee, A.K.K., Siddiqui, M.A.B., 1988. Kinetics of methyl tertiary butyl ether synthesis catalyzed by sulphuric acid. Chem. Eng. J. 39, 169–174. doi:10.1016/0300-9467(88)80024-8

Al-jarallah, A.M., Siddiqui, M.A.B., Lee, A.K.K., 1988. Kinetics of Methyl Tertiary Butyl Ether Synthesis Catalyzed by Ion Exchange Resin 66.

Alvarado-Morales, M., Hamid, M.K.A., Sin, G., Gernaey, K. V., Woodley, J.M., Gani, R., 2010. A model-based methodology for simultaneous design and control of a bioethanol production process. Comput. Chem. Eng. 34, 2043–2061. doi:10.1016/j.compchemeng.2010.07.003

Androulakis, I.P., 2000. Kinetic mechanism reduction based on an integer programming approach. AIChE J. 46, 361–371. doi:10.1002/aic.690460214

Anterroches, L., Gani, R., 2006. Computer Aided Methodology for Simultaneous Synthesis , Design & Analysis of Chemical Products- Processes 853, 853–858.

Asteasuain, M., Bandoni, A., Sarmoria, C., Brandolin, A., 2006. Simultaneous process and control system design for grade transition in styrene polymerization. Chem. Eng. Sci. 61, 3362–3378. doi:10.1016/j.ces.2005.12.012

Asteasuain, M., Brandolin, A., Sarmoria, C., Bandoni, A., 2004. Simultaneous Design and Control of a Semibatch Styrene Polymerization Reactor. Ind. Eng. Chem. Res. 43, 5233–5247. doi:10.1021/ie040021s

Asteasuain, M., Sarmoria, C., Brandolin, A., Bandoni, A., 2007. Integration of control aspects and uncertainty in the process design of polymerization reactors. Chem. Eng. J. 131, 135–144. doi:10.1016/j.cej.2006.12.029

Avraam, M.P., Shah, N., Pantelides, C.C., 1999. A decomposition algorithm for the optimisation of hybrid dynamic processes. Comput. Chem. Eng. 23, S451–S454. doi:10.1016/S0098-1354(99)80111-2

Avraam, M.P., Shah, N., Pantelides, C.C., 1998. Modelling and optimisation of general hybrid systems in the continuous time domain. Comput. Chem. Eng. 22,

S221–S228. doi:10.1016/S0098-1354(98)00058-1

Babi, D.K., Gani, R., 2014. Hybrid Distillation Schemes: Design, Analysis, and Application, in: Gorak, A., Sorensen, E. (Eds.), Distillation: Fundamentals and Principles. Elsevier, London, pp. 357–381. doi:10.1016/B978-0-12-386547-2.00009-0

Babi, D.K., Lutze, P., Woodley, J.M., Gani, R., 2014. A process synthesis-intensification framework for the development of sustainable membrane-based operations. Chem. Eng. Process. Process Intensif. 86, 173–195. doi:10.1016/j.cep.2014.07.001

Bahakim, S.S., Ricardez-sandoval, L.A., 2014. Simultaneous design and MPC-based control for dynamic systems under uncertainty : A stochastic approach. Comput. Chem. Eng. 63, 66–81. doi:10.1016/j.compchemeng.2014.01.002

Bahri, P., Bandoni, J., Romagnoli, J., 1997. Integrated flexibility and controllability analysis in design of chemical processes. AIChE J. 43, 997–1015. doi:10.1002/aic.690430415

Banga, J., Moles, C., Alonso, A., 2004. Global Optimization of Bioprocesses using Stochastic and Hybrid Methods, in: Floudas, C.A., Pardalos, P. (Eds.), Frontiers in Global Optimization SE - 3, Nonconvex Optimization and Its Applications. Springer US, pp. 45–70. doi:10.1007/978-1-4613-0251-3_3

Bansal, V., Perkins, J.D., Pistikopoulos, E.N., 2002. A Case Study in Simultaneous Design and Control Using Rigorous, Mixed-Integer Dynamic Optimization Models. Ind. Eng. Chem. Res. 41, 760–778. doi:10.1021/ie010156n

Bansal, V., Perkins, J.D., Pistikopoulos, E.N., Ross, R., Van Schijndel, J.M.G., 2000. Simultaneous design and control optimisation under uncertainty, in: Computers and Chemical Engineering. pp. 261–266. doi:10.1016/S0098-1354(00)00475-0

Bansal, V., Ross, R., Perkins, J.D., Pistikopoulos, E.N., 1998. Optimal design and control of double-effect distillation systems, in: UKACC International Conference on Control (CONTROL '98). pp. 1096–1101. doi:10.1049/cp:19980382

Bansal, V., Sakizlis, V., Ross, R., Perkins, J.D., Pistikopoulos, E.N., 2003. New algorithms for mixed-integer dynamic optimization. Comput. Chem. Eng. 27, 647–668. doi:10.1016/S0098-1354(02)00261-2

Barton, P.I., Allgor, R.J., Feehery, W.F., Galán, S., 1998. Dynamic Optimization in a Discontinuous World. Ind. Eng. Chem. Res. 37, 966–981. doi:10.1021/ie970738y

Barton, P.I., Lee, C.K., 2004. Design of process operations using hybrid dynamic optimization. Comput. Chem. Eng. 28, 955–969. doi:10.1016/j.compchemeng.2003.09.015

Bek-Pedersen, E., Gani, R., 2004. Design and synthesis of distillation systems using a driving-force-based approach. Chem. Eng. Process. Process Intensif. 43, 251–262. doi:10.1016/S0255-2701(03)00120-X

Bek-Pedersen, E., Gani, R., Levaux, O., 2000. Determination of optimal energy efficient separation schemes based on driving forces. Comput. Chem. Eng. 24, 253–259. doi:10.1016/S0098-1354(00)00474-9

Berkovitz, L.D., 1961. Variational methods in problems of control and programming. J. Math. Anal. Appl. 3, 145–169. doi:10.1016/0022-247X(61)90013-0

Bhat, N., McAvoy, T.J., 1990. Use of neural nets for dynamic modeling and control of chemical process systems. Comput. Chem. Eng. 14, 573–583. doi:10.1016/0098-1354(90)87028-N

Biegler, L.T., 2007a. An overview of simultaneous strategies for dynamic optimization. Chem. Eng. Process. Process Intensif. 46, 1043–1053. doi:10.1016/j.cep.2006.06.021

Biegler, L.T., 2007b. An overview of simultaneous strategies for dynamic optimization. Chem. Eng. Process. Process Intensif. 46, 1043–1053. doi:10.1016/j.cep.2006.06.021

Biegler, L.T., Cervantes, A.M., Wächter, A., 2002. Advances in simultaneous strategies for dynamic process optimization. Chem. Eng. Sci. 57, 575–593. doi:10.1016/S0009-2509(01)00376-1

Bildea, C.S., Dimian, A.C., Iedema, P.D., 2000. Nonlinear behavior of reactor—separator—recycle systems. Comput. Chem. Eng. 24, 209–215. doi:10.1016/S0098-1354(00)00515-9

Bristol, E., 1966. On a new measure of interaction for multivariable process control. IEEE Trans. Automat. Contr. 11, 133–134. doi:10.1109/TAC.1966.1098266

Capón-García, E., Guillén-Gosálbez, G., Espuña, A., 2013. Integrating process dynamics within batch process scheduling via mixed-integer dynamic optimization. Chem. Eng. Sci. 102, 139–150. doi:10.1016/j.ces.2013.07.039

Carvalho, A., Gani, R., Matos, H., 2008. Design of sustainable chemical processes: Systematic retrofit analysis generation and evaluation of alternatives. Process Saf. Environ. Prot. 86, 328–346. doi:10.1016/j.psep.2007.11.003

Chiu, M. Sen, Arkun, Y., 1991. New result on relative gain array, Niederlinski index and decentralized stability condition: 2x2 plant cases. Automatica 27, 419–421. doi:10.1016/0005-1098(91)90093-H

Chung, Y.-H., Peng, T.-H., Lee, H.-Y., Chen, C.-L., Chien, I.-L., 2015. Design and Control of Reactive Distillation System for Esterification of Levulinic Acid and n -Butanol. Ind. Eng. Chem. Res. 54, 3341–3354. doi:10.1021/ie500660h

Corriou, J.-P., 2004. Process Control Theory and Applications. Springer-Verlog London.

Dimian, A.C., Bildea, C.S., Kiss, A.A., 2014a. Integrated Design and Simulation of Chemical Processes. Comput. Aided Chem. Eng. 35, 1–863.

Dimian, A.C., Bildea, C.S., Kiss, A.A., 2014b. Index, in: Computer Aided Chemical Engineering, Computer Aided Chemical Engineering. Elsevier, pp. 849–863.

Dimitriadis, V.D., Pistikopoulos, E.N., 1995. Flexibility Analysis of Dynamic Systems. Ind. Eng. Chem. Res. 34, 4451–4462. doi:10.1021/ie00039a036

Downs, J.J., Vogel, E.F., 1993. A plant-wide industrial process control problem. Comput. Chem. Eng. 17, 245–255. doi:10.1016/0098-1354(93)80018-I

Dua, P., Dua, V., Pistikopoulos, E.N., 2006. Optimal delivery of chemotherapeutic agents in cancer. Comput. Aided Chem. Eng. 21, 1643–1648. doi:10.1016/S1570-7946(06)80283-X

Esposito, W., Floudas, C., 2000. Deterministic Global Optimization in Nonlinear Optimal Control Problems. J. Glob. Optim. 17, 97–126. doi:10.1023/A:1026578104213

Flores-Tlacuahuac, A., Biegler, L.T., 2007. Simultaneous mixed-integer dynamic optimization for integrated design and control. Comput. Chem. Eng. 31, 588–600. doi:10.1016/j.compchemeng.2006.08.010

Flores-Tlacuahuac, A., Biegler, L.T., Saldívar-Guerra, E., 2005. Dynamic optimization of HIPS open-loop unstable polymerization reactors. Ind. Eng. Chem. Res. 44, 2659–2674. doi:10.1021/ie049534p

Flores-Tlacuahuac, A., Grossmann, I.E., 2011. Simultaneous cyclic scheduling and control of tubular reactors: Single production lines. Ind. Eng. Chem. Res. 50, 8086–8096. doi:10.1021/ie101677e

Flores-Tlacuahuac, A., Grossmann, I.E., 2006. Simultaneous cyclic scheduling and control of a multiproduct CSTR. Ind. Eng. Chem. Res. 45, 6698–6712. doi:10.1021/ie051293d

Fraga, E.S., Hagemann, J., Estrada-Villagrana, A., Bogle, I.D.L., 2000. Incorporation

of dynamic behaviour in an automated process synthesis system. Comput. Chem. Eng. 24, 189–194. doi:10.1016/S0098-1354(00)00511-1

Francisco, M., Vega, P., Álvarez, H., 2011. Robust Integrated Design of processes with terminal penalty model predictive controllers. Chem. Eng. Res. Des. 89, 1011–1024. doi:10.1016/j.cherd.2010.11.023

Fuente, R.L.-N. de la, Flores-Tlacuahuac, A., 2009. Integrated Design and Control Using a Simultaneous Mixed-Integer Dynamic Optimization Approach. Ind. Eng. Chem. Res. 48, 1933–1943. doi:10.1021/ie801353c

Gani, R., 2015. ICAS documentation, Internal Document, Technical University of Denmark. Internal Document, Technical University of Denmark, Kongens Lyngby.

Gani, R., Bek-Pedersen, E., 2000. Simple new algorithm for distillation column design. AIChE J. 46, 1271–1274. doi:10.1002/aic.690460619

Georgiadis, M.C., Schenk, M., Pistikopoulos, E.N., Gani, R., 2002. The interactions of design, control and operability in reactive distillation systems. Comput. Chem. Eng. 26, 735–746. doi:10.1016/S0098-1354(01)00774-8

Giovanoglou, A., Barlatier, J., Adjiman, C.S., Pistikopoulos, E.N., Cordiner, J.L., 2003. Optimal Solvent Design for Batch Separation Based on Economic Performance. AIChE J. 49, 3095–3109. doi:10.1002/aic.690491211

Gollapalli, U., Dantus, M.M., High, K.A., 2000. Environment and control issues in design. Comput. Chem. Eng. 24, 1709–1712. doi:10.1016/S0098-1354(00)80016-2

Grosser, J.H., Doherty, M.F., Malone, M.F., 1987. Modeling of reactive distillation systems. Ind. Eng. Chem. Res. 26, 983–989. doi:10.1021/ie00065a023

Grossmann, I.E., Morari, M., 1983. Operability , Resiliency , and Flexibility : process design objectives for a changing world, in: Proceedings of Second International Conference on Foundations of Computer-Aided Process Design. p. 931.

Hamid, M.K.A., 2011. Model-Based Integrated Process Design and Controller Design of Chemical Processes. PhD Thesis, Technical University of Denmark, Kongens Lyngby.

Hamid, M.K.A., Sin, G., Gani, R., 2010a. Integration of process design and controller design for chemical processes using model-based methodology. Comput. Chem. Eng. 34, 683–699. doi:10.1016/j.compchemeng.2010.01.016

Hamid, M.K.A., Sin, G., Gani, R., 2010b. Integration of process design and controller design for chemical processes using model-based methodology. Comput. Chem. Eng. 34, 683–699. doi:10.1016/j.compchemeng.2010.01.016

Harmsen, G.J., 2007. Reactive distillation: The front-runner of industrial process intensification. Chem. Eng. Process. Process Intensif. 46, 774–780. doi:10.1016/j.cep.2007.06.005

Hengstebeck, R.J., 1961. Distillation Design. McGraw-Hill, New York.

Hildebrandt, D., Glasser, D., 1990. The attainable region and optimal reactor structures. Chem. Eng. Sci. 45, 2161–2168. doi:10.1016/0009-2509(90)80091-R

Hildebrandt, D., Glasser, D., 1990. The attainable region and optimal reactor structures. Chem. Eng. Sci. 45, 2161–2168. doi:10.1016/0009-2509(90)80091-R

Huusom, J.K., 2015. Challenges and opportunities in integration of design and control. Comput. Chem. Eng. 81, 138–146. doi:10.1016/j.compchemeng.2015.03.019

Jantharasuk, A., Gani, R., Górak, A., Assabumrungrat, S., 2011. Methodology for design and analysis of reactive distillation involving multielement systems. Chem. Eng. Res. Des. 89, 1295–1307. doi:10.1016/j.cherd.2011.04.016

Jenkins, H.D.B., 2008. Gibbs-Duhem Equation, in: Chemical Thermodynamics at a Glance. Blackwell Publishing Ltd, Oxford, UK, pp. 164–167.

doi:10.1002/9780470697733.ch50
Karunanithi, A.T., Achenie, L.E.K., Gani, R., 2005a. A New Decomposition-Based Computer-Aided Molecular/Mixture Design Methodology for the Design of Optimal Solvents and Solvent Mixtures. Ind. Eng. Chem. Res. 44, 4785–4797. doi:10.1021/ie049328h
Karunanithi, A.T., Achenie, L.E.K., Gani, R., 2005b. New Decomposition-Based Computer-Aided Molecular/Mixture Design Methodology for the Design of Optimal Solvents and Solvent Mixtures. Ind. Eng. Chem. Res. 44, 4785–4797. doi:10.1021/ie049328h
Karunanithi, A.T., Achenie, L.E.K., Gani, R., 2004. Optimal (Solvent) mixture design through a decomposition based CAMD methodology. Comput. Aided Chem. Eng. 18, 217–222. doi:10.1016/S1570-7946(04)80102-0
Khajuria, H., Pistikopoulos, E.N., 2011. Integrated Design and Control of Pressure Swing Adsorption Systems, Computer Aided Chemical Engineering. Elsevier B.V. doi:10.1016/B978-0-444-53711-9.50008-0
Kookos, I.K., Perkins, J.D., 2001. An Algorithm for Simultaneous Process Design and Control. Ind. Eng. Chem. Res. 40, 4079–4088. doi:10.1021/ie000622t
Larsson, T., Govatsmark, M.S., Skogestad, S., Yu, C.C., 2003. Control Structure Selection for Reactor, Separator, and Recycle Processes. Ind. Eng. Chem. Res. 42, 1225–1234. doi:10.1021/ie0200860
Lee, H.-Y., Jan, C.-H., Chien, I.-L., Huang, H.-P., 2010. Feed-splitting operating strategy of a reactive distillation column for energy-saving production of butyl propionate. J. Taiwan Inst. Chem. Eng. 41, 403–413. doi:10.1016/j.jtice.2010.03.003
Lewis, N., Hedengren, J., Haseltine, E., 2015. Hybrid Dynamic Optimization Methods for Systems Biology with Efficient Sensitivities. Processes 3, 701–729. doi:10.3390/pr3030701
Lu, X.J., Li, H.-X., Yuan, X., 2010. PSO-based intelligent integration of design and control for one kind of curing process. J. Process Control 20, 1116–1125. doi:10.1016/j.jprocont.2010.06.019
Lutze, P., Gani, R., Woodley, J.M., 2010. Process intensification: A perspective on process synthesis. Chem. Eng. Process. Process Intensif. 49, 547–558. doi:10.1016/j.cep.2010.05.002
Malcolm, A., Polan, J., Zhang, L., Ogunnaike, B.A., Linninger, A.A., 2007. Integrating systems design and control using dynamic flexibility analysis. AIChE J. 53, 2048–2061. doi:10.1002/aic.11218
Mansouri, S.S., Ismail, M.I., Babi, D., Simasatitkul, L., Huusom, J.K., Gani, R., 2013. Systematic Sustainable Process Design and Analysis of Biodiesel Processes. Processes 1, 167–202. doi:10.3390/pr1020167
Mansouri, S.S., Sales-Cruz, M., Huusom, J.K., Gani, R., 2016. Integrated Process Design and Control of Multi-element Reactive Distillation Processes, in: 11th IFAC Symposium on Dynamics and Control of Process Systems, Including Biosystems (DYCOPS-CAB 2016). p. TuB3.2.
Mansouri, S.S., Sales-Cruz, M., Huusom, J.K., Woodley, J.M., Gani, R., 2015. Integrated Process Design and Control of Reactive Distillation Processes. IFAC-PapersOnLine 48, 1120–1125. doi:10.1016/j.ifacol.2015.09.118
McCabe, W.L., Thiele, E., 1925. Graphical design of fractionating columns. Ind. Eng. Chem. 17, 605–611. doi:10.1021/ie50186a023
Mehta, S., Ricardez-sandoval, L.A., 2016. Integration of Design and Control of Dynamic Systems under Uncertainty: A New Back-O ff Approach. Ind. Eng. Chem. Res. 55, 485−498. doi:10.1021/acs.iecr.5b03522
Meidanshahi, V., Adams, T.A., 2016. Integrated design and control of

semicontinuous distillation systems utilizing mixed integer dynamic optimization. Comput. Chem. Eng. 89, 172–183. doi:10.1016/j.compchemeng.2016.03.022

Michelsen, M.L., 1994. Calculation of multiphase equilibrium. Comput. Chem. Eng. 18, 545–550. doi:10.1016/0098-1354(93)E0017-4

Mohideen, M.J., Perkins, J.D., Pistikopoulos, E.N., 1997. Robust stability considerations in optimal design of dynamic systems under uncertainty. J. Process Control 7, 371–385. doi:10.1016/S0959-1524(97)00014-0

Mohideen, M.J., Perkins, J.D., Pistikopoulos, E.N., 1996. Optimal design of dynamic systems under uncertainty. AIChE J. 42, 2251–2272. doi:10.1002/aic.690420814

Mohideen, M.J., Perkins, J.D., Pistikopoulos, E.N., 1996. Optimal synthesis and design of dynamic systems under uncertainty. Comput. Chem. Eng. 20, S895–S900.

Moles, C.G., Gutierrez, G., Alonso, A.A., Banga, J.R., 2003. Integrated Process Design and Control Via Global Optimization. Chem. Eng. Res. Des. 81, 507–517. doi:10.1205/026387603765444465

Moon, J., Kim, S., Linninger, A.A., 2011. Embedded Control for Optimizing Flexible Dynamic Process Performance. Ind. Eng. Chem. Res. 50, 4993–5004. doi:10.1021/ie1014052

Moon, J., Kim, S., Ruiz, G., Linninger, A.A., 2009a. 10th International Symposium on Process Systems Engineering: Part A, Computer Aided Chemical Engineering, Computer Aided Chemical Engineering. Elsevier.

Moon, J., Kim, S., Ruiz, G., Linninger, A.A., 2009b. Embedded Control for Optimizing Flexible Dynamic Process Performance, Computer Aided Chemical Engineering, Computer Aided Chemical Engineering. Elsevier. doi:10.1016/S1570-7946(09)70599-1

Morari, M., 1983. Design of resilient processing plants—III. Chem. Eng. Sci. 38, 1881–1891. doi:10.1016/0009-2509(83)85044-1

Nie, Y., Biegler, L.T., Wassick, J.M., 2012. Integrated scheduling and dynamic optimization of batch processes using state equipment networks. AIChE J. 58, 3416–3432. doi:10.1002/aic.13738

Nielsen, T.L., Abildskov, J., Harper, P.M., Papaeconomou, I., Gani, R., 2001. The CAPEC database. J. Chem. Eng. Data 46, 1041–1044. doi:10.1021/je000244z

Nikačević, N.M., Huesman, A.E.M., Van den Hof, P.M.J., Stankiewicz, A.I., 2012. Opportunities and challenges for process control in process intensification. Chem. Eng. Process. Process Intensif. 52, 1–15. doi:10.1016/j.cep.2011.11.006

Panda, D., Kannan, A., 2014. Equilibrium and Rate Based Simulation of MTBE Reactive Distillation Column 8, 998–1004.

Panjwani, P., Schenk, M., Georgiadis, M.C., Pistikopoulos, E.N., 2005. Optimal design and control of a reactive distillation system. Eng. Optim. 37, 733–753. doi:10.1080/03052150500211903

Paramasivan, G., Kienle, A., 2010. A reactive distillation case study for decentralized control system design using mixed integer optimization. Comput. Aided Chem. Eng. 28, 565–570.

Patel, J., Uygun, K., Huang, Y., 2008. A path constrained method for integration of process design and control. Comput. Chem. Eng. 32, 1373–1384. doi:10.1016/j.compchemeng.2007.06.005

Patil, B.P., Maia, E., Ricardez-Sandoval, L.A., 2015. Integration of scheduling, design, and control of multiproduct chemical processes under uncertainty. AIChE J. 61, 2456–2470. doi:10.1002/aic.14833

Pérez-Cisneros, E.S., 1997. Modelling , Design and Analysis of Reactive Separation

Processes. Ph.D. Thesis, Technical University of Denmark, Kongens Lyngby.
Pérez-Cisneros, E.S., Gani, R., Michelsen, M.L., 1997. Reactive separation systems—I. Computation of physical and chemical equilibrium. Chem. Eng. Sci. 52, 527–543. doi:10.1016/S0009-2509(96)00424-1
Pérez-Cisneros, E.S., Schenk, M., Gani, R., Pilavachi, P.A., 1996. Aspects of simulation, design and analysis of reactive distillation operations. Comput. Chem. Eng. doi:10.1016/0098-1354(96)00055-5
Pernebo, L., Silverman, L.M., 1982. Model reduction via balanced state space representations. IEEE Trans. Automat. Contr. doi:10.1109/TAC.1982.1102945
Petzold, L., Petzold, L., Zhu, W., Zhu, W., 1999. Model reduction for chemical kinetics: An optimization approach. AIChE J. 45, 869–886. doi:10.1002/aic.690450418
Pistikopoulos, E.N., Diangelakis, N.A., 2015. Towards the integration of process design, control and scheduling: Are we getting closer? Comput. Chem. Eng. doi:10.1016/j.compchemeng.2015.11.002
Pistikopoulos, E.N., Grossmann, I.E., 1988. Optimal retrofit design for improving process flexibility in linear systems. Comput. Chem. Eng. 12, 719–731. doi:10.1016/0098-1354(88)80010-3
Pöpken, T., Steinigeweg, S., Gmehling, J., 2001. Synthesis and Hydrolysis of Methyl Acetate by Reactive Distillation Using Structured Catalytic Packings: Experiments and Simulation. Ind. Eng. Chem. Res. 40, 1566–1574. doi:10.1021/ie0007419
Reddy, K.R., Kumar, D.B.K., Rao, G.S., Sairam, P.V.S., Anila, P., Rambabu, C., 2012. Activity Coefficients and Excess Gibbs Energies for Binary Mixtures of N -Methyl-2-pyrrolidone with Some Substituted Ethanols. J. Chem. Eng. Data 57, 1412–1416. doi:10.1021/je3002078
Ricardez Sandoval, L.A., Budman, H.M., Douglas, P.L., 2008. Simultaneous design and control of processes under uncertainty: A robust modelling approach. J. Process Control 18, 735–752. doi:10.1016/j.jprocont.2007.11.006
Ricardez-Sandoval, L.A., Budman, H.M., Douglas, P.L., 2009. Integration of design and control for chemical processes: A review of the literature and some recent results. Annu. Rev. Control 33, 158–171. doi:10.1016/j.arcontrol.2009.06.001
Rivera, D.E., Morari, M., Skogestad, S., 1986. Internal model control: PID controller design. Ind. Eng. Chem. Res. 25, 252–265. doi:10.1021/i200032a041
Ross, R., Perkins, J.D., Pistikopoulos, E.N., Koot, G.L.M., Van Schijndel, J.M.G., 2001. Optimal design and control of a high-purity industrial distillation system. Comput. Chem. Eng. 25, 141–150. doi:10.1016/S0098-1354(00)00637-2
Russel, B.M., Henriksen, J.P., Jørgensen, S.B., Gani, R., 2002. Integration of design and control through model analysis. Comput. Chem. Eng. 26, 213–225. doi:10.1016/S0098-1354(01)00742-6
Sakizlis, V., Perkins, J.D., Pistikopoulos, E.N., 2003. Parametric controllers in simultaneous process and control design. Ind. Eng. Chem. Res. 42, 4545–4563. doi:10.1016/S1570-7946(03)80442-X
Sánchez-Daza, O., Pérez-Cisneros, E.S., Bek-Pedersen, E., Gani, R., 2003. Graphical and Stage-to-Stage Methods for Reactive Distillation Column Design. AIChE J. 49, 2822–2841. doi:10.1002/aic.690491115
Sanchez-Sanchez, K., Ricardez-Sandoval, L.A., 2013. Simultaneous Process Synthesis and Control Design under Uncertainty : A Worst-Case Performance Approach. AIChE J. 59, 2497–2514. doi:10.1002/aic.14040
Schoenmakers, H.G., Bessling, B., 2003. Reactive and catalytic distillation from an industrial perspective. Chem. Eng. Process. Process Intensif. 42, 145–155. doi:10.1016/S0255-2701(02)00085-5

Schrans, S., de Wolf, S., Baur, R., 1996. Dynamic simulation of reactive distillation: An MTBE case study. Comput. Chem. Eng. doi:10.1016/0098-1354(96)00275-X

Schweiger, C., Floudas, C., 1998. Interaction of Design and Control: Optimization with Dynamic Models, in: Optimal Control SE - 19, Applied Optimization. Springer US, pp. 388–435. doi:10.1007/978-1-4757-6095-8_19

Seferlis, P., Georgiadis, M.C., 2004. The Integration of Process Design and Control. Comput. Aided Chem. Eng. 17, 1–639.

Sendin, O.H., Moles, C.G., Alonso, A.A., Banga, J.R., 2004. Multi-objective integrated design and control using stochastic global optimization methods, Computer Aided Chemical. Elsevier Masson SAS. doi:10.1016/S1570-7946(04)80074-9

Sharifzadeh, M., 2013a. Integration of process design and control: A review. Chem. Eng. Res. Des. 91, 2515–2549. doi:10.1016/j.cherd.2013.05.007

Sharifzadeh, M., 2013b. Integration of process design and control: A review, Chemical Engineering Research and Design. Institution of Chemical Engineers. doi:10.1016/j.cherd.2013.05.007

Sharifzadeh, M., Thornhill, N.F., 2013. Integrated design and control using a dynamic inversely controlled process model. Comput. Chem. Eng. 48, 121–134. doi:10.1016/j.compchemeng.2012.08.009

Sharma, N., Singh, K., 2010. Control of Reactive Distillation Column: A Review. Int. J. Chem. React. Eng. doi:10.2202/1542-6580.2260

Skogestad, S., 2003. Simple analytic rules for model reduction and PID controller tuning. J. Process Control 13, 291–309. doi:10.1016/S0959-1524(02)00062-8

Skogestad, S., Morari, M., 1987. Implications of Large RGA Elements on Control Performance. Ind. Eng. Chem. Res. 26, 2323–2330. doi:10.1021/ie00071a025

Sneesby, M.G., Tade, M.O., Smith, T.N., 1999a. Two-point control of a reactive distillation column for composition and conversion. J. Process Control 9, 19–31. doi:10.1016/S0959-1524(98)00007-9

Sneesby, M.G., Tade, M.O., Smith, T.N., 1999b. Two-point control of a reactive distillation column for composition and conversion. J. Process Control 9, 19–31. doi:10.1016/S0959-1524(98)00007-9

Straub, D.A., Grossmann, I.E., 1990. Integrated stochastic metric of flexibility for systems with discrete state and continuous parameter uncertainties. Comput. Chem. Eng. 14, 967–985. doi:10.1016/0098-1354(90)87053-R

Trainor, M., Giannakeas, V., Kiss, C., Ricardez-sandoval, L.A., 2013. Optimal process and control design under uncertainty : A methodology with robust feasibility and stability analyses. Chem. Eng. Sci. 104, 1065–1080. doi:10.1016/j.ces.2013.10.017

Tuchlenski, A., Beckmann, A., Reusch, D., Düssel, R., Weidlich, U., Janowsky, R., 2001. Reactive distillation — industrial applications, process design & scale-up. Chem. Eng. Sci. 56, 387–394. doi:10.1016/S0009-2509(00)00240-2

Tula, A.K., Eden, M.R., Gani, R., 2015. Process synthesis, design and analysis using a process-group contribution method. Comput. Chem. Eng. 81, 245–259. doi:10.1016/j.compchemeng.2015.04.019

Yuan, Z., Chen, B., Sin, G., Gani, R., 2012. State-of-the-art and progress in the optimization-based simultaneous design and control for chemical processes. AIChE J. 58, 1640–1659. doi:10.1002/aic.13786

APPENDIX A

The reactive element operating lines are given as follows (Pérez-Cisneros, 1997):

$$W_A^v = \frac{RR}{RR+1} W_A^l + \frac{1}{RR+1} W_A^D \quad \text{(Reactive operating line for the rectifying section)} \tag{A.1}$$

$$W_A^v = \frac{RB+1}{RB} W_A^l - \frac{1}{RB} W_A^B \quad \text{(Reactive operating line for the stripping section)} \tag{A.2}$$

Substituting these equations in Eq. (23) for W^v_A gives the top and bottom element product composition with respect to the driving force as follows:

$$W_A^D = DF\ (RR+1) + W_A^l \tag{A.3}$$

$$W_A^B = W_A^l - DF \cdot RB \tag{A.4}$$

Next, equations (A.3) and (A.4) are differentiated with respect to *DF* (driving force) and result in the following expressions:

$$\frac{dW_A^D}{dDF} = (RR+1) + \frac{dW_A^l}{dDF} = (RR+1) + \left(\frac{dDF}{W_A^l}\right)^{-1} \tag{A.5}$$

$$\frac{dW_A^B}{dDF} = \frac{W_A^l}{dDF} - RB = \left(\frac{dDF}{dW_A^l}\right)^{-1} - RB \tag{A.6}$$

The total element *A* mass balance is written as follows:

$$F_f \cdot z_{W_{Af}} = W_A^D b^D + W_A^B b^B \tag{A.7}$$

Where, b^D and b^B are element *A* mass flows in top and bottom of the column, respectively. Substituting (A.3) and (A.4), one at the time, into (A.7) for $W_A{}^D$ and $W_A{}^B$, the total element *A* mass balance in terms of driving force is expressed as:

$$F_f \cdot z_{W_{Af}} = DF\ (RR+1) b^D + W_A^l b^D + W_A^B b^B \tag{A.8}$$

or

$$F_f \cdot z_{W_{Af}} = W_A^D b^D + W_A^l b^B - b^B \cdot DF \cdot RB \tag{A.9}$$

Differentiating equations (A.8) and (A.9) with respect to the F_f and z_{WAf} (assuming that the changes in composition, and, top and bottom element flowrates (b^D and b^B) with respect to the feed flowrate is negligible), the expressions for dW_A^l / dF_f, $dW_A^l / dz_{W_{Af}}$ are obtained. Having these derivatives, the solution to (4.19) is expressed by (4.20) as described in algorithm 4.4. Note that a more detailed derivation for a binary compound system involving the methanol-water non-reactive system is given in Appendix C.

APPENDIX B

Equation (A.3) is differentiated with respect to RR as follows:

$$\frac{dW_A^D}{dRR} = DF + (RR+1)\frac{dDF}{dRR} + \frac{dW_A^l}{dRR} \tag{A.10}$$

The previous equation can be further expressed as a function of $\frac{dDF}{dW_A^l}$ as follows:

$$\frac{dW_A^D}{dRR} = DF + (RR+1)\left(\frac{dDF}{dW_A^l}\right)\left(\frac{dW_A^l}{dRR}\right) + \frac{dW_A^l}{dRR} \tag{A.11}$$

Differentiating the expression of the top product composition with respect to RB gives:

$$\frac{dW_A^D}{dRB} = DF\frac{dRR}{dRB} + (RR+1)\frac{dDF}{dRB} + \frac{dW_A^l}{dRB} \tag{A.12}$$

It is assumed that d*RR*/d*RB*=0, then equation is simplified and is expressed as a function of $\frac{dDF}{dW_A^l}$ as follows:

$$\frac{dW_A^D}{dRB} = (RR+1)\left(\frac{dDF}{dW_A^l}\right)\left(\frac{dW_A^l}{dRB}\right) + \frac{dW_A^l}{dRB} \tag{A.13}$$

The expression of the bottom product composition (W_A^B) in terms of driving force is given by equation (A.4).

Differentiating the above equation with respect to *RR* gives:

$$\frac{dW_A^B}{dRR} = \frac{dW_A^l}{dRR} - \frac{dDF}{dRR}RB - DF\frac{dRB}{dRR} \tag{A.14}$$

It is assumed that d*RR*/d*RB*=0, then the above equation is simplified and is expressed as a function of as $\frac{dDF}{dW_A^l}$ follows:

$$\frac{dW_A^B}{dRR} = \frac{dW_A^l}{dRR} - \left(\frac{dDF}{dW_A^l}\right)\left(\frac{dW_A^l}{dRR}\right)RB \tag{A.15}$$

Similarly, differentiating the expression of bottom product composition (W_A^B) with respect to *RB* gives:

$$\frac{dW_A^B}{dRB} = \frac{dW_A^l}{dRB} - DF \tag{A.16}$$

Using these derivations, equation (4.22) or (4.23) is obtained for a binary or multi-element system. Note that a more detailed derivation for a binary compound system involving the methanol-water non-reactive system is given in Appendix C.

APPENDIX C

In this appendix, methanol-water control structure is determined. It must be noted that the vectors $\mathbf{y} = \begin{bmatrix} x^D & x^B \end{bmatrix}$, $\mathbf{d} = \begin{bmatrix} F_f & z_f \end{bmatrix}$, $x = x^l$ and $\theta = DF$. Note that the x^l here corresponds to liquid composition of methanol. Note that the derivations are the same as those for a binary element or multi-element systems, except that the composition domain is different. That is instead of binary element composition or equivalent binary element composition, binary comound composition is used,

$$\frac{d\mathbf{y}}{d\mathbf{d}} = \begin{bmatrix} \frac{dx^D}{dF_f} & \frac{dx^D}{dz_f} \\ \frac{dx^B}{dF_f} & \frac{dx^B}{dz_f} \end{bmatrix} = \begin{bmatrix} \left(\frac{dx^D}{dDF}\right)\left(\frac{dDF}{dx^l}\right)\left(\frac{dx^l}{dF_f}\right) & \left(\frac{x^D}{dF_{Di}}\right)\left(\frac{dDF}{dx^l}\right)\left(\frac{dx^l}{dz_f}\right) \\ \left(\frac{dx^B}{dDF}\right)\left(\frac{dDF}{dx^l}\right)\left(\frac{dx^l}{dF_f}\right) & \left(\frac{dx^B}{dDF}\right)\left(\frac{dDF}{dx^l}\right)\left(\frac{dx^l}{dz_f}\right) \end{bmatrix}$$

(A.17)

After performing mathematical derivations for each of derivative terms (see Appendix A for detailed derivation), the following equation is obtained, similar to a binary element system or a multi-element system.

$$\frac{d\mathbf{y}}{d\mathbf{d}} = \begin{bmatrix} \left((RR+1)+\left(\frac{dDF}{dx^l}\right)^{-1}\right)\left(\frac{dDF}{dx^l}\right)\left(\frac{-a_7}{\left[a_5\frac{dDF}{dx^l}-a_6-\left(\frac{dx^D}{dDF}\right)\left(\frac{dDF}{dx^l}\right)\right]}\right) & \left((RR+1)+\left(\frac{dDF}{dx^l}\right)^{-1}\right)\left(\frac{dDF}{dx^l}\right)\left(\frac{-a_8}{\left[a_5\frac{dDF}{dx^l}-a_6-\left(\frac{dx^D}{dDF}\right)\left(\frac{dDF}{dx^l}\right)\right]}\right) \\ \left(\left(\frac{dDF}{dx^l}\right)^{-1}-RB\right)\left(\frac{dDF}{dx^l}\right)\left(\frac{a_3}{\left[a_1\frac{dDF}{dx^l}+a_2+\left(\frac{dx^B}{dDF}\right)\left(\frac{dDF}{dx^l}\right)\right]}\right) & \left(\left(\frac{dDF}{dx^l}\right)^{-1}-RB\right)\left(\frac{dDF}{dx^l}\right)\left(\frac{a_4}{\left[a_1\frac{dDF}{dx^l}+a_2+\left(\frac{dx^B}{dDF}\right)\left(\frac{dDF}{dx^l}\right)\right]}\right) \end{bmatrix}$$

(A.18)

Selection of the controller structure (pairing between controlled-manipulated variables). It can be seen from Eq. (A.19) that the best controller structure can easily be determined by looking at the value of $d\mathbf{y}/d\mathbf{u}$. Since values of dx_d/dRR and dx_b/dRB

are bigger, controlling x^D by manipulating *RR* and controlling x^B by manipulating *RB* will require less control action. This is because only small changes in *RR* and *RB* are required to move x^D and x^B in a bigger direction. It must be noted that in Eq. (A.19), $\mathbf{y} = \begin{bmatrix} x^D & x^B \end{bmatrix}$, $\mathbf{u} = \begin{bmatrix} RR & RB \end{bmatrix}$.

$$\frac{dy}{du} = \begin{bmatrix} \frac{dx^D}{dRR} & \frac{dx^D}{dRB} \\ \frac{dx^B}{dRR} & \frac{dx^B}{dRB} \end{bmatrix} = \begin{bmatrix} DF & 0 \\ 0 & -DF \end{bmatrix} \tag{A.19}$$

For methanol/water binary compound system, the corresponding driving force diagram is given below (see Figures A1 and A2):

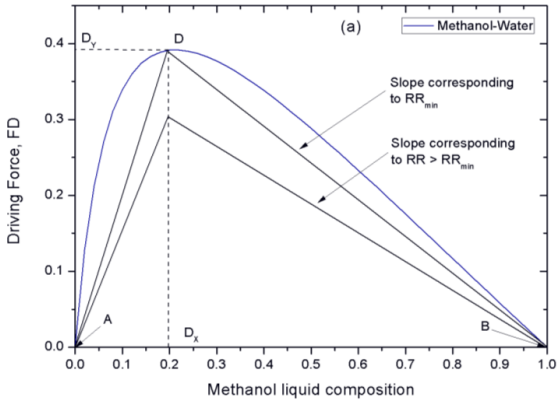

Figure A1 Driving force diagram with illustration of the distillation design parameters at point A (maximum driving force) (Hamid, 2011)

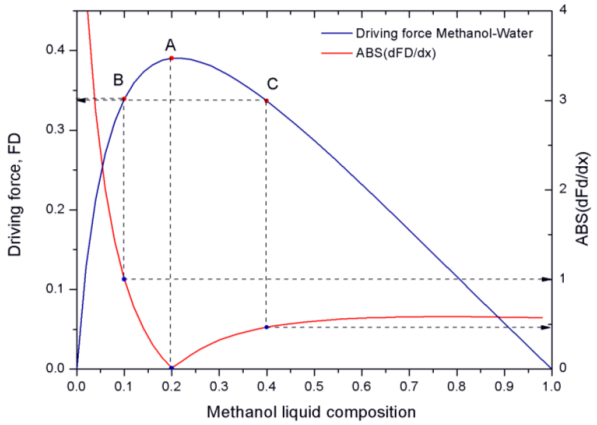

Figure A2 Plot of driving force and derivative of driving force with respect to composition as a function of composition for methanol-water (Hamid, 2011).

In Table A1, the design parameters for the binary methanol-water distillation at the maximum driving force (design A) and two alternative design points (B and C) are given

Table A1. Values of design variable and steady-state simulation at different operating points

Point	No. Stage	Feed Stage	RR	RB	D (kmol/h)	B (kmol/h)	T_{cond} (K)	T_{reb} (K)	Q_{reb} (MJ/h)	Q_{cond} (MJ/h)
A	22	17	0.6606	1.9845	30.82	29.18	330.35	384.30	20.95	17.52
B	22	20	0.3361	2.6383	47.15	12.85	338.81	390.81	23.33	19.94
C	22	13	1.4073	1.7665	48.12	11.88	328.10	372.57	21.21	19.07

Values of dDF/dx^l are calculated and shown in Figure A2. Note that in Figure A1, two other points (Points B and C) which are not at the maximum are identified as candidate alternative designs for a distillation column which will be used for verification purposes. The value of dx^D/dF_f from equation (A.18) is calculated as follows (only for the first element of the two by two matrix):

at point A (maximum driving force)

$$\left.\frac{dx^D}{dF_f}\right|_{point\ A} = \left((RR+1)+\left(\frac{dDF}{dx^l}\right)^{-1}\right)\left(\frac{dDF}{dx^l}\right)\left(\frac{-a_7}{\left[a_5\frac{dDF}{dx^l}-a_6-\left(\frac{dx^D}{dDF}\right)\left(\frac{dDF}{dx^l}\right)\right]}\right) =$$

$$\left((0.6606+1)+(0)^{-1}\right)(0)\left(\frac{-0.016}{[(1.98)(0)-0.946-1]}\right)=0$$

at point B

$$\left.\frac{dx^D}{dF_f}\right|_{point\ B} = \left((RR+1)+\left(\frac{dDF}{dx^l}\right)^{-1}\right)\left(\frac{dDF}{dx^l}\right)\left(\frac{-a_7}{\left[a_5\frac{dDF}{dx^l}-a_6-\left(\frac{dx^D}{dDF}\right)\left(\frac{dDF}{dx^l}\right)\right]}\right) =$$

$$\left((0.3361+1)+(1)^{-1}\right)(1)\underbrace{\left(\frac{-0.011}{[(0.71)(1)-0.27-2.33]}\right)}_{\geq 0}\geq 0$$

at point C

$$\left.\frac{dx^D}{dF_f}\right|_{point\ C} = \left((RR+1)+\left(\frac{dDF}{dx^l}\right)^{-1}\right)\left(\frac{dDF}{dx^l}\right)\left(\frac{-a_7}{\left[a_5\frac{dDF}{dx^l}-a_6-\left(\frac{dx^D}{dDF}\right)\left(\frac{dDF}{dx^l}\right)\right]}\right) =$$

$$\left((1.4073+1)+(0.49)^{-1}\right)(0.49)\underbrace{\left(\frac{-0.01}{[(0.43)(0.49)-0.24-2.17]}\right)}_{\geq 0}\geq 0$$

It can be seen that the sensitivity of the design to the disturbances in the feed at the maximum driving force (point A) is the less than any other point on the driving force diagram. Similarly, the same conclusion can be made if the values of other elements in Eq. (A.16) are calculated. For the choice of the controller structure (given by Eq. A.19) the values of the derivatives at the points A (maximum driving force), B and C is calculated as follows:

$$\frac{d\mathbf{y}}{d\mathbf{u}}\Big|_{Point\,A} = \begin{bmatrix} \frac{dx^D}{dRR} & \frac{dx^D}{dRB} \\ \frac{dx^B}{dRR} & \frac{dx^B}{dRB} \end{bmatrix} = \begin{bmatrix} 0.38 & 0 \\ 0 & -0.38 \end{bmatrix}$$

$$\frac{d\mathbf{y}}{d\mathbf{u}}\Big|_{Point\,B} = \begin{bmatrix} \frac{dx^D}{dRR} & \frac{dx^D}{dRB} \\ \frac{dx^B}{dRR} & \frac{dx^B}{dRB} \end{bmatrix} = \begin{bmatrix} 0.34 & 0 \\ 0 & -0.34 \end{bmatrix}$$

$$\frac{d\mathbf{y}}{d\mathbf{u}}\Big|_{Point\,C} = \begin{bmatrix} \frac{dx^D}{dRR} & \frac{dx^D}{dRB} \\ \frac{dx^B}{dRR} & \frac{dx^B}{dRB} \end{bmatrix} = \begin{bmatrix} 0.34 & 0 \\ 0 & -0.34 \end{bmatrix}$$

Therefore, it is also established that the highest sensitivity of the controlled variables to manipulated variables is at the maximum driving force.

Department of Chemical and Biochemical Engineering
Technical University of Denmark
Søltofts Plads, Building 229
2800 Kgs. Lyngby
Denmark

Phone: +45 45 25 28 00
Web: www.kt.dtu.dk/